INTERNATIONAL ATOMIC ENERGY AGENCY
UNITED NATIONS EDUCATIONAL, SCIENTIFIC AND CULTURAL ORGANIZATION

INTERNATIONAL CENTRE FOR THEORETICAL PHYSICS
34100 TRIESTE (ITALY) - P.O.B. 586 - MIRAMARE - STRADA COSTIERA 11 - TELEPHONE: 2240-1
CABLE: CENTRATOM - TELEX 460392 - I

SMR/459- 9

SPRING COLLEGE IN CONDENSED MATTER
ON
'PHYSICS OF LOW-DIMENSIONAL STRUCTURES'
(23 April - 15 June 1990)

AN INTRODUCTION TO THE THEORY OF ELECTRON TRANSPORT IN LOW-DIMENSIONAL SEMICONDUCTOR STRUCTURES

P.N. BUTCHER
University of Warwick
Department of Physics
Coventry CV4 7AL
United Kingdom

An Introduction to the
Theory of Electron Transport
in Low-Dimensional
Semiconductor Structures

P.N. Butcher
University of Warwick
Coventry CV4 7AL
England

An Introduction to the Theory of Electron Transport in Low-Dimensional Semiconductor Structures

P. N. Butcher, University of Warwick, Coventry CV4 7AL, England

Abstract

Several different approaches to electron transport theory in semiconductor microstructures are discussed. The main emphasis in on the behaviour of a 2D electron gas in zero magnetic field at liquid helium temperatures. Boltzmann transport theory is developed for this system and applied to the calculation of low-field transport coefficients in the absence of inelastic scattering. A 2D electron gas coupled to a 3D phonon gas is also treated from the point of view of Boltzmann transport theory so as to evaluate the large phonon drag contribution to the thermopower. Kubo formulae are introduced and used to discuss Onsager symmetry, weak localisation corrections to the transport coefficients and universal fluctuations of conductivity and thermopower. The scattering matrix formalism for a semiconductor microstructure is developed. It is used to obtain relationships between fluxes of charge and heat in the terminals and changes of chemical potentials and temperatures in the resevoirs feeding them. Applications are made to mesoscopic and ballistic systems and to the integer quantum Hall effect.

1. Introduction

Low-dimensional semiconductor structures have interesting transport properties. Several methods have been developed for investigating them from a theoretical point of view. Here we discuss Boltzmann transport theory[1] which is physically transparent, Kubo formulae[2] which are more general but less easy to evaluate and the Laudauer-Buttiker formalism which is paticularly useful in mesoscopic and ballistic systems.[3, 4] To keep the mathematical complications to a minimum we concentrate on the behaviour of a 2D electron gas (2DEG) in zero applied magnetic field. Apart from a few introductory remarks we leave magneto-transport to other lecturers who will treat it in the rich detail which it deserves. Similarly we avoid the complications which arise in low-dimensional hole gasses because of the degenerate valence band structure. Finally, we generally only quote results for a 1D electron gas (1DEG) because the detailed analysis is similar to that for a 2DEG. These omissions allow us to develop the aspects of transport theory that we have chosen to emphasise in enough detail to be useful.

In Section 2 we introduce a simple description of the energy band structure of 2DEGS and 1DEGS. This is used in Section 3 to develop Boltzmann transport theory for a 2DEG. The relaxation time approximation is employed to obtain the standard formulae for the transport coefficients when the electrons are scattered elastically by static defects and phonons are ignored. In Section 4 the formulae are used to discuss the quantum size effects which arise at liquid helium temperatures when the Fermi level moves through one of the discrete energy levels associated with the confining potential. In Section 4.1 we discuss the sharp discontinuities of the electrical conductivity which are predicted for a 2DEG by Boltzmann transport theory. In Section 4.2 we introduce energy level broadening which is ignored in Boltzmann's equation. It has a strong smoothing effect on the discontinuities in the conductivity. However, we show in Section 4.3 that the quantum size effects

predicted for the thermopower of a 2DEG are much more striking and are also much more resistant to the effects of level broadening. Similar, but stronger effects are predicted for 1DEGS in Section 4.4.

Phonons are neglected throughout Sections 3 and 4. Consequently, the thermopower calculated is what is usually referred to as "electron diffusion" thermopower.(1) Experiment shows that this is proportional to the absolute temperature T and it is dominant when T< 0·5K. In the temperature range 1-10K, however, experiment also shows that "phonon drag" thermopower(1) in a 2DEG is proportional to T^3 and greatly exceeds the electron diffusion contribution. To see how this comes about and to investigate the phonon drag effect in detail we consider coupled 3D phonon and 2DEG Boltzmann equations in Section 5.

In Section 6 we give an elementary derivation of the Kubo-Greenwood formula for the electrical conductivity of a system of independent electrons. It is used to derive corresponding formulae for the other transport coefficients when the magnetic induction field $\underline{B} = 0$. Kubo formulae for electrical conductivity and the thermal and thermoelectric transport coefficients are also given there when $\underline{B} \neq 0$. The formulae are used to discuss Onsager symmetry and to introduce weak localisation corrections to the transport coefficients and universal fluctuations in mesoscopic systems.

Section 7 is devoted to the Landauer-Buttiker formalism. We extend Buttiker's treatment of the conductance matrix of a many-terminal microstructure(4) to obtain corresponding formulae for the thermal and thermoelectric matrices. The formulae are used to discuss Onsager symmetry and reciprocity for electrical, thermal and thermoelectric configurations. They are also used in Section 8 to discuss the Aharonov-Bohm effect, quantum point contacts and the integer quantum Hall effect.

This is a convenient place to survey, very briefly, the semiconductor

microstructures which are the principal concern of the Spring College. The subject began with the study of 2DEGS in n-channel Si MOSFETS. The work done prior to 1985 is summarised in the seminal review by Ando, Fowler and Stern.(5) In this system, which is illustrated in Figure 1, Si is separated from a metal gate by an insulating layer of SiO_2. Biasing the gate positive drives holes away from the Si/SiO_2 interface. Biasing beyond a threshold voltage produces a narrow, degenerate "inversion layer" of electrons at the interface which conducts electricity between a source electrode and a drain electrode in the Si. The width of the inversion layer is in the order of 3-10nm. The electrons are confined on one side by the steep potential barrier presented by the insulating SiO_2. On the other side they are confined by the linear potential barrier arising from the ionised acceptors in the depletion layer as shown in Figure 2. Electrons may only move freely parallel to the Si/SiO_2 interface. Their charge distribution in the inversion layer may be calculated by solving the Schrodinger equation in the triangular potential well self-consistently.(5) This is our first example of the "quantum wells" which are ubiquitous in low-dimensional semiconductor physics.

At liquid helium temperatures the electron mobility in an n-channel MOSFET is determined by scattering from Coulomb centres in the SiO_2 and imperfections in the nominally planar Si/SiO_2 interface. Values in the order of 15,000 $cm^2\ V^{-1}\ s^{-1}$ are obtained at 1·5K in recently fabricated structures.(6) Much higher mobilities can be achieved in the 2DEGS which can be created at GaAs/AlGaAs heterojunctions. Values in excess of $10^6\ cm^2\ V^{-1}\ s^{-1}$ are commonplace and the World record at the time of writing appears to be $12 \times 10^6\ cm^2 V^{-1} s^{-1}$.(7) In this system the GaAs is pure and the AlGaAs is an alloy containing typically 30% Al and 70% Ga. There is a 250 meV potential barrier between the GaAs and the alloy. With

p-type doping in the GaAs and n-type doping in the AlGaAs, a triangular potential well appears in the GaAs which confines the 2DEG to the neighbourhood of the interface as shown in Figure 3. The very high mobility is due to two factors. Firstly, the high degree of perfection of the GaAs/AlGaAs interface which is usually grown by molecular beam epitaxy.(8) Secondly, the dramatic reduction of scattering by the ionised donors in the AlGaAs which is achieved by separating them from the interface with a spacer layer as shown in Figure 3. This system, which was pioneered by Stormer et al,(9) has been used in many of the developments of low-dimensional semiconductor physics in recent years.

Using molecular beam epitaxy, it is also possible to confine a 2DEG in a square quantum well consisting of several atomic planes of GaAs sandwiched between thick layers of AlGaAs (see Figure 4). Multiple quantum well structures (i.e. superlattices) may also be fabricated by laying down successive layers of GaAs and AlGaAs. Finally, while GaAs and AlGaAs are the favourite pair of materials, there are many other combinations. The ability to fabricate many different layered semiconductor structures with essentially atomic precision is the driving force behind modern research on low-dimensional semiconductors. Some of these structures have already been discussed by Bastard(10) and Foxon.(8) Subsequently lecturers will return to them again and again.

A further reduction of dimensionality, from 2 to 1, may be achieved by laterally confining a 2DEG. There are many ways of doing this. Probably the most successful for heterojunctions is the split gate technique pioneered by Pepper et al.(11) The electrons in the 2DEG are driven away by a negative bias on an overlayed metal gate except in the vicinity of a narrow split in the gate. The electrons under the split constitute a 1D system with a lateral width which is controlled by the gate voltage. This technique may be extended to produce 2DEGS with an unlimited variety of shapes by appropriately

patterning the gate. The multi-terminal microstructures which we discuss in Sections 7 and 8 may be fabricated in this way. They may involve quantum point contacts if constrictions are introduced in which the 2DEG moves ballistically.(12) A striped gate yields a laterally confined superlattice in the 2DEG. A gate containing holes can yield quantum dots in which the electrons are confined in all three directions. Stern will treat quantum wires and dots in detail.(13)

2. The Energy Band Structure of 2D and 1D Electron Gases

2.1 Two Dimensional Electron Gas

The variation of the conduction band edge with distance (z) in the direction of confinment is the potential energy V(z) for an electron in the conduction band. In the effective mass approximation the one-electron Hamiltonian is

$$H = \underline{p}^2/2m^* + V(z) \qquad (2.1)$$

where $\underline{p} = -i\hbar\underline{\nabla}$ and a constant isotropic effective mass m^* has been assumed for simplicity. To determine the eigenfunctions of H we consider a macroscopic square of side L in the xy-plane and apply periodic boundary conditions in the x and y directions. Since H is independent of x and y the eigenfunctions take the form

$$\psi_{\alpha\underline{k}}(\underline{r}, z) = L^{-1}e^{i\underline{k}\cdot\underline{r}}\phi_\alpha(z) \qquad (2.2)$$

where $\underline{r} = (x,y)$ and $\underline{k} = (k_x, k_y)$ with both k_x and k_y equal to integer multiples of $2\pi/L$. By substituting equation (2.2) in the eigenvalue equation for H we find that the eigenvalue associated with $\psi_{\alpha\underline{k}}$ is

$$\epsilon_{\alpha\underline{k}} = \epsilon_\alpha + \hbar^2 k^2/2m^* \qquad (2.3)$$

where ϵ_α and $\phi_\alpha(z)$ are determined by the 1D Schrodinger equation

$$-\hbar^2 d^2\phi_\alpha(z)/dz^2 2m^* + V(z)\phi_\alpha(z) = \epsilon_\alpha\phi_\alpha(z) \qquad (2.4)$$

and $k^2 = k_x^2 + k_y^2$.

We see that the subscript α in equation (2.2) is a quantum number labelling the solutions of equation (2.4). We set $\alpha = 0,1,2,\ldots$ in the discrete spectrum of equation (2.4) where $\alpha = 0$ is the ground state. When $V(z) = 0$ we have, by inspection, $\phi_\alpha(z) = L^{-1/2}\exp(ik_z z)$ with $k_z = \alpha 2\pi/L$ if we impose periodic boundary conditions over a distance L in the z direction. When $L\to\infty$, k_x, k_y and k_z all become quasi-continuous and equation (2.3) gives the familiar 3D form $\hbar^2(k_x^2 + k_y^2 + k_z^2)/2m^*$ for the energy. In the cases of interest to us V(z) has the form of a potential well and the low values of ϵ_α are discrete. Then, if we use equation (2.3) to plot energy against k, we obtain a distinct parabola for each α with a minimum at ϵ_α. We refer to this plot and the associated eigenfunctions as subband α. the value of ϵ_α depend on V(z). For a simple square well of width w having infinite side walls $\phi_\alpha(z)$ and ϵ_α have the familiar forms

$$\phi_\alpha(z) = (2/w)^{1/2}\sin[(\alpha + 1)\pi z/w] \qquad (2.5a)$$

$$\epsilon_\alpha = \hbar^2(\alpha + 1)^2\pi^2/2m^*w^2 \qquad (2.5b)$$

where z is measured from one side of the well. Formulae appropriate to a triangular well are given in reference 5 in which self-consistent calculations are also discussed.

The density of states per unit area in sub-band α is readily evaluated in the manner familiar from 3D calculations for free electrons, Introducing a factor 2 for spin it is

$$N_\alpha(\epsilon) = 2.(1/2\pi)^2\, 2\pi\, k\, dk/d\epsilon\, \theta(\epsilon - \epsilon_\alpha) = N_{ssb}\, \theta(\epsilon - \epsilon_\alpha) \qquad (2.6a)$$

where

$$N_{ssb} = m^*/\pi\hbar^2 \qquad (2.6b)$$

is the density of states when $\epsilon > \epsilon_\alpha$ and θ denotes the unit step function. The subscript ssb in equation (2.6) is an abbreviation for "single subband." The density of states for all the subbands is

$$N(\epsilon) = N_{ssb} \sum_\alpha \theta(\epsilon - \epsilon_\alpha)\,. \qquad (2.7)$$

We see that $N(\epsilon)$ has the form of the staircase sketched in Figure 5(a). It increased by N_{ssb} whenever a subband minimum is crossed. The quantum size effects exhibited by a 2DEG are due to the subband structure and reflect the discontinuities in $N(\epsilon)$.

2.2 One-Dimensional Electron Gas

A 2DEG may be converted to a 1DEG by introducing a potential well U(y) in the y direction. Then the electrons are only free to move in the x-direction. Hence equation (2.2) becomes

$$\psi_{\alpha k}(x,y,z) = L^{-1/2}\, e^{ikx}\, \phi_\alpha(y,z) \qquad (2.8)$$

where $\phi_\alpha(y,z)$ is determined by the 2D Schrodinger equation

$$-\hbar^2[\partial^2/\partial y^2 + \partial^2/\partial z^2]\phi_\alpha(y,z)/2m^* + [U(y) + V(z)]\phi_\alpha(y,z) = \epsilon_\alpha\phi_\alpha(y,z). \qquad (2.9)$$

and equation (2.3) remains formally the same but k is now the wave number in

the x direction. We may still speak of subbands and the eigenvalue ϵ_α in equation (2.9) is the minimum energy in subband α. The most important result of reducing the dimensionality from 2 to 1 is that the calculation of the density of states per unit length in subband α now takes the form

$$N_\alpha(\epsilon) = 2(1/2\pi)\, 2dk/d\epsilon\, \theta(\epsilon - \epsilon_\alpha) = (2N_{ssb}/\pi)^{-1/2}\, \theta(\epsilon - \epsilon_\alpha)^{-1/2} \qquad (2.10)$$

where N_{ssb} is again given by equation (2.5b). In 1D there is a square root singularity at the subband minimum. The density of states $N(\epsilon)$ for all the subbands is obtained by summing equation (2.10) over all α as shown in Figure 5(b). The quantum size effects exhibited by 1DEGS reflect the discontinuous nature of this function. They are expected to be sharper than they are for 2DEG because the discontinuities are much more severe for a 1DEG.

The additional confining potential U(y) may be created in various ways. The most obvious, and technically the most difficult,is to etch away the material in the 2DEG structure so as to reduce the width in the y direction to a few nanometres.[14] It is also possible to introduce additional electrodes on either side of the 2DEG and squeeze it in electrostatically.[15, 16] Another option is the split gate technique described in the Introduction.[11] All these procedures yield a potential well in the yz-plane which is more complicated than the simple additive form U(y) + V(z) which we have assumed here and the calculation of ϵ_α and $\phi_\alpha(y,z)$ is a difficult problem.[13] Even in the elementary case in which the 2D potential well is zero inside and infinite outside the rectangle $0<z<a$ and $0>y>b$ it is best to abandon the integer notation for successive subbands and write instead $\alpha = (m,n)$ where m and n are positive integers. Then $\phi_{mn}(y,z)$ and $\epsilon_{m,n}$ have the familiar forms

$$\phi_{mn}(y,z) = 2(ab)^{-1/2}\sin(m\pi z/a)\sin(n\pi y/b) \qquad (2.11a)$$

$$\epsilon_{mn} = \hbar[m^2/a^2 + n^2/b^2]\pi^2/2m^* \qquad (2.11b)$$

3. Boltzmann Transport Theory

3.1 The Transport Coefficient

We confine our attention to a 2DEG. The modifications of the formalism required to treat a 1DEG are easily made. For simplicity we suppose that the Fermi level (chemical potential) is uniform and that the 2DEG is subjected to a weak electric field $\underline{E}$ and a weak temperature gradient $\underline{\nabla}T$ in the xy- plane. We are concerned with the response which the 2DEG produces in the form of electric and heat current densities per unit length which are denoted by $\underline{J}$ and $\underline{Q}$ respectively. These quantities are obtained by integrating the 3D electric and heat current densities across the 2DEG in the z (confinment) direction. They are linearly related to $\underline{E}$ and $\underline{\nabla}T$ by the macroscopic transport equations

$$\underline{J} = \sigma \underline{E} + L \underline{\nabla} T \qquad (3.1a)$$

$$\underline{Q} = M \underline{E} + N \underline{\nabla} T \qquad (3.1b)$$

We consider 2DEGS which are isotropic in the xy-plane so that the transport coefficients σ,L,M and N are all scalars,

Equations (3.1) are the theoretician's standard form for the macroscopic transport equations. Experimentalists usually rewrite them as

$$\underline{E} = \rho \underline{J} + S \underline{\nabla} T \qquad (3.2a)$$

$$\underline{Q} = \pi \underline{J} - \kappa \underline{\nabla} T \qquad (3.2b)$$

where $\rho = \sigma^{-1}$, $S = -\sigma^{-1}L$, $\pi = M\sigma^{-1}$ and $\kappa = M\sigma^{-1}L - N$ are respectively the resistivity, thermopower, Peltier coefficient and thermal conductivity. These are the quantities which are directly measured in electron transport

experiments.

3.2 Boltzmann's Equation in the Quantum Limit

It is convenient to begin with the case in which only the ground subband with $\alpha = 0$ is occupied by electrons (i.e. the "quantum limit"). The modifications of the formalism neccessary when several subbands are occupied are easy to make.

We are concerned with average effects produced by many electrons. It is therefore convenient to introduce a distribution function $f(\underline{k},\underline{r},t)$ which is proportional to the density of electrons in $(\underline{k},\underline{r})$-space. The proportionality constant is fixed so that $f(\underline{k},\underline{r},t)$ is equal to the probability that an electron will occupy a state with wave vector $\underline{k}$ and a given spin orientation in the neighbourhood of the point $\underline{r}$ at time t. Then, for a 2DEG, the density of electrons in $(\underline{k},\underline{r})$-space is $(2\pi^2)^{-1}f(\underline{k},\underline{r},t)$. It follows that n, (the areal density of electrons), $\underline{J}$ and $\underline{Q}$ are given by

$$n = (2\pi^2)^{-1} \int f \, d\underline{k} \qquad (3.3a)$$

$$\underline{J} = -e(2\pi^2)^{-1} \int f \, \underline{v}(\underline{k}) \, d\underline{k} \qquad (3.3b)$$

$$\underline{Q} = (2\pi^2)^{-1} \int f \, \underline{v}(\underline{k}) \, [\epsilon_{0\underline{k}} - \epsilon_F] \, d\underline{k} \qquad (3.3c)$$

Here: ϵ_F is the Fermi level, $\epsilon_{0\underline{k}} = \epsilon_0 + \hbar^2\underline{k}^2/2m^*$ is the energy in the ground subband and $\underline{v}(\underline{k}) = \hbar\underline{k}/m^*$ is the associated group velocity.

To determine $f(\underline{k},\underline{r},t)$ we use Boltzmann's equation.[1,2,17] The equation expresses the conservation of electrons as they follow semiclassical trajectories in $(\underline{k},\underline{r})$-space. Its derivation follows the same lines as those used for a 3D system[17] and the result is

$$\partial f/\partial t + \underline{v}.\underline{\nabla} f - e/\hbar \, \underline{E} \, . \, \underline{\nabla}_{\underline{k}} f = (\partial f/\partial t)_c \qquad (3.4)$$

where $(\partial f/\partial t)_c$ is the rate of change of f due to collisions, $\underline{\nabla} = (\partial/\partial x, \partial/\partial y)$,

$\nabla_k = (\partial/\partial k_x, \partial/\partial k_y)$ and $\underline{k}$ is left understood.

3.3 The relaxaton Time Ansatz in the Quantum Limit

We consider only static situations for which $\partial f/\partial t = 0$ and replace f by its thermal equilibrium value $f_0(\epsilon_{0\underline{k}})$ in the other two terms on the left-hand side of equation (3.4). The terms which are neglected in this approximation are second order in $\underline{E}$ and ∇T. The form of $f_0(\epsilon_{0\underline{k}})$ is given by the Fermi-Dirac function

$$f_0(\epsilon_{0\underline{k}}) = [\exp\{(\epsilon_{0\underline{k}} - \epsilon_F)/k_B T\} + 1]^{-1} \tag{3.5}$$

We introduce the relaxation time ansatz by writing

$$(\partial f/\partial t)_c = -(f - f_0')/\tau(\epsilon_{0\underline{k}}) \tag{3.6}$$

on the right hand-side of equation (3.4). Then the calculation of f is trivial. When the result is substituted into equation (3.3) we find that n is not effected by $\underline{E}$ and ∇T while $\underline{J}$ and $\underline{Q}$ are given by (3.3) with

$$\sigma = -\int f_0'(\epsilon)\, \sigma(\epsilon)\, d\epsilon \tag{3.7a}$$

$$L = -(eT)^{-1} \int f_0'\, \sigma(\epsilon)\, (\epsilon - \epsilon_F)\, d\epsilon \tag{3.7b}$$

$$M = -TL \tag{3.7c}$$

$$N = (e^2T)^{-1} \int f_0'\, \sigma(\epsilon)\, (\epsilon - \epsilon_F)^2\, d\epsilon \tag{3.7d}$$

where $f_0(\epsilon)$ is the energy-derivative of the Fermi-Dirac function and

$$\sigma(\epsilon) = n_0(\epsilon) e^2\, \tau(\epsilon)/m^* \tag{3.8}$$

In equation (3.8) $n(\epsilon) = k_0(\epsilon)^2 2\pi$ is the areal electron density when all the states inside a circle of radius $k_0(\epsilon) = \hbar^{-1}[2m^*(\epsilon - \epsilon_0)]^{1/2}$ are full.

When $T \to 0$, $f_0'(\epsilon) \to -\delta(\epsilon - \epsilon_F)$ and equation (3.7a) gives $\sigma = \sigma(\epsilon_F)$. Hence $\sigma(\epsilon)$ may be interpreted as the conductivity when $T \to 0$ with the Fermi level at ϵ. A low temperature formula for $S = -L/\sigma$ is obtained by expending $\sigma(\epsilon)$ about ϵ_F in equation (3.7b). Up to terms linear in T it is

$$S = -(\pi^2 k_B T/3e)\, \sigma'(\epsilon_F)/\sigma(\sigma_F). \tag{3.9a}$$

A similar calculation of κ yields the Wiedemann-Franz law

$$\kappa = L_0 \sigma(\epsilon_F) T \tag{3.9b}$$

where $L_0 = 1/3(\pi k_B/e)^2$ is the Lorentz number. Finally we note that $\sigma(\epsilon)$ may be written in the alternative form

$$\sigma(\epsilon) = e^2 N_{ssb} D_0(\epsilon) \tag{3.10}$$

where N_{ssb} is the density of states in subband 0 and

$$D(\epsilon) = 1/2[\hbar k_0(\epsilon)/m^*]^2 \tau(\epsilon\} \tag{3.11}$$

is the diffusion constant at $T = 0$ when the Fermi level is at ϵ. Equation (3.10) is one form of the Einstein relation for a degenerate electron gas.[17]

The only unknown in equations (3.7) to (3.11) is the relaxation time. For elastic scattering which is even in the scattering angle we may derive an

explicit formula for $\tau(\epsilon)$ by substituting f in terms of $\tau(\epsilon)$ into equation (3.6) with $(\partial f/\partial t)_c$ replaced by the standard Boltzmann collision integral:(17)

$$(\partial f/\partial t)_c = (L/2\pi)^2 \int d\underline{k}' [f'(1 - f)P(\underline{k}', \underline{k}) - f(1 - f')P(\underline{k}, \underline{k}')] \qquad (3.12)$$

where $f = f(\underline{k})$, $f' = f(\underline{k}')$ and $P(\underline{k}', \underline{k})$ is the transition rate from $\underline{k}'$ to $\underline{k}$. Then, in the linear regime we find that

$$1/\tau(\epsilon_{0\underline{k}}) = (L/2\pi)^2 \int P(\underline{k}, \underline{k}')[1 - \cos\theta]\, d\underline{k}' \qquad (3.13)$$

where θ is the scattering angle between $\underline{k}'$ and $\underline{k}$.

3.4 Boltzmann Transport Theory for more than One Subband

The analysis of Sections 3.2 and 3.3 may be generalised easily to the case when more than one subband is occupied. We introduce a distribution function $f_\alpha(\underline{k}, \underline{r}, t)$ for αth subband and sum over subbands in calculating n, $\underline{J}$ and $\underline{Q}$ from the generalisation of equation (3.3). Boltzmann's equation (3.4) remains formally the same apart from the addition of a subscript α to f. Of course, $(\partial f_\alpha/\partial t)_c$ is more complicated in the multi-subband case. To use the relaxation time ansatz (3.6), however, we have only to add a subscript α to both f and τ and replace $\epsilon_{0\underline{k}}$ by $\epsilon_{\alpha\underline{k}}$. Then the calculation of the transport coefficients leads to equation (3.7) in which $\sigma(\epsilon)$ is replaced by

$$\sigma(\epsilon) = \sum_\alpha n_\alpha(\epsilon)\, e^2\, \tau_\alpha(\epsilon)/m^* \qquad (3.14)$$

With this understanding, the low temperature approximations to σ, S and κ are still given by $\sigma(\epsilon_F)$ and equation (3.9).

Equations (3.13) generalises to a set of equations for the relaxation times of the subbands which are occupied at energy ϵ when $T = 0$. With $\hbar k_\alpha = [2m^*(\epsilon - \epsilon_\alpha)]^{1/2}$ we have

$$\tau^{-1}(\epsilon) = (L/2\pi)^2 \sum_\beta \int d\underline{k}'\, P(\alpha\underline{k}, \beta\underline{k}')[1 - \cos\theta\, k_\beta\, \tau_\beta(\epsilon)/k_\alpha\, \tau_\alpha(\epsilon)] \qquad (3.15)$$

where $P(\alpha\underline{k}, \beta\underline{k}')$ is the transition rate from $\psi_{\alpha\underline{k}}$ to $\psi_{\beta\underline{k}'}$ for the elastic scattering process considered. For simplicity in what follows we confine our attention to a randomly distributed array of δ-function scatterers. In that case the system averaged transition rate is independent of the orientation of $\underline{k}$ and $\underline{k}'$. Hence the contribution to the integral in equation (3.15) from the term involving $\cos\theta$ vanishes and $\tau_\alpha(\epsilon)$ reduces to the lifetime of a state with energy ϵ in subband α.

4. Quantum Size Effects in the Transport Coefficients

4.1 The Boltzmann Transport Approximation to the Electrical Conductivity of a 2DEG

We saw in Section 3 that the Boltzmann approximation to the electrical conductivity of a 2DEG at 0K is given by equation (3.14) with $\epsilon = \epsilon_F$. Thus we have

$$\sigma = \sum_\alpha n_\alpha(\epsilon_F) e^2\, \tau_\alpha(\epsilon_F)/m^* \qquad (4.1)$$

Moreover, we see from equation (2.6) that the density of states in subband α is $N_{ssb}\theta(\epsilon - \epsilon_\alpha)$. Hence

$$n_\alpha(\epsilon_F) = N_{ssb}(\epsilon_F - \epsilon_\alpha)\,\theta(\epsilon_F - \epsilon_\alpha) \tag{4.2}$$

Finally, we see from the remarks at the end of Section 3 that a reasonable ansatz for $\tau_\alpha(\epsilon_F)$ is the lifeline of a state at the Fermi level in subband α. This is proportional to the inverse of the density of final states available at energy ϵ_F which increases by N_{ssb} whenever ϵ_F crosses a subband minimum. Consequently σ takes the form shown in Figure 6. The Wiedemann-Franz relation (3,9a) implies that κ will behave similarly.

Discontinuities in $\sigma(\epsilon_F)$ of this type are an inevitable consequence of Boltzmann transport theory for any elastic scattering mechanism. They arise because the theory takes no account of the effect of the scattering on the electronic states and energy levels. We show in Section 4.2 that when this is allowed for, even in the crudest approximation, the discontinuities are rounded off and will be difficult to see unless the electron mean free path is very large in comparison to the Fermi wavelength.

4.2 The effect of level broadening on the electrical conductivity of a 2DEG

The analysis given in Sections 2 and 3 assumes that the energy levels are sharp. In fact they are broadened by the scattering potential. The primary effect of level broadening is to round off the "staircase" structure in the density of states which is shown in Figure 5.

To take this effect into account in an approximate way we use the general Born approximation.[18] The density of states is written in the form

$$N(\epsilon) = (2/A\pi)\sum_\alpha \sum_{\underline{k}} \mathrm{Im}\; G_{\alpha\alpha}(\underline{k}) \tag{4.3}$$

where $G_{\alpha\alpha}(\underline{k})$ is the $(\alpha\underline{k}, \alpha\underline{k})$th matrix element of the Green's operator in the

unperturbed energy representation and $A = L^2$. We may write

$$G_{\alpha\alpha}(\underline{k}) = [\epsilon - \epsilon_\alpha(\underline{k}) + i\,\Gamma_{\alpha\alpha}(\epsilon)]^{-1} \tag{4.4}$$

where

$$\Gamma_{\alpha\alpha}(\epsilon) = \hbar/2\tau_\alpha(\epsilon) \tag{4.5}$$

with $\tau_\alpha(\epsilon)$ denoting the lifetime of a state with energy ϵ in subband α. (For the δ-function scattering potential which we consider below there is no distinction between $\tau_\alpha(\epsilon)$ in equations (4.5) and (4.1). It is for this reason that we use the same notation for both quantities.)

When equation (4.4) is sustituted into equation (4.3) we may evaluate the sum over $\underline{k}$ by taking the limit $A \to \infty$ for which

$$A^{-1}\sum_{\underline{k}} \to (4\pi^2)^{-1}\int d\underline{k} \tag{4.6}$$

The intergral over the 2D $\underline{k}$ space is readily evaluated to yield

$$N(\epsilon) = \sum_\alpha N_{ssb}\,[\pi/2 + \tan^{-1}\{(\epsilon - \epsilon_\alpha)/\Gamma_{\alpha\alpha}(\epsilon)\}]/\pi \tag{4.7}$$

We see by inspection of equation (4.7) that, when $\Gamma_{\alpha\alpha}(\epsilon) \to 0$, the contribution to $N(\epsilon)$ from subband α reduces to 0 when $\epsilon < \epsilon_\alpha$ (so that the inverse tangent $\to -\pi/2$) and reduces to N_{ssb} when $\epsilon > \epsilon_\alpha$ (so that the inverse tangent $\to +\pi/2$). Thus we regain the staircase density of states function discussed in Section 2 in the absence of scattering. To go beyond this it is necessary to make a self-consistent calculation of $\Gamma_{\alpha\alpha}(\epsilon)$. This is

easy to do in only one case. We suppose that the scattering potential is a superposition of randomly located 3D δ-functions with strength U i.e.

$$U_s(r, z) = U \sum_i \delta(x - x_i)\,\delta(y - y_i)\,\delta(z - z_i) \tag{4.8}$$

Then we may use equation (4.5) and Fermi Golden Rule transitions rates to write down an expression for $\Gamma_{\alpha\alpha}(\epsilon)$ involving transitions to each subband with a strength proportional to the contribution of that subband to the total density of states. A self-consistent equation for $\Gamma_{\alpha\alpha}(\epsilon)$ is obtained when the latter is given by equation (4.7) with a factor 2 removed because the scattering potential does not flip spins. Thus we obtain[18]

$$\Gamma_{\alpha\alpha}(\epsilon) = \pi n_s \sum_\beta M_{\alpha\beta}{}^2 N_{ssb}\,[\pi/2 + \tan^{-1}\{(\epsilon - \epsilon_\alpha)/\Gamma_{\alpha\alpha}(\epsilon)\}]\,/\pi \tag{4.9}$$

where n_s is the 2D density of scatterers and

$$M_{\alpha\beta}{}^2 = U^2 \int dz_i P(z_i) \phi_\alpha{}^2(z_i) \phi_\beta{}^2(z_i) \tag{4.10}$$

is the mean square matrix element associated with an individual scatterer located at (x_i, y_i, z_i). In equation (4.10) $P(z_i)$ denotes the probability density for z_i.

Equation (4.9) has been solved numerically after using subband wavefunctions (2.5a) to evaluate $M_{\alpha\beta}{}^2$.[18] Thus the electrons are confined to a channel of width w. To be definite we take $P(z_i)$ to be w^{-1} in the channel and 0 outside it. (In writing equations (4.9) and (4.10) the probability

distribution of r_i has been assumed to be uniform over A.)

The above calculation of the effect of level broadening on the density of states may be used to develop a heuristic formula for $\sigma(\epsilon_F)$ in the presence of level broadening. To do so we start from the equation (4.1) and rewrite it in the suggestive form

$$\sigma(\epsilon_F) = e^2 \sum_\alpha N_{ssb}\,\theta(\epsilon_F - \epsilon_\alpha)\,D_\alpha(\epsilon_F) \tag{4.11}$$

where, as we indicated in equation (3.11),

$$D_\alpha(\epsilon_F = (\epsilon_F - \epsilon_\alpha)\,\tau_\alpha(\epsilon_F)/m^* \tag{4.12}$$

has an immediate interpretation as the electron diffusivity in subband α. The coefficient of $D_\alpha(\epsilon_F)$ in (4.11) is the zeroth order approximation to the density of states in subband α. To improve the formula we simply replace this by the better approximation derived by inspection of equation (4.7). Thus we have

$$\sigma(\epsilon_F) = e^2 \sum_\alpha N_{ssb}[\pi/2 + \tan^{-1}(\epsilon_F - \epsilon_\alpha)/\Gamma_{\alpha\alpha}(\epsilon_F)]\,D_\alpha(\epsilon_F)/\pi \tag{4.13}$$

There is a problem with equation (4.13). Equation (4.12) implies that $D_\alpha(\epsilon_F)$ is negative when $\epsilon_F < \epsilon_\alpha$. Hence subbands with Fermi energies in this range make a negative contribution to $\sigma(\epsilon_F)$. This result is physically wrong. To put it right requires a full diagrammatic calculation of $\sigma(\epsilon_F)$.[18] We do not give the details here because the final result turns out to be a very simple

modification of equation (4.13). It is only necessary to add $e^2/\pi\hbar$ to the contribution to $\sigma(\epsilon_F)$ from each subband. Thus we obtain the final result in the general Born approximation:

$$(e^2/\pi\hbar)\sum_{\alpha}([\pi/2 + \tan^{-1}\{(\epsilon_F - \epsilon_\alpha)/\Gamma_{\alpha\alpha}(\epsilon_F)\}]\{(\epsilon_F - \epsilon_\alpha)/\Gamma_{\alpha\alpha}(\epsilon_F)\} + 1) \qquad (4.14)$$

where $\Gamma_{\alpha\alpha}(\epsilon_F)$ is to be determined by solving equation (4.9).

The final results of the calculation are shown in Figure 7. For each curve we start with the Fermi level in the lowest subband so that the system is strictly 2D. The number labelling the curves is the value of $k_F\ell$ in that case (i.e. $(k_F\ell)_{2D}$) where ℓ is the mean free path and k_F is the radius of the Fermi circle. Each curve is generated by increasing k_F with $k_F\ell$ held fixed. We see that strong fine structure remains when $(k_F\ell)_{2D} \sim 11$ but it has almost disappeared when $(k_F\ell)_{2D} \sim 2$. The latter value is close to that appropriate to the original experiments of Sernelius et al [19] who did not see any quantum size effects.

4.3 Quantum Size Effect in the Thermopower of a 2DEG

In Section 3 we saw that Boltzmann transport theory predicts that the thermopower $S = -L/\sigma$ where S and σ are given in terms of $\sigma(\epsilon)$ by equation (3.7). At low temperatures we obtain equation (3.9a) provided that $\sigma(\epsilon)$ varies slowly on the scale of k_BT near the Fermi level. A naive application of this equation using $\sigma(\epsilon)$ as given in Figure 6 produces a negative contribution to S (proportional to T) as ϵ_F moves between subband minima and a positive,

δ-function-like, contribution to S (with a strength in the order of k_BT) whenever ϵ_F crosses a subband minimum. Of course, in the latter case, the assumption that $\sigma(\epsilon)$ varies slowly on the scale of k_BT is no longer valid and a more careful evaluation of the integrals in equation (3.7) is necessary. When this is carried out[20] we find that S is the sum of a negative contribution which is proportional to T and behaves in the way shown in Figure 8 when ϵ_F moves through a subband minimum and a positive contribution behaving in the way shown in Figure 9, This is a thermally broadened version of the δ-function peak found in the elementary discussion. It has a width $\sim k_BT$ at temperature T. Since the strength (i.e.the area under the curve) is in the order of k_BT its height remains constant ($\sim 2k_B \ln 2/e$) as $T \to 0$. Consequently S must change sign as $T \to 0$ when ϵ_F lies in the neighbourhood of a subband minimum.

In Section 6 we develop exact formulae for the transport coefficients of a non-interacting electron gas. It is shown there that equations (3.7) have general validity outside the Boltzmann transport regime when $\sigma(\epsilon)$ is correctly identified. Consequently, we may calculate the effect of level broadening on the thermopower by substituting the $\sigma(\epsilon)$ for this case which has already been evaluated in Section 4.2.[21] Numerical evaluation of the integrals yields the results presented in Figures 10-12 in which the subband minima are assumed to lie at 0, 5, 10 and 15 meV. In Figure 10, which is drawn for T = 1K, the for the (full curve) case $(k_F\ell)_{2D} = 50$ represents the Boltzmann transport limit, It shows the very large effect of the positive quasi-δ-function peaks in the neighbourhood of the subband minima. We see from the dashed curve ($(k_F\ell)_{2D} = 6$) that peaks remain at this scattering level but the sign changes are eliminated except near the second subband minimum.

Figure 11 shows plots of S against T for $(k_F\ell)_{2D} = 6$ when ϵ_F is near the second subband minimum at 5meV. We find the normal metallic behaviour predicted by equation (3.9a) when ϵ_F is well away from 5meV, and also when it is just above 5meV. The sign change which is expected from Figure 10 when $T \to 0$ appears for $T \sim 1.2K$ when $\epsilon_F = 4.8$ meV. In Figure 12 we plot S against ϵ_F for T = 1K and 6K for $(k_F\ell)_{2D} = 2$ which is a strong scattering case. The details are washed out but significant structure is still present.

Quantum size effects in the thermopower have recently been observed in GaAs/AlGaAs heterojunctions at temperatures in the order of 300mK by Ruf et al.[22] We show some of their data in Figure 13 in the form of a plot of -S/T against ϵ_F. The electron density is increased by means of the persistent photoconductivity effect. The arrow on the horizontal axis indicates the expected location of the first excited subband minimum. The minimum in the curve which preceeds it indicates a positive value of S at T = 320 mK and 300 mK in accordance with the theoretical predictions.

4.4 Quantum Size Effect in a 1DEG

The analysis which we have given for a 2DEG retains much the same character for 1DEG. Both systems have subband structures and therefore both exhibit quantum size effects. In the Boltzmann transport theory of Section 3 all the equations are valid with minor changes to take account of the reduced dimensionality. Thus all the vectors in equation (3.1) and (3.2) point along the wire and $\underline{J}$ and $\underline{Q}$ refer to the total electric and heat currents in that direction. Everywhere $\underline{k}$ and $\underline{k}'$ are replaced by k and k' and in equation (3.3) the factor $(2\pi^2)^{-1}$ becomes π^{-1}. In equations (3.8) and (3.14) $n_\alpha(\epsilon) = 2k_\alpha(\epsilon)/\pi$ and in equations (3.12), (3.13) and (3.15) $L^2/4\pi^2$ becomes $L/2\pi$ where L is the length of the quantum wire. The central equations (3.7)

to (3.11), together with (3.14) have exactly the same form in 1D.

Kearney and Butcher have calculated σ and S for a 1DEG using Boltzmann transport theory.[23] The full force of the square root singularities in the density of states (see equation (2.10)) are felt in this case. The relaxation time for each subband vanishes at the subband minimum and so does $\sigma(\epsilon_F)$. This sharp structure is rapidly removed by thermal broadening above liquid helium temperatures. The effects of level broadening are more interesting.[24] The analysis may again be carried out within the framework of the general Born approximation which we discuss in detail for a 2D system in Section 4.2. It is easily adapted to the 1D case. We present only some of the results obtained by numerical solution of the self-consistent equations for the damping parameters $\Gamma_{\alpha\alpha}(\epsilon)$ in Figures 14 to 17.

4.5 Discussion

The theoretical situation regarding quantum size effects is clear. They are an inevitable consequence of Boltzmann transport theory and are fairly robust when level broadening is taken into account. We have discussed σ and S in detail. The behaviour of κ will be similar to that of σ. The experimental situation at the time of writing is much less clear. Quantum size effects of the type predicted for σ have never been observed. In the case of S the predicted behaviour has been seen in only one 2DEG.[22] There have been no quantum size effect measurements at all for 1DEGS and none involving κ in 2DEGS. The experimental study of quantum size effects in low-dimensional semiconductor structures is ripe for further development.

5. Phonon Drag Thermopower of a 2DEG

5.1. Introduction

The treatment of electron transport theory given in Section 4 makes no mention of phonons or electron-phonon interactions. This is often a good starting point for T < 1K but as T increases above 1K phonons and electron-phonon interactions become increasingly important. We concentrate here on the thermopower of a 2DEG in the temperature range 1 to 10K which has been the subject of several recent experimental and theoretical investigations. The thermopower is observed to be one or two orders of magnitude larger than predicted by the formulae in Section 4. The reason is that these formulae give only the "electron diffusion" contribution which takes no account of the effect of a temperature gradient on the phonon distribution. What is observed is dominated by the "phonon drag" contribution which is due to the momentum imparted to the electrons by the perturbed phonons.

5.2. An Elementary Treatment of Phonon Drag Thermopower

The phonon drag contribution to the thermopower is denoted by S_g. There are several simple ways of deriving approximate formulae for S_g which are appropriate in various limits. They have been reviewed recently by Smith and Butcher[25]. Here we concentrate on the case in which the electron statistics are degenerate. We are concerned with a 2DEG but it is useful to begin by considering a 3D electron gas coupled to 3D acoustic phonons in a system with volume Ω. For simplicity we give all the phonons a common sound velocity v_s and

write $N_{\underline{Q}}$ for the phonon distribution function (i.e. the number of phonons with wave vector $\underline{Q}$). The following formulae for the phonon system are well known[1,25].

The phonon heat flux and momentum density are given by

$$\underline{Q}_p = \Omega^{-1} \sum_{\underline{Q}} \hbar\omega_{\underline{Q}} N_{\underline{Q}} v_s (\underline{Q}/Q) \qquad (5.1)$$

and

$$\underline{P}_p = \Omega^{-1} \sum_{\underline{Q}} \hbar \underline{Q} N_{\underline{Q}} \qquad (5.2)$$

respectively. Moreover, by writing $\omega_{\underline{Q}} = Qv_s$ in equation (5.1) we see that

$$\underline{P}_p = \underline{Q}_p / v_s^2 \qquad (5.3)$$

The phonon specific heat is given by

$$C_p = \Omega^{-1} \sum_{\underline{Q}} (dN_{\underline{Q}}/dT)\, \hbar\omega_{\underline{Q}} \qquad (5.4)$$

and the thermal conductivity of the phonons is

$$\kappa_p = C_p v_s^2 \tau_p / 3 \qquad (5.5)$$

In equation (5.5) τ_p is the momentum relaxation time of the phonons. We may conveniently write τ_p^{-1} in the form

$$\tau_p^{-1} = \tau_{pp}^{-1} + \tau_{pe}^{-1} \qquad (5.6)$$

where τ_{pp} arises from phonon-phonon and phonon-boundary interactions while τ_{pe} is due to phonon-electron interactions.

With these preliminaries a simple formula for S_g may easily be derived. Suppose that a temperature gradient $\underline{\nabla}T$ is applied. Then $\underline{Q}_p = -\kappa_p \underline{\nabla}T$ and, from equation (5.3),

$$\underline{P}_p = -(\kappa_p / v_s^2)\underline{\nabla}T \qquad (5.7)$$

The rate at which $\underline{P}_p$ is annihilated is $\underline{P}_p/\tau_p$ and the rate at which this annihilated phonon momentum appears in the electron system is $(\underline{P}_p/\tau_p)(\tau_p/\tau_{pe})$. Hence the steady state balance equation for the 3D electron momentum density $\underline{P}_e$ is

$$0 = d\underline{P}_e/dt = -en\underline{E} + \underline{P}_p/\tau_{pe} \qquad (5.8)$$

When equation (5.8) is solved for the emf $\underline{E} = S_g \underline{\nabla}T$ with $\underline{P}_p$ and κ_p given by equations (5.7) and (5.5) respectively we find that

$$S_g = -\alpha C_p/3ne \qquad (5.9)$$

where

$$\alpha = \tau_p/\tau_{pe} \qquad (5.10)$$

is the fraction of the phonon momentum annihilated each second which appears in the electron system.

Equation (5.9) is the standard approximate formula for 3D metals[1]. The modifications which are necessary when we consider a 2DEG are easy to identify. We remark, first of all, that the interfaces which lead to the confinement of the electron gas seldom have much effect on the acoustic phonons which retain their 3D character. Thus, the system which interest us is a 2DEG confined to a narrow channel which is coupled to 3D phonons in a phonon bath with a macroscopic extent L_z in the z direction (i.e. the direction of confinement). To formulate the steady state balance equation for the 2D electron momentum density we have only to average equation (5.8) across the phonon bath in the z direction. Then the 3D electron density is replaced by n/L_z where n now denotes the 2D electron density. The same change is necessary in equation (5.8) which becomes

$$S_g = -\alpha L_z C_p/3ne \qquad (5.11)$$

where the 2D interpretation of n is left understood.

Equation (5.9) tells us a great deal about the behaviour of S_g for a 2DEG. Since the electron-phonon interaction is confined to a narrow channel we ignore τ_{pe}^{-1} in equation (5.6). Hence, α in equation (5.10) becomes τ_{pp}/τ_{pe}. In the temperature range 1-10K τ_{pp} is determined by boundary scattering. Thus, apart from a trivial geometrical factor, $\tau_{pp} = L_z/v_s$ which is independent of both T and n. We shall find in Section 5.3 that τ_{pe} is also only weakly dependent on T and n in a degenerate electron gas. Consequently S_g is proportional to T^3 (because C_p is proportional to T^3) and inversely proportional to n. The data of Ruf et al[22] exhibited in Figure 18 clearly shows the T^3 dependence predicted when $1 < T < 10K$. We also see that $|S| \sim 100$ μVK^{-1} in this temperature range. Finally, $|S| \sim 1$ μVK^{-1} below 1K and S changes sign at $T = 0.35$ K when $n = 3.49 \times 10^{11}$ cm^{-2}. Ruf et al suggest that <u>electron diffusion</u> thermopower is dominant when $T < 1K$ and that the change of sign is due to quantum size effects. This behaviour has already been discussed in Section 4.3 in connection with Fig. 13 which shows more of their data.

We give data showing the proportionality of S_g to n^{-1} in the next Section after making a more exact calculation exhibiting a maximum in the temperature dependence of α which is also seen experimentally. It is important to emphasise that this behaviour is characteristic of a <u>degenerate</u> electron gas. In a non-degenerate electron gas τ_{pe}^{-1} is proportional to n and S_g is independent of n[25].

5.3 Calculation of the Phonon Drag Thermopower from Coupled Electron and Phonon Boltzmann Equations

We suppose for simplicity that the electrons occupy only the ground subband with energy $\varepsilon_{0\underline{k}}$ and wave function $\Phi_0(z)$. Then Boltzmann's equation for the electrons is just equation (3.4) with the collision term given by

$$(\partial f/\partial t)_c = -(f-f_0)/\tau + (\partial f/\partial t)_a + (\partial f/\partial t)_e \qquad (5.10)$$

Here f_0 is the Fermi-Dirac function given by equation (3.5) and τ is the electron momentum relaxation time associated with static defects.

The terms $(\partial f/\partial t)_a$ and $(\partial f/\partial t)_e$ in equation (5.10) are the contributions to $(\partial f/\partial t)_c$ from phonon absorption and emission respectively:

$$(\partial f(\underline{k}/\partial t)_{a(e)} = \sum_{\underline{k}'\underline{Q}} \{f'[1-f]P_{\underline{Q}}^{a(e)}(\underline{k}',\underline{k}) - f[1-f']P_{\underline{Q}}^{a(e)}(\underline{k},\underline{k}')\} \qquad (5.11)$$

where $f = f(\underline{k})$, $f' = f(\underline{k}')$ and

$$P_{\underline{Q}}^{a}(\underline{k},\underline{k}') = A(\underline{Q})N_{\underline{Q}}\,\delta[\varepsilon_{0\underline{k}'} - \varepsilon_{0\underline{k}} - \hbar\omega_{\underline{Q}}]\,\delta_{\underline{k}',\underline{k}+\underline{q}} \qquad (5.12)$$

is the transition rate from $\underline{k}$ to $\underline{k}'$ due to phonon absorption when there are $N_{\underline{Q}}$ phonons with wavevector $\underline{Q}$.

The corresponding formula for $P_{\underline{Q}}^{e}(\underline{k},\underline{k}')$ is obtained by replacing $N_{\underline{Q}}$ by $N_{\underline{Q}} + 1$ in equation (5.11) and changing the signs in front of $\hbar\omega_{\underline{Q}}$ and $\underline{q}$ in the δ-symbols. The 3D phonon wave vector $\underline{Q} = (\underline{q},q_z)$ with $\underline{q}$ in the (x,y)-plane. Finally $A(\underline{Q})$ is proportional to the squared electronic matrix element of the screened electron-phonon interaction.

We give an explicit formula for $A(\underline{Q})$ only in the case of an isotropic deformation potential interaction with the interaction energy

$$U(\underline{r},z) = E_1\,\underline{\nabla}.\underline{u}(\underline{r},z) \qquad (5.13)$$

In equation (5.13) $\underline{r} = (x,y)$, $\underline{u}(\underline{r},z)$ is the 3D lattice displacement and E_1 is the deformation potential constant. In the single subband screening approximation (which is usually adequate)

$$A(\underline{Q}) = (\pi E_1^2 Q^2/\rho\Omega\omega_{\underline{Q}}\varepsilon^2(\underline{q}))\,|\int\Phi_0^2(z)\exp(iq_z z)dz|^2 \qquad (5.14)$$

where $\varepsilon(\underline{q})$ is the dielectric function for the ground subband. Equation (5.14) is derived by Cantrell and Butcher[26] but with $\varepsilon(\underline{q}) = 1$ because they ignore screening effects. They also derive the corresponding formula for an anisotropic deformation potential interaction[27]. A multi-subband treatment of screening is given by Smith and Butcher[28] who use it to confirm that the single subband approximation to $\varepsilon(\underline{q})$ may be used in equation (5.14) to interpret data for current experimental systems. The corresponding formula for a piezoelectric interaction is given by Lyo[29].

To solve Boltzmann's equation (3.4) for the electrons we set $\partial f/\partial t = 0$, $\underline{E} = 0$ and suppose that a temperature gradient $\underline{\nabla}T$ is established in the (x,y) plane. Then we may write

$$\underline{v}.\underline{\nabla}f = \underline{v}.\nabla f_0 = f_0'[(\varepsilon_{0\underline{k}}) - \varepsilon_F]\underline{v}.\underline{\nabla}T/T \qquad (5.15)$$

so that

$$f = f_0 - \tau\{f_0'[\varepsilon_{0\underline{k}} - \varepsilon_F]\underline{v}.\underline{\nabla}T/T - (\partial f/\partial t)_a - (\partial f/\partial t)_e\} \qquad (5.16)$$

There are two contributions to $(\partial f/\partial t)_a$ and $(\partial f/\partial t)_e$ in the linear regime. The first is proportional to $f-f_0$ and consequently

involves only the thermal equilibrium value of $N_{\underline{Q}}$:

$$N_{\underline{Q}}^{o} = [\exp(\hbar\omega_{\underline{Q}}/k_B T) - 1]^{-1} \qquad (5.17)$$

It may be allowed for by renormalising τ in equation (5.16) and dropping $(\partial f/\partial t)_a$ and $(\partial f/\partial t)_e$ altogether. The renormalisation required is negligible at liquid helium temperatures because electron scattering by equilibrium phonons is small compared to scattering by static defects. Thus, the effect of the first contribution to $(\partial f/\partial t)_a$ and $(\partial f/\partial t)_e$ is simply to reproduce the solution of the electron Boltzmann equation already obtained in Section 3.3. When substituted into equation (3.3b) it finally yields the electron diffusion thermopower given by equation (3.9a).

The second contribution to $(\partial f/\partial t)_a$ and $(\partial f/\partial t)_e$ in equation (5.16) is proportional to $\Delta N_{\underline{Q}} = N_{\underline{Q}} - N_{\underline{Q}}^{o}$. It yields the perturbation Δf of f which is responsible for phonon drag thermopower. In the linear regime it involves only the thermal equilibrium value f_o of f, i.e. the Fermi-Dirac function given by equation (3.5). Consequently, using equations (5.16), (5.11), (5.12) and the subsequent remarks about $P_{\underline{Q}}^{e}(\underline{k},\underline{k}')$, we find that

$$\Delta f = \tau \sum_{\underline{Q}} \Delta N_{\underline{Q}} \, [R_1(\underline{k}|\underline{Q}) - R_2(\underline{k}|\underline{Q})] \qquad (5.18)$$

where

$$R_1(\underline{k}|\underline{Q}) = \sum_{\underline{k}'} f_o'(1-f_o)[P_{\underline{Q}}^{ao}(\underline{k}',\underline{k})/N_{\underline{Q}}^{o} + P_{\underline{Q}}^{eo}(\underline{k}',\underline{k})/(N_{\underline{Q}}^{o} + 1)] \qquad (5.19a)$$

and

$$R_2(\underline{k},\underline{Q}) = \sum_{\underline{k}'} f_o(1-f_o')[P^{ao}(\underline{k},\underline{k}')/N_{\underline{Q}}^{o} + P_{\underline{Q}}^{eo}(\underline{k},\underline{k}')/(N_{\underline{Q}}^{o} + 1)] \; . \qquad (5.19b)$$

In these equations Δf, τ and f_o are all evaluated when the electron wave number is $\underline{k}$ and f_o' is evaluated when the electron wave number is $\underline{k}'$ (It is not the energy derivation of f_o). The superscript o on the P-symbols indicates that they are to be evaluated with $N_{\underline{Q}} = N_{\underline{Q}}^{o}$.

Following Cantrell and Butcher[26] we introduce the quantity

$$\Gamma_{\underline{k}'\underline{k}}(\underline{Q}) = f^{o}(1 - f_o') \, P_{\underline{k}\underline{k}'}^{ao}(\underline{Q}) \qquad (5.20a)$$

which is the electron flux from $\underline{k}$ to $\underline{k}'$ due to the absorption of thermal equilibrium phonons. Then the following detailed balance relations are easily verified:

$$\Gamma_{\underline{k}'\underline{k}}(\underline{Q}) = f_o'[1 - f_o] \, P_{\underline{k}'\underline{k}}^{eo}(\underline{Q}) \qquad (5.20b)$$

and

$$\Gamma_{\underline{k}\underline{k}'}(\underline{Q}) = f_o'[1 - f_o] \, P_{\underline{k}'\underline{k}}^{ao}(\underline{Q}) \qquad (5.20c)$$

$$= f_o[1 - f_o'] \, P_{\underline{k}\underline{k}'}^{eo}(\underline{Q}) \qquad (5.20d)$$

When equations (5.20) are used in equation (5.19) we find that equation (5.18) simplifies to

$$\Delta f = \tau \sum_{\underline{Q}} \{\sum_{\underline{k}'} (\Gamma_{\underline{k}\underline{k}'} - \Gamma_{\underline{k}'\underline{k}})\} \, \Delta N_{\underline{Q}}/N_{\underline{Q}}^{o}(N_{\underline{Q}}^{o} + 1) \qquad (5.21)$$

The contribution J_g which Δf makes to the electric current density $\underline{J}$ is most conveniently written down by expressing the integral in equation (3.3b) as a sum over $\underline{k}$ values for a 2DEG with area A in the (x,y) plane:

$$\underline{J}_g = -(2e/A) \sum_{\underline{k}} \Delta f \; \underline{v}(\underline{k}) \qquad (5.22)$$

Thus we find that

$$\underline{J}_g = (-2e/A) \sum_{\underline{Q}} [\sum_{\underline{k}} \sum_{\underline{k}'} (\Gamma_{\underline{k}\underline{k}'} - \Gamma_{\underline{k}'\underline{k}}) \underline{v}(\underline{k}) \tau(\underline{k})] \Delta N_{\underline{Q}} / N^{o}_{\underline{Q}} (N^{o}_{\underline{Q}} + 1)$$

$$= (2e/A) \sum_{\underline{Q}} [\sum_{\underline{k}} \sum_{\underline{k}'} \Gamma_{\underline{k}'\underline{k}} \{\underline{v}\tau - \underline{v}'\tau'\}] \Delta N_{\underline{Q}} / N^{o}_{\underline{Q}} (N^{o}_{\underline{Q}} + 1) \quad (5.23)$$

where $\underline{v}$ and τ are evaluated when the electron wave vector is $\underline{k}$ and $\underline{v}'$ and τ' are evaluated when the electron wave vector is $\underline{k}'$. In the second line of equation (5.23) we have interchanged $\underline{k}$ and $\underline{k}'$ in the first term in the summation in the first line.

To complete the calculation of $\underline{J}_g$ we must determine $\Delta N_{\underline{Q}} = N_{\underline{Q}} - N^{o}_{\underline{Q}}$ from the phonon Boltzmann equation

$$\partial N_{\underline{Q}}/\partial t + \underline{v}_p(\underline{Q}).\underline{\nabla} N_{\underline{Q}} = (\partial N_{\underline{Q}}/\partial t)_c \quad (5.24)$$

where $\underline{v}_p(\underline{Q})$ is the velocity of phonons with wave vector $\underline{Q}$. In the steady state $\partial N_{\underline{Q}}/\partial t = 0$. Moreover, for small temperature gradients

$$\underline{\nabla} N_{\underline{Q}} \simeq \underline{\nabla} N^{o}_{\underline{Q}} = \underline{\nabla} T \, dn^{o}_{\underline{Q}}/dT \quad (5.25)$$

Finally, the collision term in equation (5.24) is

$$(\partial N_{\underline{Q}}/\partial t)_c = - \Delta N_{\underline{Q}}/\tau_{pp}(\underline{Q}) + (\partial N_{\underline{Q}}/\partial t)_a + (\partial N_{\underline{Q}}/\partial t)_e \quad (5.26)$$

where $\tau_{pp}(\underline{Q})$ is the phonon momentum relaxation time due to phonon-phonon and phonon-boundary collisions and the last two terms in equation (5.26) are the contributions to $(\partial N_{\underline{Q}}/\partial t)_c$ due to phonon absorption and emission. They are given by

$$(\partial N_{\underline{Q}}/\partial t)_{a(e)} = \mp 2 \sum_{\underline{k}} \sum_{\underline{k}'} f(1-f') P^{a(e)}_{\underline{Q}} (\underline{k},\underline{k}') \quad (5.27)$$

where the summation includes all electron transitions with a given spin orientation in which a phonon with wave vector $\underline{Q}$ is absorbed (emitted). The factor of 2 allows for the two possible spin

orientations of each electron.

In equation (5.26) $\tau_{pp}(\underline{Q})$ depends on $\underline{Q}$. It therefore differs from τ_{pp} in Section 5.2 which is an appropriate average of $\tau_{pp}(\underline{Q})$. It is also convenient to introduce here a $\underline{Q}$-dependent generalisation of the time-constant τ_{pe} used in Section 2.2 to quantify the effect of the electron-phonon interaction on the phonons. To do so we set $f = f_o$ and $f' = f_o'$ in equation (5.27). Then, making use of the detailed balance relations (5.20), we may write

$$(\partial N_{\underline{Q}}/\partial t)_a + (\partial N_{\underline{Q}}/\partial t)_e = -\Delta N_{\underline{Q}}/\tau_{pe}(\underline{Q}) \quad (5.28)$$

with

$$\tau^{-1}_{pe}(\underline{Q}) = 2 \sum_{\underline{k}} \sum_{\underline{k}'} \Gamma_{\underline{k}'\underline{k}}/N^{o}_{\underline{Q}}(N^{o}_{\underline{Q}} + 1) \quad (5.29)$$

In the case of interest to us the last two terms in equation (5.26) may be neglected in comparison to the first. Hence by using equation (5.25), we find that the solution of the phonon Boltzmann equation (5.24) is simply

$$\Delta N_{\underline{Q}} = -\tau_{pp}(\underline{Q}) \underline{v}_p(\underline{Q}).\underline{\nabla} T \, dN^{o}_{\underline{Q}}/dT \quad (5.30)$$

and equation (5.23) gives

$$\underline{J}_g = -(2e/A) \sum_{\underline{Q}} [\sum_{\underline{k}} \sum_{\underline{k}'} \Gamma_{\underline{k}'\underline{k}} \{\underline{v}\tau - \underline{v}'\tau'\}] \times \tau_{pp}(\underline{Q}) \, \underline{v}_p(\underline{Q}).\underline{\nabla} T.\hbar\omega_{\underline{Q}}/k_B T^2 \quad (5.31)$$

In deriving equation (5.31) we have used the relation

$$dN^{o}_{\underline{Q}}/dT = N^{o}_{\underline{Q}} (N^{o}_{\underline{Q}} + 1) \, \hbar\omega_{\underline{Q}}/k_B T^2 \quad (5.32)$$

which follows immediately from equation (5.17).

The system under discussion is isotropic in the xy-plane. We see from the remarks following equation (3.2) that S_g may therefore be identified with $-\sigma^{-1}$ times the coefficient of $\partial T/\partial x$ in the x component of equation (5.31) or with $-\sigma^{-1}$ times the coefficient of $\partial T/\partial y$ in the y component of equation (5.31) or (most symmetrically) with the mean of these two expressions. Thus we obtain the final formula[27]:

$$S_g = (e/A\sigma) \sum_{\underline{Q}} \sum_{\underline{k}} \sum_{\underline{k}'} \Gamma_{\underline{k}'\underline{k}} \{\underline{v}\tau - \underline{v}'\tau'\}.\underline{v}_p(\underline{Q})\, \tau_{pp}(\underline{Q})/k_B T^2 \quad (5.33)$$

5.4 Recovering the Elementary Formula for Phonon Drag

Equation (5.33) is relatively complicated and is the result of considerable algebraic manipulation. To gain confidence in its use we begin by rederiving the elementary formula (5.9). Thus, we suppose that τ is independent of $\underline{k}$ and write $\sigma = ne^2\tau/m^*$. and $\underline{v} - \underline{v}' = \hbar(\underline{k} - \underline{k}')/m^* = -\hbar\underline{q}/m^*$ because of the momentum conservation law contained in $\Gamma_{\underline{k}'\underline{k}}$ through equations (5.20a) and (5.12). Then τ/m^* may be taken outside the summation signs in equation (5.33) to cancel with the corresponding factor in σ. Thus we obtain

$$S_g = -(L_z/ne\Omega) \sum_{\underline{Q}} \sum_{\underline{k}} \sum_{\underline{k}'} \Gamma_{\underline{k}'\underline{k}}\, \tau_{pp}(\underline{Q})\, \hbar\underline{q}.\underline{v}_p(\underline{Q})\hbar\omega_{\underline{Q}}/k_B T^2 \quad (5.34)$$

where $\Omega = AL_z$ is the volume of the phonon bath. For acoustic phonons $\underline{v}_p(\underline{Q}) = v_s(\underline{q},q_z)/Q$, where v_s is the velocity of sound, and $\hbar v_s Q = \hbar\omega_{\underline{Q}}$. The last factor in the summand of equation (5.34) can therefore be written in the form

$$(q/Q)^2(\hbar\omega_{\underline{Q}})^2/k_B T^2 = (q/Q)^2\hbar\omega_{\underline{Q}} d\overset{\circ}{N}_{\underline{Q}}/dT\, [\overset{\circ}{N}_{\underline{Q}}(\overset{\circ}{N}_{\underline{Q}} + 1)]^{-1} \quad (5.35)$$

where we have used equation (5.32). Hence equation (5.34) becomes

$$S_g = -(L_z/2ne\Omega) \sum_{\underline{Q}} \alpha(\underline{Q})(d\overset{\circ}{N}_{\underline{Q}}/dT)\, \hbar\omega_{\underline{Q}}(q/Q)^2 \quad (5.36)$$

where $\alpha(\underline{Q}) = \tau_{pp}(\underline{Q})/\tau_{pe}(\underline{Q})$ in which $\tau_{pe}(\underline{Q})$ is given by equation (5.29). We see that $\alpha(\underline{Q})$ is the fraction of the collisions suffered by phonons with wave vector $\underline{Q}$ which involve the electron-phonon interaction. It is the $\underline{Q}$-dependent analogue of α in equations (5.10) and (5.11). To recover the equation (5.11) from equation (5.36) we have only to approximate $\alpha(\underline{Q})$ and $(q/Q)^2$ by average values α and 2/3 respectively and use equation (5.4) for C_p.

5.5 Comparison of Theory and Experiment

Extensive calculations of S_g have been made from equation (5.33) by Smith and Butcher[6,28,30] and Lyo[29] for Si MOSFETS and GaAs/AlGaAs heterojunctions. All the parameters needed are measured in other experiments and are known in principle. In practice, of course, there is considerable uncertainty in some of their values. The phonon relaxation time $\tau_{pp}(\underline{Q})$ is usually assumed to be independent of $\underline{Q}$ and is either approximated by L_z/v_s or is derived from measured values of the phonon thermal conductivity which is given by equation (5.5).

In Fig. 19 we compare values of $-S_g/T^3$ calculated for a Si MOSFET with measured values of the total thermopower divided by $-T^3$[6]. The data points are fairly flat for $T > 2.5$ K which reflects the basic T^3 dependence predicted by the elementary treatment given in Section 5.2. The measured values also increase as n decreases in rough accord with the n^{-1} behaviour predicted there. What is not

predicted by the elementary treatment is the maximum exhibited by the data at a temperature proportional to $n^{\frac{1}{2}}$. This behaviour is due to a "Kohn anomaly" in the summand of equation (5.33)[6,27] which is illustrated in Figure 20 and is discussed below.

We may remove the sum over $\underline{k}'$ from equation (5.33) by using the momentum conservation condition $\underline{k}' = \underline{k} + \underline{q}$ which is inherent in $\Gamma_{\underline{k}'\underline{k}}$ (see equations (5.20a) and (5.12)). The summation over $\underline{k}$ may then be evaluated by writing

$$\sum_{\underline{k}} = (A/4\pi^2) \int_0^{\infty} k\, dk \int_{-\pi}^{\pi} d\theta \qquad (5.37)$$

where k and θ are polar coordinates in the (k_x,k_y)-plane. The k integration can be evaluated when $\hbar\omega_{\underline{Q}} \ll \varepsilon_{o\underline{k}}$ by approximating the product of the Fermi-Dirac factors involved in $\Gamma_{\underline{k}'\underline{k}}$ by $\delta(\varepsilon-\varepsilon_F)$ times an appropriate normalising factor. The integral over θ may be similarly evaluated by exploiting the energy conserving δ-function in $\Gamma_{\underline{k}'\underline{k}}$. The remaining sum over $\underline{Q}$ is dominated by contributions from $q_z = 0$ because of the electronic matrix element involved in $\Gamma_{\underline{k}'\underline{k}}$ via $A(\underline{Q})$ which is given in equation (5.14). When $q_z = 0$ the summand is the product of two factors: one involving $N_{\underline{Q}}^{o}$ which has a peak at the "dominant phonon wave number"[6]

$$q_D \simeq 4.96\, k_B T/\hbar v_s \qquad (5.38a)$$

and one involving the availability of final electron states which diverges when $q \simeq 2k_F$. The peak in the theoretical curves is at the temperature T_D at which

$$q_D = 2k_F \qquad (5.38b)$$

This relationship shows that q_D is proportional to $n^{-\frac{1}{2}}$, as is

observed, and is accurately followed by the peaks in the data when an appropriate average value of v_s is used[6].

The curves are calculated using Fang and Howard wavefunctions[5,28], deformation potentials E_u = 9 eV and E_d = -6 eV[5], phonon velocities $v_T = 5.5 \times 10^3$ m s^{-1} and $v_L = 8.8 \times 10^3$ m s^{-1}[6] and effective masses $m^* = 0.19\, m_o$ in the xy plane and $m_z^* = 0.916\, m_o$ in the z-direction where m_o is the free electron mass[5]. They are in excellent agreement with the data except when T ~ 1K when electron diffusion thermopower may be expected to dominate (see Section 4.3). The sign change observed for the largest value of n (labelled f in Figure 19) is believed to be due to the predominance of electron scattering by interface roughness which makes $\sigma'(\varepsilon_F)$ negative at high n so that the electron diffusion thermopower in equation (3.9a) becomes positive[6,31].

Lyo points out that the contribution of piezoelectric scattering to S_g is about the same as that of deformation potential scattering in GaAs/AlGaAs heterojunctions[29]. In Figure 21 we compare recent calculations[30] with experimental data on S_g due to Ruf et al[32]. The calculated curves (full lines) allow for the inelasticity of electron-phonon scattering (which is neglected, by Lyo) and assume that the momentum relaxation time of the electrons is proportional to ε^p with p = 0, 1 or 2. The corresponding value of electron diffusion thermopower has been subtracted from the observed values to obtain the experimental curves (dashed lines). The numbers on the curves give the value of p. The calculations are made with standard parameters for GaAs[5], E_1 = 16 eV and $v_s\tau_p = 0.14$ mm which is close to the value

determined from thermal conductivity data. In Figure 22 we compare curves calculated with p = 1 (chain line) with the data of Fletcher et al[33] corrected for electron diffusion thermopower (broken curve). The full curve is calculated on the assumption that electron-phonon scattering is elastic to assess the error involved in doing so. It is not very large. The theoretical curves is drawn for E_1 = 9.3 eV and $v_s\tau_p$ = 0.30 mm which is close to the mean free path estimated by Fletcher et al[33] and Lyo[29]. Taking E_1 = 16.0 eV, as was done in Figure 21 would require us to put $v_s\tau_p$ = 0.1 mm to obtain as good a fit between theory and experiment in Figure 22. This value of $v_s\tau_p$ is too small to be reasonable. Values of E_1 between 7 and 16 eV are quoted in recent papers[30]. New experiments on bulk GaAs designed to remove this large uncertainty would be useful.

The diagonal component of the phonon drag thermopower tensor of a 2DEG in a transverse magnetic induction field B has been evaluated by Kubakaddi et al in the quantum limit[34]. We show their results for a GaAs/AlGaAs heterojunction when B = 15T and T = 6K in Figure 23. Curve 1 is for piezoelectric scattering alone, curve 2 is for deformation potential scattering alone and curve 3 is for the realistic situation in which both scattering mechanisms are present. Standard parameters are assumed for GaAs[5] with E_1 = 11.5 eV and $v_s\tau_p$ = 0.3 mm which is close to the value estimated in the experiments[33]. Screening is ignored and a Lorentz line shape is assumed for the ground Landau subband with a half-width γ of 1.12 meV chosen to fit the data points. Similar agreement in a screened calculation may be achieved by reducing γ. In a screened calculation Lyo finds that good

agreement can be achieved with the oscillations seen at lower magnetic induction fields by making realistic phenomenological assumptions about the overall density of states[35].

6. Quantum Corrections to the Boltzmann Transport Formalism

6.1 Introduction

Most of our preceding discussioon has been in terms of the Boltzmann transport formalism. An exception was the approximate treatment of level broadening in Sections 4.2 and 4.3. In this Section we turn to more exotic quantum-mechanical corrections to the predictions of semi-classical theory. In Section 6.2 exact formulae are derived for the scalar transport coefficients of an isotropic 2DEG in zero magnetic induction field. The formulae are used to verify the assumption made in Section 4.3 that they may be put in the form of equation (3.7). In Section 6.3 we give exact Kubo formulae for the tensor transport coefficients of a 2DEG when $\underline{B} \neq 0$. They are used in Section 6.4 to discuss Onsager symmetry.[2] Section 6.5 is devoted to "weak localisation" corrections to the transport coefficients which are due to coherent back scattering.[36] Finally, in Section 6.6 we discuss the "universal fluctuations" which arise in specimens which are so small that they do not self-average, i.e. they are mesoscopic.[37]

Sections 6.2 and 6.4 are necessarily rather formal. To keep the formalism as simple as possible we ignore phonons altogether and suppose that the electrons are scattered by randomly located static impurities.

6.2 Kubo-Greenwood Formulae when $\underline{B} = 0$[38, 39]

An exact quantum-mechanical formula for the dc electrical conductivity σ may be derived by treating σ as the dc limit of the real part, $\mathrm{Re}[\sigma(\omega)]$, of the ac conductivity $\sigma(\omega)$. The latter is easily related to the power absorbed from an ac electric field which may be evaluated quantum- mechanically.

Thus, let us suppose that a uniform ac electric field

$$E(t) = \mathrm{Re}\,[E_0 e^{i\omega t}] \tag{6.1}$$

is established in the x direction in the plane of a 2DEG with effective mass m^* and area A. Then the x component of the 2D current density is

$$J(t) = \mathrm{Re}[\sigma(\omega)E_0 e^{i\omega t}] \tag{6.2}$$

and the power absorbed per unit area is given by the time average of E(t)J(t), i.e. :

$$P(\omega) = \mathrm{Re}\,\sigma(\omega)\,|E_0|^2 / 2 \tag{6.3}$$

To write down a quantum-mechanical formula for $P(\omega)$ we concentrate on the electrons with one spin orientation and label the one-electron orbital energy eigenfunctions with Greek letters: λ, μ etc. (These states are understood to include the effect of the random scatterers.) The ac field can only induce a transition from state λ to state μ if λ is full and μ is empty. The probability that this is so in thermal equilibrium is $f_0(\epsilon_\lambda)[1 - f_0(\epsilon_\mu)]$ where f_0 is the Fermi-Dirac function. Let $R_{\lambda\mu}$ denote the transition rate from a full state λ with enegy ϵ_λ an empty state μ with energy ϵ_μ. Then

$$P(\omega) = (2/A)\sum_{\lambda}\sum_{\mu} R_{\lambda\mu}\, f_0(\epsilon_\lambda)\,[1 - f_0(\epsilon_\mu)]\,(\epsilon_\mu - \epsilon_\lambda) \tag{6.4}$$

where the factor of 2 allows for the 2 possible spin orientations.

A comparison of equations (6.3) and (6.4) shows that the dc conductivity is given by

$$\sigma = \lim_{\omega \to 0} (4/A|E_0|^2) \sum_{\lambda} \sum_{\mu} R_{\lambda\mu} f_0(\epsilon_\lambda)[1 - f_0(\epsilon_\mu)](\epsilon_\mu - \epsilon_\lambda) \qquad (6.5)$$

This equation is exact. It is identical to the more sophisticated Kubo-Greenwood and Kubo formulae [2, 39 - 42] which we discuss here and in the next Section.

We may conveniently write $E(t) = -\partial a(t)/\partial t$ where

$$a(t) = \mathrm{Re}[-(E_0/i\omega)\, e^{i\omega t}] \qquad (6.6)$$

is the x component of a vector potential $\underline{A} = [a(t), 0, 0]$. The Hamiltonian for an electron in the ac field may then be expressed in the form

$$H = (\underline{p} + e\,\underline{A})^2/2m^* + V \qquad (6.7)$$

where V is a function of x, y and z which includes the confining potential as well as the potentials of the random scatterers. For small field strengths we may linearise H as follows

$$H \simeq H_0 - ja(t) \qquad (6.8)$$

where $j = -ep_x/m^*$ is the x component of the current operator $-e\underline{p}/m^*$ and $H_0 = \underline{p}^2/2m^* + V$. In deriving equation (6.8) we have used the fact that a(t) is spatially uniform. Fermi's golden rule for $R_{\lambda\mu}$ is

$$R_{\lambda\mu} = (2\pi/\hbar)|\langle\mu|j|\lambda\rangle|^2 (E_0/2\omega)^2 \times [\delta(\epsilon_\mu - \epsilon_\lambda - \hbar\omega) + \delta(\epsilon_\mu - \epsilon_\lambda + \hbar\omega)] \qquad (6.9)$$

in which the first and second δ-functions account for photon absorption and emission respectively.

When equation (6.9) is used in equation (6.5) it is convenient to interchange λ and μ in the term associated with the second δ-function. We find that the product $f_0(\epsilon_\mu)\, f_0(\epsilon_\mu)$ cancels out to leave

$$\sigma = \lim_{\omega \to 0} (2\pi/A\hbar\omega^2) \sum_{\lambda} \sum_{\mu} [f_0(\epsilon_\lambda) - f_0(\epsilon_\mu)]$$

$$\times (\epsilon_\mu - \epsilon_\lambda)\,|\langle\mu|j|\lambda\rangle|^2\, \delta(\epsilon_\mu - \epsilon_\lambda - \hbar\omega)$$

$$= (\hbar/A) \sum_{\lambda} \sum_{\mu} f_0'(\epsilon_\lambda)\,|\langle\mu|j|\lambda\rangle|^2\, \delta(\epsilon_\mu - \epsilon_\lambda) \qquad (6.10)$$

In the second line of equation (6.10) we have used the energy conservation condition $\epsilon_\mu = \epsilon_\lambda + \hbar\omega$ which allows us to write the limit of $[f_0(\epsilon_\lambda) - f_0(\epsilon_\lambda + \hbar\omega)]/\hbar\omega$ when $\omega \to 0$ as minus the derivative, $f_0'(\epsilon_\lambda)$, of the Fermi-Dirac function. We may formally rewrite equation (6.10) as

$$\sigma = -\int f_0'(\epsilon)\, \sigma(\epsilon) \qquad (6.11)$$

where

$$\sigma(\epsilon) = (\hbar/A) \sum_{\lambda} \sum_{\mu} |\langle\mu|j|\lambda\rangle|^2\, \delta(\epsilon - \epsilon_\mu)\, \delta(\epsilon - \epsilon_\lambda) \qquad (6.12)$$

This is the Kubo-Greenwood formula for the dc conductivity at 0K when the Fermi level is at ϵ.[39, 41] To calculate σ at temperature T we must take the thermal average of σ(ϵ) in accordance with equation (6.11). We see by inspection that equation (6.11) is identical in structure to equation (3.7a). Thus, the assertion made in Section 4.3 that equation (3.7a) has validity

outside the semiclassical domain is justified.

We now give a heuristic argument showing that equation (3.7c) for M is also valid when $\sigma(\epsilon)$ is given by equation (6.12). Thus, by using equation (6.11), we see that the electric current density produced by an electric field $\underline{E}$ may be written in the form

$$\underline{J} = -\int f_0'(\epsilon)\, \sigma(\epsilon)\, \underline{E}\, d\epsilon \tag{6.13}$$

Hence the contribution to the flux of charge from the energy range ϵ to $\epsilon + d\epsilon$ is just

$$\Delta\underline{J} = -f_0'(\epsilon)\, \sigma(\epsilon)\, \underline{E}\, d\epsilon \tag{6.14}$$

To calculate the corresponding contribution to the heat flux $\underline{Q}$ we have to multiply $\Delta\underline{J}$ by $-(\epsilon - \epsilon_F)/e$ because $\underline{Q}$ involve the transport of the energy (measured from the Fermi level) instead of the charge -e. When the integration is restored we obtain $\underline{Q} = M\underline{E}$ with M given by equations (3.7c) and (6.12).

It remains for us to show that equation (3.7b) for L and equation (3.7d) for N also have validity outside the semiclassical domain. This is more difficult than was the case for σ and M because L and N describe the response of the 2DEG to a temperature gradient which cannot be included in a Hamiltonian. A purely quantum-mechanical calculation of L and N is therefore impossible. However, we may obtain Kubo-Greenwood type formulae for them by combining the heuristic argument used to calculate M with a consideration of local equilibrium conditions. The effect of a non-uniform chemical potential (which is ignored in Section 3) may be calculated in the same way. This familiar problem provides a useful introduction to the calculation of L and N. Let us

therefore suppose that $\underline{E} = 0$ while the uniform equilibrium value ϵ_F of the chemical potential is replaced by $\epsilon_F + \mu$ where μ is a small, slowly-varying perturbation. Then the Fermi-Dirac function for state λ becomes

$$f(\epsilon_\lambda) = [\exp\{(\epsilon_\lambda - \epsilon_F - \mu)/k_BT\} + 1]^{-1} \tag{6.15}$$

The diffusion current density which flows in this case is conveniently written in the form $\sigma'\underline{\nabla}\mu/e$ where σ' remains to be determined.

When an electric field $\underline{E} = -\underline{\nabla}\phi$ is also present it produces an additional current density $\sigma\underline{E}$. To find σ' we suppose that μ is adjusted to establish thermal equilibrium in the presence of an electrostatic potential ϕ. The Fermi-Dirac function $f(\epsilon_\lambda)$ is then identical to equation (6.15) with $\mu = e\phi$. Consequently, the diffusion current density is $\sigma'\underline{\nabla}\phi = -\sigma'\underline{E}$. This must cancel out the conduction current $\sigma\underline{E}$, i.e. $\sigma\underline{E} - \sigma'\underline{E} = 0$ for all $\underline{E}$. Hence $\sigma' = \sigma$. This deceptively simple result is an expression of the Eistein relation between conduction and diffusion processes.[1] It shows that diffusion may be taken into account in the transport equations by replacing the electric field $\underline{E}$ by the emf $\underline{E} + e^{-1}\underline{\nabla}\mu$.

Let us now turn to the case in which the chemical potential has a constant value ϵ_F but the uniform equilibrium value of the temperature T is replaced by $T + \theta$ where θ is a small slowly-varying perturbation. Then $f(\epsilon_\lambda)$ is given by equation (6.15) with $\mu = 0$ and T replaced by $T + \theta$. To first order in θ we may continue to write $f(\epsilon_\lambda)$ in the form of equation (6.15) but with

$$\mu = \theta(\epsilon - \epsilon_F)/T \tag{6.16}$$

Our discussion of the diffusion current density shows that the

contribution which $\nabla\theta$ makes to $\underline{J}$ in the energy interval ϵ to $\epsilon + d\epsilon$ is given by (6.14) with $\underline{E}$ replaced by $\nabla\mu/e$ where μ is now given by equation (6.15). We therefore find, after integration, that $\underline{J} = L\nabla\theta$ with L given by equations (3.7b) and (6.12). Similarly, to calculate the heat flux produced by $\nabla\theta$ we have only to multiply the $\Delta\underline{J}$ calculated above by $-(\epsilon - \epsilon_F)/e$ and integrate. The result is $\underline{Q} = N\nabla\theta$ with N given by equations (3.7d) and (6.10). Luttinger[40] gives a more rigorous treatment of thermal transport in terms of the Kubo formalism[2, 41] which we outline in the next Section.

The Kubo-Greenwood formulae are useful because they immediately establish a connection between the quantum-mechanical and semiclassical treatment of electron transport in an isotropic 2DEG when $\underline{B} = 0$. They provide justification for our treatment of level broadening in Section 4.3. Moreover, they show that the Wiedemann-Franz law (3.9b) is valid outside the weak scattering regime.[42] An experimental verification of this law has been made recently in a 2DEG.[43] It is clear, however, that equation (6.12) is useless for actual calculations of $\sigma(\epsilon)$ because it is expressed in the energy representation and the energy eigenfunctions include the effect of the random scatterers. While we may take the scatterers into account in principle, it is impossible to do so in practice. The Kubo formulae to which we now turn have the advantage that they maybe evaluated in any convenient representation.

6.3 Kubo Formulae when $\underline{B} \neq 0$[40, 41]

When the applied static magnetic induction field $\underline{B} \neq 0$ the conductivity tensor σ in the transport equation (3.1) is a 2D tensor. It has a symmetric part which governs power absorption and may be calculated in the manner of Section 6.2. It also has an antisymmetrical part which is responsible for the Hall effect but which cancels out of the power absorption. An alternative method of calculation is therefore necessary. The simplest approach is to make a direct calculation of $\underline{J}$ when an ac electric field $\underline{E}$ is applied in an

arbitrary direction in the xy plane of a 2DEG. The same calculation in 3D has been treated by many authors (see for example, references 2, 39, 40, 41 and 44). We therefore simply state the corresponding result for a 2DEG. The ac conductivity tensor at frequency ω is given by

$$\sigma_{ab}(\omega) = (ne^2/i\omega m^*)\delta_{ab} + (2/i\omega A)\int_0^\infty e^{-i\omega t} g_{ab}(t)dt \qquad (6.17a)$$

where, with a and b denoting x and y,

$$g_{ab}(t) = (i\hbar)^{-1}\langle[j_a(t), j_b]\rangle \qquad (6.17b)$$

The angular brackets in equation (6.17b) signify a thermal average of the commutator taken with the equilibrium Fermi-Dirac operator

$$f_0(H_0) = [\exp\{(H_0 - \epsilon_F)/k_BT\} + 1]^{-1}, \qquad (6.18)$$

i.e.

$$g_{ab}(t) = (i\hbar)^{-1}\mathrm{Tr}\{f_0(H_0)[j_a(it), j_b]\} \qquad (6.19)$$

where the trace may be evaluated in <u>any</u> representation. In equation (6.17a) ω is given a small negative imaginary part to ensure that the integral converges. The dc conductivity tensor $[\sigma_{ab}]$ is the limit of $[\sigma_{ab}(\omega)]$ as $\omega \to 0$. In what follows we always give ac formulae in which the dc limit remains to be taken.

In equation (6.17b) and (6.19)

$$H_0 = (\underline{p} + e\underline{A}^0)^2/2m^* + V \qquad (6.20)$$

is the unperturbed Hamiltonian of an electron in the 2DEG. Here, :

$\underline{A}^0 = 1/2\ \underline{B} \times \underline{r}$ accounts for the applied magnetic induction field and, as usual, V includes the potential energies of the random scatterers as well as the confining potential. Moreover,

$$j_b = -e(p_b + eA_b^0)/m^* \tag{6.21a}$$

is the bth component of the current operator $\underline{j}$ in the presence of $\underline{B}$ and $j_a(t)$ is the Heisenberg operator associated with j_a :

$$j_a(t) = \exp(iH_0 t/\hbar)\ j_a \exp(-iH_0 t/\hbar). \tag{6.21b}$$

In the energy representation specified by H_0 the matrix element of $j_a(t)$ is

$$\langle \lambda |\ j_a(t)\ | \mu \rangle = \exp\{i(\epsilon_\lambda - \epsilon_\mu)\ t/\hbar\}\ \langle \lambda |\ j_a |\ \mu \rangle \tag{6.21c}$$

When this representation is used to evaluate $\sigma_{ab}(\omega)$ from equations (6.15) to (6.19) we find that

$$\sigma_{ab}(\omega) = (ne^2/i\omega m^*)\ \delta_{ab} - (2/i\omega A) \sum_\lambda \sum_\mu \langle \mu |\ j_a |\ \lambda \rangle \langle \lambda |\ j_b |\ \mu \rangle$$

$$\times [f(\epsilon_\lambda) - f(\epsilon_\mu)]/[\epsilon_\mu - \epsilon_\lambda - \hbar\omega] \tag{6.22}$$

It is not difficult to show that equation (6.22) reproduces the Kubo-Greenwood equations (6.11) and (6.12) when $\omega \to 0$ with $\underline{B} = 0$ and b = a. However, the whole point of the Kubo formula (6.17) is that the trace may be evaluated in <u>any</u> convenient representation. This flexibility helps with the evaluation of the

trace. Of course, the evaluation remains a difficult technical problem which lies outside the scope of these introducing lectures. The book by Mahan[2] gives a good description of how the problem is usually solved.

It is easy to show that the Kubo formula for M_{ab}, the ab th element of the 2D tensor which determines $\underline{Q}$ in an applied electric field, is obtained from equation (6.17) as follows. In the first term of equation (6.17a) n is replaced by -U/e where U is the energy density

$$U = (2/A) \sum_\lambda f_0(\epsilon_\lambda)\ \epsilon_\lambda \tag{6.23}$$

In equation (6.17b) $j_a(t)$ is replaced by the Heisenberg operator derived from the a th component of the heat flux operator

$$\underline{q} = 1/2[(H - \epsilon_F)\ \underline{v} + \underline{v}\ (H - \epsilon_F)] \tag{6.24}$$

where $\underline{v} = -\underline{j}/e$ is the velocity operator. The Kubo formulae for the thermal transport tensors L and N may also be derived by extending the heuristic arguments already developed when in Section 6.2. Details of several other approaches to the calculation of Kubo formulae for L and N are given by Mahan,[2] Luttinger[40] and Kubo et al.[41] The results are that L_{ab} is obtained from equation (6.17) as follows. In the first term in equation (6.17a) n is replaced by U/eT and in equation (6.17b) j_b is replaced by q_b/T. Finally : N_{ab} is obtained from equation (6.17) as follows. In equation (6.17a) n is replaced by $-W/e^2T$ where

$$W = 2/A \sum_\lambda f_0(\epsilon_\lambda)(\epsilon_\lambda - \epsilon_f)^2 \tag{6.25}$$

and in equation (6.17b) $j_a(t)$ and j_b are replaced by $q_a(t)$ and $-q_b/T$ respectively. Thus, to summarise, we have

$$M_{ab} = -(Ue/i\omega m^*)\,\delta_{ab} - (2/\hbar\omega A)\int_0^\infty e^{-i\omega t}\,\langle[q_a(t),j_b]\rangle\,dt \qquad (6.26a)$$

$$L_{ab} = (Ue/Ti\omega m^*)\,\delta_{ab} - (2/\hbar\omega AT)\int_0^\infty e^{-i\omega t}\,\langle[j_a(t),q_b]\rangle\,dt \qquad (6.26b)$$

$$N_{ab} = -(W/Ti\omega m^*)\,\delta_{ab} + (2/\hbar\omega AT)\int_0^\infty e^{-i\omega t}\,\langle[q_a(t),q_b]\rangle\,dt \qquad (6.26c)$$

where U and N are given by equations (6.23) and (6.25) respectively. It is again not difficult to verify that these equations reproduce the Kubo-Greenwood formulae when they are evaluated in the energy representation with $\underline{B} = 0$ and $a = b$.

6.4 Onsager symmetry

The tensor transport coefficients in equation (3.1) have properties which are due to the time-reversal symmetry of the underlying equations of motion.[44-46] They are :

$$\sigma_{ab}(-\underline{B}) = \sigma_{ba}(\underline{B}) \qquad (6.27a)$$

$$M_{ab}(-\underline{B}) = -TL_{ba}(\underline{B}) \qquad (6.27b)$$

$$N_{ab}(-\underline{B}) = N_{ba}(\underline{B}) \qquad (6.27c)$$

When $\underline{B} = 0$ all the tensors reduce to scalars and equations (6.27a) and (6.27c) are trivial while equation (6.27b) is identical to equation (3.7c) which we derived using Boltzmann transport theory with $\underline{B} = 0$. When $\underline{B} \neq 0$, Boltzmann transport theory also leads to the tensorial relations given in equation (6.27).[45]

To derive these equations from the Kubo formulae for the transport coefficients we simply write them down in the energy representation which is defined by the eigenvalue equation $H_0\psi_\lambda = \epsilon_\lambda\psi_\lambda$ where H_0 is given in equation (6.20). Now $\underline{p} = -i\underline{\nabla}$ and $\underline{A}_0$ is linear in $\underline{B}$. It therefore follows that ψ_λ is replaced by ψ_λ^* while ϵ_λ is unaltered when $\underline{B}$ is replaced by $-\underline{B}$. Hence the matrix elements of $\underline{j}$ and $\underline{q}$ are replaced by minus their complex conjugates under this transformation. Equations (6.27) follow immediately when we combine this result of time-reversal symmetry with the Hermitian character of $\underline{j}$ and $\underline{q}$. In particularly, equation (6.27a) is obvious by inspection of equation (6.22) for $\sigma_{ab}(\omega)$. There is no need to go to the limit $\omega \to 0$. Onsager symmetry is exhibited by the tensors defined in Section 6.3 when $\omega \neq 0$.[44]

It is often convenient to rewrite the "theoreticians" transport equations (3.1) in the "experimentalists" form which is given in equations (3.2). When $\underline{B} \neq 0$ the resistivity ρ, thermopower S, Peltier coefficient π and thermal conductivity κ in these equations are all 2D tensors. They are related to the coefficient in equations (3.1) by

$$\rho = \sigma^{-1} \qquad (6.28a)$$

$$S = -\sigma^{-1}L \qquad (6.28b)$$

$$\pi = M\sigma^{-1} \qquad (6.28c)$$

$$\kappa = M\sigma^{-1}L - N \qquad (6.28d)$$

The Onsager symmetry relations given in equation (6.27) imply that the tensor

coefficients in equations (3.2) have the corresponding symmetry properties

$$\rho_{ab}(-\underline{B}) = \rho_{ba}(\underline{B}) \tag{6.29a}$$

$$\pi_{ab}(-\underline{B}) = \pi_{ba}(\underline{B}) \tag{6.29b}$$

$$\kappa_{ab}(-\underline{B}) = \kappa_{ab}(\underline{B}) \tag{6.29c}$$

6.5 Weak Localisation Corrections to the Conductivity

When $\underline{B} = 0$ the ac conductivity $\sigma(\omega)$ of a 2DEG is a scalar. We know from linear response theory that

$$\sigma(\omega) = \int_0^\infty \gamma(t)\, e^{-i\omega t}\, dt \tag{6.30}$$

where $\gamma(t)$ is the impulse response function.[2] Hence the dc conductivity $\sigma = \sigma(0)$ is simply the area under the $\gamma(t)$ curve. Unfortunately, the only property of $\gamma(t)$ which is easy to calculate is its initial value. When an electron is subjected to an electric field $\delta(t)$ in the x direction it aquires a velocity $-e/m^*$. Hence the initial current density is $\gamma(0) = -en(-e/m^*) = ne^2/m^*$ where n is the electron density. We have used a classical argument to derive this result but the Kubo formula (6.17) may be manipulated to show the same thing.

To determine σ we also need to know the shape of the $\gamma(t)$ curve. It is clear on general physical grounds that $\gamma(t)$ decays to zero as $t \to \infty$. For the want of anything better, let us assume exponential decay with a time constant τ. Then we have, when $t > 0$,

$$\gamma(t) = (ne^2/m^*)\exp(-t/\tau) \tag{6.31}$$

so that $\sigma = ne^2\tau/m^*$. This is just equation (3.8) for a single subband which we derived in Section 3.3 in a much more complicated way by using Boltzmann transport theory. There we identified τ with the relaxation time due to elastic scattering of the electrons. We may continue to do so here. It is perhaps also worthwhile to point out that equations (6.30) and (6.31) with $\omega \neq 0$ yields the familiar Drude formula[1]

$$\sigma(\omega) = \sigma(0)/(1 + i\omega\tau) \tag{6.32}$$

which describes the ac behaviour of many weakly scattered free electron systems very well.

Over the last three decades there has been a growing realised that there is a small departure from equation (6.31) which has a simple physical origin and which can be both calculated and measured. This is the "weak localisation correction" to the conductivity which we discuss briefly here. Extensive reviews have been given by Bergmann[36] and Lee and Ramakrishnan.[47]

The name "weak localisation correction" is derived from the idea, originally due to Anderson[48], that interference effects can completely localise the electron wave functions in a strongly disordered system. Most transport experiments are concerned with systems which are only weakly disordered. In that case Boltzmann transport theory gives the main contribution to σ. However, interference effects between multiple scattering paths (which are ignored in Boltzmann's equation) make a small, negative, "weak localisation correction" to σ when $\underline{B} = 0$ which we denote by $\Delta\sigma_{WL}$.

To see how this comes about let us consider a scattering process when $\underline{B} = 0$ in which an electron starts from a state with wave vector $\underline{k}$ and finishes in a state with wave vector $-\underline{k}$ after passing elastically through N intermediate states with wave vectors $\underline{k}_1, \underline{k}_2, \cdots \underline{k}_N$. This process is illustrated by the

arrows in the upper half of Figure 24 for the case N = 3. The contribution that it makes to the amplitude of state $-\underline{k}$ after some time interval t is determined by the following product of matrix elements of the scattering potential V :

$$A = \langle -\underline{k} | V | \underline{k}_N \rangle \langle \underline{k}_N | V | \underline{k}_{N-1} \rangle \cdots \langle \underline{k}_2 | V | \underline{k}_1 \rangle \langle \underline{k}_1 | V | \underline{k} \rangle \qquad (6.33a)$$

Let us also consider a second process in which the sequence $\underline{k}_1, \underline{k}_2, \cdots \underline{k}_N$ is replaced by $-\underline{k}_N, -\underline{k}_{N-1} \cdots, -\underline{k}_1$. This is illustrated by the arrows in the lower half of Fig. 24. For the second process , A is replaced by

$$A' = \langle -\underline{k} | V | -\underline{k}_1 \rangle \langle -\underline{k}_1 | V | \underline{k}_2 \rangle \cdots \langle -\underline{k}_{N-1} | V | -\underline{k}_N \rangle \langle -\underline{k}_N | V | \underline{k} \rangle \qquad (6.33b)$$

Now, the states $|\underline{k}_i\rangle$ in equation (6.33) are plane wave states and V is real. We therefore see by inspection that A′ and A are identical in both amplitude and phase.

These two processes therefore contribute coherently to the back scattering for all $\underline{k}_1, \underline{k}_2 \cdots \underline{k}_N$. Consequently, the back scattering rate is larger than is assumed in Boltzmann transport theory and, since back scattering destroys momentum, $\gamma(t)$ falls below the Boltzmann transport value given in equation (6.31) as illustrated in Figure 25. The positive full curve shows the Boltzmann approximation to $\gamma(t)$ and the negative dashed curve is a greatly exagerated sketch of the weak localisation correction which we denote by $\gamma_{WL}(t)$. It has the dimensions of conductance over time. Detailed calculations show that it also has a universal form in a 2DEG :

$$\gamma_{WL}(t) = -e^2/\pi\hbar t \qquad (6.34)$$

when $\tau < t < \tau_i$ where τ_i is the relaxation time due to inelastic collisions.[36, 47] Outside this time range $\gamma_{WL}(t)$ is negligible. For $t < \tau$ this comes about because the Boltzmann transport approximation to $\gamma(t)$ already gives the correct value of $\gamma(0)$. For $t > \tau_i$ it comes about because inelastic collisions (which we have previously ignored) are phase randomising and therefore destroy the coherent back scattering. Hence, to obtain the weak localisation correction to σ we have only to integrate $\gamma_{WL}(t)$ in equation (6.34) between the time cut-offs τ and τ_i. Thus we obtain

$$\sigma_{WL} = -(e^2/\pi\hbar) \ln(\tau_i/\tau) \qquad (6.35)$$

Equation (6.35) gives σ_{WL} in a 2DEG. The weak localisation correction to σ takes different forms in 3D and 1D.[47] The transition in the behaviour of σ_{WL} from 2D → 3D and from 2D → 1D is treated by Cantrell and Butcher[49] and Kearney and Butcher.[50] The latter authors also discuss weak lacalisation corrects to the thermal and thermoelectric transport coefficients which arise inevitably at low temperatures because these quantities are determined by the conductivity through relations of the type given in equation (3.7).[42]

Most experimental work has been concerned with σ_{WL} in 2D. At liquid helium temperatures τ is constant and $\tau_i \propto T^{-p}$ with $p \sim 1 - 2$.[51] Consequently, weak localisation produces a logarithmic reduction of σ which increases with decreasing T. In Figure 26 we give resistance data showing behaviour of this type.[51] We would also expect to find that σ increases in a magnetic induction field because that will remove the time reversal symmetry and consequently destroy the phase coherence which is responsible for σ_{WL}. In Figure 27 we give negative magnetoresistance data for a Si MOSFET with the

expected behaviour.[51] Spin-orbit coupling also modifies the coherent back scattering in a way which is well understood both theoretically and experimentally.[36]

6.6 Universal Fluctuations

Macroscopic conductors always differ from one another microscopically. We usually choose to measure physical quantities which are insensitive to the microscopic differences. Moreover, in theoretical calculations, it is traditional to remove microscopic fluctuations by taking an average over an appropriate ensemble of systems which are identical macroscopically although different microscopically. Experiments are usually carried out on one sample. However, provided the sample is large enough, it may be regarded as constituting an ensemble of smaller (but still macroscopic) samples in which "self-averaging" occurs.

The above point of view has been the standard one in electron transport physics until very recently. The rapidly diminishing size of electronic microstructures has now made it untenable in many cases at liquid helium temperatures. Conductance measurements , for example, often exhibit reproducible, sample-specific, fluctuations when a parameter like the strength B of the magnetic induction field is varied. We show two examples in Figure 28 which is taken from a recent review of universal fluctuations by Stone.[52] The left-hand and centre curves show results for an 0.8μm diameter gold ring[53] and a quasi-1D Si MOSFET[54] respectively. The fluctuations produced by changing B reflect the changes induced in the phases of the one-electron wave functions for the specific distribution of static scatterers present in the experimental samples. To make the fluctuations show up it is necessary to cool the specimen until the sample length L is in the order of or less than the distance $L_i = (D\tau_i)^{1/2}$ which an electron at the Fermi

level ϵ_F diffuses in the mean free time τ_i between inelastic scattering events. Here D is the diffusion constant. It evolves the mean free time τ between elastic scattering events (which are overwhelmingly more numerous than inelastic scattering events, and is given by equation (3.11) with $\epsilon = \epsilon_F$. Inelastic collisions are phase randomising because they involve the excitation of another system (e.g. phonons) with an uncontrolled phase. The condition $L \lesssim L_i$ ensures that phase randomisation is unimportant. In the opposite extreme, when $L >> L_i$, the inelastic collisions have a self-average effect which destroys the fluctuations and bring back conventional macroscopic behaviour. Specimiens whose dimensions lie between L_i (which marks the beginning of macroscopic behaviour) and atomic length scales (which guarantee microscopic behaviour) are called mesoscopic.[37]

Conductance fluctuations had been observed in small systems for many years before their origin was appreciated. They are much more interesting than might have been supposed because, in mesoscopic systems, they have a universal character. The rms deviation ΔG of the conductance G is in the order of e^2/h. We see by inspection that this is so for the experimental curves in Figure 28. The result was originally discovered in numerical calculations made by Stone.[55] We show one of his curves on the right in Figure 28. It has since been confirmed by Lee, Stone and Fukayama[56] in an analytical treatment of the statistical behaviour of G when the distribution of static scatterers is changed. These authors also verify numerically their "ergodic hypothesis" that ΔG is independent of what is varied in a mesoscopic system : the distribution of static scatterers, B or ϵ_F. Calculations of the fluctuations of G for all three cases are shown in Figure 29 which is taken from reference 56. The ergodic hypothesis is important because it allows the results of the analytical theory (in which the distribution of static scatterers is varied) to be

used to interpret experiments (in which either B or ϵ_F is varied). Lee et al also give the energy scale ϵ_c on which the fluctuations of G are correlated when ϵ_F is varied as in the right-hand diagram of Figure 29. It is essentially determined via the uncertainty principle by the time that an electron at the Fermi level takes to diffuse across the conductor : $\epsilon_c = \hbar\pi^2 D/L^2$.

Universal fluctuations and weak localisation corrections have the same origin; the phase coherence of the one-electron wave function in the elastic scattering regime. The relationship of the other transport coefficients to conductivity through equations (3.7) means that both effects should also occur in themopower and thermal conductivity. We drew attention to that in Section 6.5 in the case of weak localisation. However, no relevent experimental data has been reported at the time of writing. Thermopower fluctuations have been discussed by Esposito et al,[57] using an approach similar to that of Lee et al,[56] and by Kearney[58] who replaces $\sigma(\epsilon)$ by a model conductance function $G(\epsilon)$ in equations (3.7). The model function is shown in Figure 30. It has a mean value of $6e^2/h$ and $\Delta\epsilon = 60\mu eV$ which is appropriate to a sample with L = $1\mu m$ and $D = 10^{-2} m^2 s^{-1}$. A naive application of the low-temperature equation (3.9a) with this $G(\epsilon)$ indicates that the thermopower will fluctuate about zero. In Figure 31 we show the results of detailed evaluation of the integrals in equation (3.7) when T = 60mK (i.e. $k_B T \sim 0{\cdot}1\epsilon_c$). Strong fluctuations about zero are exhibited. Kearney shows that they are smoothed out by thermal broadening when $T \sim 0{\cdot}3K$ (i.e. $k_B T \sim 0{\cdot}5\epsilon_c$).

We lay stress here on thermopower fluctuations because the first observations of them have recently been reported for GaAs wires.[59] Typical plots of the thermoelectric voltage fluctuations as B varies are shown in Figure 32. The temperature gradient is zero for trace A and increases for trace B and again for trace C. The latter two traces have been offset by $4\mu V$

trace B and again for trace C. The latter two traces have been offset by $4\mu V$ and $7\mu V$ respectively for clarity. The fluctuations about zero which are to be expected on the basis of the above discussion and the ergodic hypothesis are clearly demonstrated. The magnitude of the fluctuations is in reasonably good agreement with the theory of Esposito et al.[57, 59]

7 Thermal and Electrical Transport Formalism for Electronic Microstructures with Many Terminals

7.1 Introduction

In 1957 Landauer [60] proposed a formula for the electrical conductance of a two-terminal electron system. This has been expressed by Buttiker [4] in a way which is convenient for a many-terminal system of the type shown in Figure 33. The Buttiker formalism directly relates the conductance matrix G to the electron scattering matrix S. The formalism has been useful for the interpretation of experiments on low-dimensional systems relating to universal fluctuations [52,55], Aharanov-Bohm oscillations [53], ballistic transport [61-63], the integer quantum Hall effect [64] and its quenching at low magnetic fields [65-67].

In this section we derive the Landauer-Buttiker formula for G. We also derive corresponding formulae for the thermal and thermoelectric transport matrices which are associated with a multi-terminal microstructure [68]. They are the terminal analogues of the local tensors describing thermopower, Peltier effect and thermal conductivity in bulk solids which are discussed in Sections 3.1, 6.3 and 6.4. In the macroscopic regime the local tensors determine the corresponding matrices via the solution of macroscopic conservation equations with appropriate boundary conditions. In the mesoscopic and ballistic regimes this is no longer the case. The thermal and thermoelectric transport matrices are controlled by Schrodinger's equation and, like G, they may be directly expressed in terms of S.

Universal fluctuations of thermopower have recently been measured [59]. That apart, there is no current experimental data on the thermal and thermoelectric transport matrices of mesoscopic and

ballistic systems. Nevertheless, interesting and challenging experiments are easily envisaged and several authors have discussed the theory of thermal and thermoelectric transport in microstructures. Sivan and Imry [69] relate the fluxes of charge and heat in the terminals to chemical potentials and temperatures which are also measured in the terminals in a particular way. Esposito et al [57] discuss universal fluctuations of thermopower. Kearney and Butcher [42] comment on that problem and they also discuss the analogue of the Wiedemann-Franz law. Finally, Streda [70] outlines a calculation of the thermopower of a quantum point contact. These discussions are all restricted to two-terminal microstructures in zero applied magnetic induction field.

We present here a general formalism in which all the transport matrices are expressed in terms of S for a microstructure with any number of terminals which is subjected to an applied magnetic induction field. To do so we relate the fluxes of charge and heat in the terminals to chemical potentials and temperatures in the resevoirs feeding the terminals. Buttiker has stressed the overall utility of proceeding in this way in the case of electrical measurements [4]. His arguments are easily extended to thermal and thermoelectric measurements. The resulting formalism may be used to interpret experiments in which chemical potentials and temperatures are measured in the resevoirs. It may also be used to interpret experiments in which these quantities are measured in the terminals provided that the measurement procedures are defined. The results of Sivan and Imry [69], for example, may be recovered by using their definitions.

In Section 7.2 we outline the salient properties of the electron energy eigenstates in the terminals when a uniform magnetic induction field is present. The scattering matrix is discussed briefly in Section 7.3. With these preliminaries out of the way, the many-terminal transport relations for a microstructure containing non-interacting electrons are easily written down in Section 7.4. We initially give them in a nonlinear form which relates the fluxes of charge and heat in the terminals to the chemical potentials and temperatures in the resevoirs. Then we linearise the equations by assuming small departures from equilibrium. The formulae for the transport matrices in the linearised equations are given both exactly and as low temperature approximations which are particularly simple and instructive.

In the general linear analysis it is convenient to use the changes of the chemical potentials and temperatures in all the resevoirs as independent variables. However, the fluxes are all controlled by differences between these quantities and the total fluxes of charge and heat into the microstructure both vanish. In Section 7.5 we use these observations to simplify the terminal relations. The simplified equations have the advantage that it is possible to invert them so as to use the charge fluxes in the terminals as independent variables instead of the changes of the chemical potentials in the resevoirs. This is analogous to what is usually done in bulk solids (see equation (3.2)). In Section 7.6 we discuss Onsager symmetry and reciprocity in electrical, thermal and thermoelectric configurations.

The analysis developed here is, for the most part, relatively new[68]. It is consequently rather more formal than is the case elsewhere in these lecture notes. Simple applications are given in Section 8 which will fill out the bare bones of the analysis.

7.2 The electron states in the terminals

We follow Buttiker [4] and suppose that free electrons with effective mass m^* enter the microstructure through ideal terminals in the form of long, straight electron waveguides. To discuss the energy eigenfunctions in a particular terminal it is convenient to introduce a local Cartesian coordinate system, Oxyz, with Oz parallel to the axis of the terminal and z increasing towards the microstructure. (In the present context this convention is more convenient than taking Oz parallel to a direction of confinement as we did in Section 2). The one-electron Hamiltonian is given by

$$H = \frac{1}{2m^*} (\underline{p} + e \underline{A}^o)^2 + V(x,y) \qquad (7.1)$$

where $\underline{A}^o$ is the vector potential and $V(x,y)$ is the potential energy field confining the electrons in the terminal.

We suppose that the local magnetic induction field $\underline{B}$ is uniform and choose $\underline{A}^o = (-B_z y, 0, B_x y - B_y x)$ so that H does not involve z. Then the energy eigenfunctions take the

$$\psi_{\alpha k}(x,y,z) = \ell^{-1/2} \exp(ikz) \phi_{\alpha k}(x,y) \qquad (7.2a)$$

with energies

$$\varepsilon_{\alpha k} = E_\alpha(k) + \hbar^2 k^2 / 2m^*. \qquad (7.2b)$$

In equation (7.2a) ℓ is the length of the terminal considered and α labels the normalised transverse eigenfunctions $\phi_{\alpha k}(x,y)$. These are determined, together with the transverse energies $E_\alpha(k)$, by the 2D Schrodinger equation

$$H\phi_{\alpha k}(x,y) = \varepsilon_{\alpha k} \phi_{\alpha k}(x,y) \qquad (7.3)$$

in which $p_z = \hbar k$.

To quantise k we introduce periodic boundary conditions over the terminal length ℓ. Then we may verify that the diagonal matrix element $\langle\alpha k|v_z|\alpha k\rangle$ of the longitudinal velocity operator $v_z = (p_z+eA_z)/m^*$ is equal to the group velocity $v_{\alpha k} = \hbar^{-1}d\varepsilon_{\alpha k}/dk$ (cf reference 45). Moreover, the density of states $N_{\alpha k}$ per unit energy range per unit length of the terminal is $N_{\alpha k} = [\pi d\varepsilon_{\alpha k}/dk]^{-1}$ where we have included a factor of 2 to allow for spin degeneracy. Hence

$$N_{\alpha k}\langle\alpha k|v_z|\alpha k\rangle = 2h^{-1} \qquad (7.4)$$

The elegance of the Landauer-Buttiker formalism is due to this simple fundamental result.

In the above discussion we use a particular gauge to make the treatment transparent. However, the essential results are all gauge invariant. Thus, suppose that we change to a new gauge in which the vector potential becomes $\underline{A}^o = \underline{A}^o + \underline{\nabla}\chi$. Then $\psi_{\alpha k}$ is replaced by $\psi_{\alpha k}$ exp $(-ie\chi/\hbar)$ and α and k may still be used to label the eigenfunctions. It is, therefore, easy to verify that $\varepsilon_{\alpha k}$, $N_{\alpha k}$, the diagonal matrix element of the longitudinal velocity operator and the fundamental result (7.4) remain the same in the new gauge.

7.3 The scattering matrix

The terminal transport relationships all involve the scattering matrix S evaluated at some value ε of the one-electron energy. In this Section we outline the definition of S and discuss its symmetry properties.

The case in which $\underline{B} \to 0$ in the terminals is well known [4]. Then $E_\alpha(k) = E_\alpha$ which is independent of k. We see from equation (7.2b) that the channels (i.e. eigenfunctions) with $E_\alpha > \varepsilon$ are evanescent and decay to zero away from the microstructure. In the asymptotic regions of the terminals we are concerned only

with the propagating channels with $E_\alpha < \varepsilon$. Equation (7.2b) determines $|k|$ for each propagating mode and we may identify an incident wave with $k = |k|$ and $v_{\alpha k} = h|k|/m^*$ and a reflected wave for which both these quantities are negated. The general case in which $\underline{B} \neq 0$ in the terminals is similar but more complicated because $E_\alpha(k)$ in equation (7.2b) depends on k in a way which involves the detailed structure of the terminals. Nevertheless, there are still evanescent channels which may be ignored and propagating channels with incident and reflected waves for which we write $k = k_i$ and $k = k_r$ respectively. They are distinguished by the sign of $v_{\alpha k}$: $v_{\alpha k_i} > 0$ and $v_{\alpha k_r} < 0$.

In the general case it is convenient to write the wave function in the asymptotic regions of the terminals in the form:

$$\psi = \sum_\alpha [a_\alpha(\ell/v_{\alpha k_i})^{1/2}\psi_{\alpha k_i} + b_\alpha(\ell/|v_{\alpha k_r}|)^{1/2}\psi_{\alpha k_r}]. \qquad (7.5)$$

In equation (7.5) we have generalised the interpretation of α : it now labels a channel in <u>any</u> of the terminals and the sum ranges over the propagating channels in <u>all</u> the terminals. The square root factors have been introduced to give a convenient normalisation to the coefficients a_α and b_α of the incident and reflected waves. Their contributions to the longitudinal particle flux $\ell^{-1}\langle\psi|v_z|\psi\rangle$ are simply $|a_\alpha|^2$ and $-|b_\alpha|^2$ respectively.

The scattering matrix S determines the relation imposed by the microstructure between the coefficients $\underline{a} = \{a_\alpha\}$ of the incident waves and the coefficients $\underline{b} = \{b_\alpha\}$ of the reflected waves. We write the relation in the form

$$\underline{b} = S\,\underline{a} \qquad (7.6)$$

where $\underline{a}$ and $\underline{b}$ are column matrices. Since particles are conserved we must have (with the normalisation introduced above) $|\underline{b}|^2 = |\underline{a}|^2$ for

all $\underline{a}$. Hence S is unitary, i.e. $S^{-1} = S^{\dagger}$. Another important symmetry property of S follows from the time-reversal symmetry of Schrodinger's equation for the entire microstructure at energy ϵ. The Hamiltonian has the form given in equation (7.1) with $\underline{A}$ now describing the entire applied magnetic field $\underline{B}(\underline{r})$ and V(x,y) replaced by the entire potential energy field V(x,y,z). Now suppose that $\underline{B}(\underline{r})$ is reversed everywhere by changing the sign of $\underline{A}$. The new wave function for the entire system is the complex conjugate of the old one (cf. Section 6.4). Consequently, since complex conjugation interchanges incident and reflected waves, we have the time-reversal symmetry property: $S(-\underline{B}) = [S^{-1}(\underline{B})]^{*}$. Finally, when this property is combined with the unitary character of S we obtain the reciprocity relation $S(-\underline{B}) = \widetilde{S(\underline{B})}$ (4).

7.4 General Terminal Transport Relations for Microstructures

The terminal transport relations involve real quantities. The scattering matrix enters into them through the real matrix T of transmission and reflection probabilities with elements

$$T_{\alpha\beta} = |S_{\alpha\beta}|^2 \tag{7.7}$$

We see by inspection that $T_{\alpha\beta}$ is the probability that an electron incident in channel β will appear in channel α, when $\alpha \neq \beta$, or will be reflected in channel β when $\alpha = \beta$. The reciprocity relation for S which is derived at the end of Section 7.3 implies that T is transposed when the magnetic induction field is reversed, i.e.

$$T_{\alpha\beta}(-\underline{B}) = T_{\beta\alpha}(\underline{B}). \tag{7.8}$$

Moreover, the unitary nature of S may be exploited easily to show that

$$\sum_{\alpha} T_{\alpha\beta} = \sum_{\beta} T_{\alpha\beta} = 1 \tag{7.9}$$

We make extensive use of equations (7.8) and (7.9) in Sections 7.5 and 7.6.

Following Buttiker (4) and Sivan and Imry (69) we suppose that the occupation probability $f_{\alpha}(\epsilon)$ of the incident wave in channel α is given by a Fermi-Dirac function:

$$f_{\alpha}(\epsilon) = [\exp[(\epsilon - \mu_{\alpha})/k_B T_{\alpha}] + 1]^{-1} \tag{7.10}$$

where μ_{α} is the chemical potential and T_{α} is the temperature. Then the total charge flux towards the microstructure in channel α is

$$\begin{aligned} J_{\alpha} &= -e\int d\epsilon f_{\alpha}(\ell N_{\alpha k_i})(v_{\alpha k_i}/\ell) \\ &\quad + e\sum_{\beta}\int d\epsilon f_{\beta}(\ell N_{\beta k_i})(v_{\beta k_i}/\ell) T_{\alpha\beta} \\ &= -e^{-1}\sum_{\beta}\int d\epsilon f_{\beta}\Gamma_{\alpha\beta} \end{aligned} \tag{7.11a}$$

where we have used equation (7.4) and

$$\Gamma_{\alpha\beta} = \frac{2e^2}{h}(\delta_{\alpha\beta} - T_{\alpha\beta}). \tag{7.11b}$$

Similarly, to obtain the total heat flux Q_{α} flowing towards the microstructure in channel α we have only to divide J_{α} by -e and insert a factor $(\epsilon - \mu_{\alpha})$ in the integrand of equation (7.11a). Thus we obtain

$$Q_{\alpha} = e^{-2}\sum_{\beta}\int d\epsilon \Gamma_{\alpha\beta}(\epsilon - \mu_{\alpha}). \tag{7.11c}$$

In equation (7.11) it is left understood that α and β always refer to propagating channels.

To linearise equation (7.11) we put

$$\mu_{\alpha} = \epsilon_F - eV_{\alpha} \tag{7.12a}$$

and

$$T_{\alpha} = T - \theta_{\alpha} \tag{7.12b}$$

where eV_{α} and θ_{α} are small perturbations of the chemical potential and temperature in channel α from equilibrium values ϵ_F and T which are common to all channels. Then

$$f_{\alpha} \simeq f_0 + f_0'[eV_{\alpha} - \frac{\epsilon-\epsilon_F}{T}\theta_{\alpha}] \tag{7.13}$$

where f_o is given by equation (7.10) with $\mu_\alpha = \epsilon_F$ and $T_\alpha = T$ and f_o' is the energy derivative of f_o. (In contrast to the notation used in Section 6.2, we have inserted minus signs in equation (7.12) to enhance the analogy between the final transport relations for microstructures and those for bulk solids). When equation (7.13) is substituted into equation (7.11) we see that f_o makes no contribution to J_α and Q_α because of equation (7.9). Hence we obtain

$$J_\alpha = \sum_\beta [G_{\alpha\beta} V_\beta + L_{\alpha\beta} \theta_\beta], \tag{7.14a}$$

$$Q_\alpha = \sum_\beta [M_{\alpha\beta} V_\beta + N_{\alpha\beta} \theta_\beta]. \tag{7.14b}$$

where

$$G_{\alpha\beta} = -\int d\epsilon\, f_o' \Gamma_{\alpha\beta} \equiv \Gamma_{\alpha\beta}, \tag{7.15a}$$

$$L_{\alpha\beta} = -\frac{1}{eT} \int d\epsilon\, f_o' \Gamma_{\alpha\beta} (\epsilon - \epsilon_F) \equiv L_o e T \Gamma'_{\alpha\beta}, \tag{7.15b}$$

$$M_{\alpha\beta} = -T L_{\alpha\beta} = -L_o e T^2 \Gamma'_{\alpha\beta} \tag{7.15c}$$

and

$$N_{\alpha\beta} = \frac{1}{e^2 T} \int d\epsilon f'_o \Gamma_{\alpha\beta} (\epsilon - \epsilon_F)^2 = -L_o T \Gamma_{\alpha\beta} \tag{7.15d}$$

with $L_o = (\pi k_B/e)^2/3$ denoting the Lorentz number. In these equations the first formula is exact. The second formula is the leading term in a Sommerfeld expansion [71] at low temperatures in which $\Gamma_{\alpha\beta}$ and its energy derivative $\Gamma'_{\alpha\beta}$ are evaluated at $\epsilon = \epsilon_F$ (cf. Section 3.3).

7.5 Simplification of the Terminal Transport Relations for a Microstructure.

The similarity between the terminal relations (7.14) and the local relations (3.1) is obvious. However, some care is needed in developing the analogy. The Greek subscripts in equation (7.14) label propagating channels. We are more interested in terminals. Each terminal may contain several propagating channels which are all fed

from a common resevoir so that they have common values of V_β and θ_β. Moreover, only the total fluxes of charge and heat in each terminal are accessible to measurement. To allow for these facets of the microstructure problem we have only to reinterpret α and β in equation (7.14) as terminal labels and replace $\Gamma_{\alpha\beta}$ in equation (7.15) by

$$\Gamma_{\alpha\beta} \rightarrow \sum_{\alpha'\beta'} \Gamma_{\alpha'\beta'} \tag{7.16}$$

where the summation is over all propagating channels α' in terminal α and β' in terminal β. Then the terminal relations may be written as matrix equations:

$$\underline{J} = G.\underline{V} + L.\underline{\theta} \tag{7.17a}$$

$$\underline{Q} = M.\underline{V} + N.\underline{\theta} \tag{7.17b}$$

In equation (7.17), with N_t denoting the number of terminals, $\underline{J}$, $\underline{Q}$, $\underline{V}$ and $\underline{Q}$ are $N_t \times 1$ column matrices with elements J_α, Q_α, V_β and θ_β respectively. The elements of the $N_t \times N_t$ square matrices G, L, M and N are defined by equations (7.14) and (7.16).

Equations (7.17) may be further simplified because equations (7.9) and (7.15) show that the rows and columns of all the transport matrices in them sum to zero. The first property reflects the fact that $\underline{J}$ and $\underline{Q}$ are determined only by differences of the terminal voltages and temperatures. The second property reflects the fact that $\sum_\alpha J_\alpha = \sum_\alpha Q_\alpha = 0$ because of particle conservation. We are therefore free to choose terminal N_t as a reference (ground) terminal at which we set $V_{N_t} = \theta_{N_t} = 0$. Moreover, we have no need to calculate J_{N_t} and Q_{N_t} because they may be determined subsequently from J_α and Q_α in the other terminals.

To take these observations into account we have only to remove the N_tth row and column from all the matrices in equation (7.17). We leave this operation understood. The reduced form of equation (7.17) which results is closely analagous to the theoretician's form (3.1) of the local transport equations. Moreover, it has the advantage that G now has an inverse $R = G^{-1}$ so that we may rewrite the equations as

$$\underline{V} = R.\underline{J} + S.\underline{\theta} \qquad (7.18a)$$

$$\underline{Q} = \Pi.\underline{J} - \kappa.\underline{\theta} \qquad (7.18b)$$

which are the analogues of the experimentalist's form (3.2) of the local transport relations. The $(N_t-1)x(N_t-1)$ matrices R, S, Π and κ in equation (7.18) are given in terms of those in the reduced form of equation (7.17) by equations (6.28) with G and R replacing σ and ρ respectively. In equation (7.18) we use the conventional notation S for thermopower because there is no likelyhood of it ever being confused with the scattering matrix.

7. Onsager Symmetry and Reciprocity

The Onsager symmetry of the matrices in equation (7.14), in the reduced forms of equation (7.17) and in equation (7.18) are all dictated by equation (7.8). Together with equation (7.11b) this equation implies that $\Gamma_{\alpha\beta}(-\underline{B}) = \Gamma_{\beta\alpha}(\underline{B})$. Consequently, all the matrices in equations (7.14) and (7.17) are transposed when the magnetic induction field is reversed. Thus the Onsager symmetry relations (6.27a) and (6.27c) survive intact in the microstructure (with G replacing σ) while equation (6.27b) is replaced by the simpler symmetry relation $L(-\underline{B}) = \widetilde{L}(\underline{B})$. However, since equation (7.15c) implies that $M = -TL$ in the microstructure, we may (if we wish) recast this simple symmetry relation in a more complicated form which is analagous to equation (6.27b): $L(-\underline{B}) = -\widetilde{M}(\underline{B})/T$.

The Onsager symmetry relations (6.29) all survive intact in a microstructure with R replacing ρ. We note that equation (6.29b) cannot generally be simplified in a microstructure in an analagous way to equation (6.27b) because R, which replaces ρ in equation (6.29), does not commute with L and M. However, in a two-terminal network all the transport matrices in equation (7.18) reduce to scalars and we have the simple relation $\Pi = -TS$ in which both Π and S are even functions of $\underline{B}$.

Electrical reciprocity is discussed by Buttiker [4]. It rests on the Onsager symmetry relation (6.27a) with σ replaced by G. We give a simple treatment which is easily extended to deal with thermal and thermoelectric reciprocity. Thus we set $\underline{\theta} = 0$ in the reduced form of equation (7.17a). Then, we have

$$\begin{aligned}\widetilde{\underline{V}}(-\underline{B}).\underline{J}(\underline{B}) &= \widetilde{\underline{V}}.(-\underline{B}).\ G(\underline{B}).\underline{V}(\underline{B}) \\ &= \widetilde{V}(\underline{B}).\ \widetilde{G}(\underline{B}).\ V(-\underline{B}) \\ &= \widetilde{V}(\underline{B}).\ \underline{J}(-\underline{B}) \end{aligned} \qquad (7.19)$$

Here $\underline{V}(\pm\underline{B})$ is related to $\underline{J}(\pm\underline{B})$ by equation (7.17a) in magnetic induction fields $\pm\underline{B}$ with $\underline{\theta}=0$ but are otherwise arbitrary. In the second line of equation (7.19) we transpose the scalar product and in the last line we use $\widetilde{G}(\underline{B}) = G(-\underline{B})$.

Let us consider a two-terminal network. When terminal 2 is grounded equation (7.19) gives

$$V_1(-\underline{B})/J_1(-\underline{B}) = V_1(\underline{B})/J_1(\underline{B}) \qquad (7.20)$$

i.e. the two-terminal resistance is an even function of $\underline{B}$. Now consider a four-terminal network. When terminal 4 is grounded equation (7.19) gives

$$\sum_{\alpha=1}^{3} V_\alpha(-\underline{B})\, J_\alpha(\underline{B}) = \sum_{\alpha=1}^{3} V_\alpha(\underline{B}) J_\alpha(-\underline{B}) \qquad (7.21)$$

Suppose that, in the magnetic induction fields + $\underline{B}$ and - $\underline{B}$, we connect an ideal voltmeter between terminals 1 and 2 and between terminals 3 and 4 respectively. Then, for + $\underline{B}$ we have $J_1(\underline{B}) = J_2(\underline{B}) = 0$ and for $-\underline{B}$ we have $J_3(-\underline{B}) = J_4(-\underline{B}) = 0$ so that charge conservation gives $J_2(\underline{B}) = - J_1(-\underline{B})$. Hence equation (7.21) reduces to

$$\frac{V_3(-\underline{B})}{J_1(-\underline{B})} = \frac{V_1(\underline{B}) - V_2(\underline{B})}{J_3(\underline{B})} \qquad (7.22)$$

i.e.

$$R_{12,34}(-\underline{B}) = R_{34,12}(\underline{B}) \qquad (7.23)$$

in the notation of Buttiker [4]. Here: $R_{\alpha\beta,\gamma\delta}$ denotes a four-terminal resistance which is determined by measuring the voltage drop from γ to δ with an ideal voltmeter (which draws no current) and dividing it by a current which enters through α and leaves through β. Equation (7.23) expresses the electrical reciprocity theorem: $R_{\alpha\beta,\gamma\delta}$ is unaltered when the current source and voltmeter are interchanged provided that $\underline{B}$ is reversed [4]. It has been verified experimentally by Benoit et al[72].

Since $N(\underline{B})$ and $K(\underline{B})$ have the same Onsager symmetry as $G(\underline{B})$ we may immediately write down analagous reciprocity relations for thermal "resistances" measured when $\underline{V} = 0$ or $\underline{J} = 0$ by using a heat flux source and an ideal temperature meter which draws no heat flux. Similarly, since $L(\underline{B})$ and $\underline{M}(\underline{B})$ also have the same Onsager symmetry as $G(\underline{B})$, we may also write down analagous reciprocity relations for thermoelectric "resistances" measured (when $\underline{V} = 0$) by using a current source and an ideal temperature meter which transmits no charge flux and (when $\underline{\theta}=0$) by using a heat flux source and an ideal voltmeter which transmits no heat flux. These relationships are not readily tested

experimentally. Most importantly: when $\underline{J} = 0$, which is the usual situation in thermopower measurements, no 4-terminal reciprocity exists because $S(-\underline{B}) \neq \widetilde{S(\underline{B})}$. In the two-terminal case, however, all the transport matrices, including S, reduce to scalars which are even functions of $\underline{B}$.

7.7. Conclusion

The transport relations in the general form of equation (7.14), in the reduced form of equation (7.17), or in the alternative form of equation (7.18), all give a complete description of the linear electrical, thermal and thermoelectric transport properties of a microstructure. The formulae (7.15) and (7.16) for the transport matrices are exact when the microstructure contains independent electrons which do not have any phase-breaking interactions with another system, e.g. phonons. They have the transparent simplicity which is characteristic of the Landauer-Buttiker formalism. Nevertheless, of course, evaluating the formulae is complicated when there are many terminals.

The theory developed in this Section puts the formulae for the thermal and thermoelectric matrices of a microstructure with many terminals on the same footing as those for the conductance matrix. For simplicity we have ignored spin-splitting, spin-orbit coupling and periodic crystal fields. Further development of the formalism is required to take account of these effects. The incorporation of electron-phonon coupling would greatly enhance the scope of the theory. Thermal and thermoelectric measurements on microstructures with more than two terminals present an interesting experimental challenge.

8. The Aharonov-Bohm Effect,[53, 73] Quantum Point Contacts[61-63] and the Integer Quantum Hall Effect.[64,75-78]

8.1 Introduction

The phenomena which we discuss now provide simple illustrations of the Landauer-Buttiker formalism developed in Section 7. They are simple because, for the most part, we confine our attention to two-terminal microstructures at low temperatures. The full subscript notation used in Section 7 then becomes over elaborate. The reduced form of equation (7.17a) when $\underline{\theta} = 0$ is simply $J_1 = G_{11} V_1$ because $V_2 = 0$. We use the notation G for $G_{11} = J_1/V_1$ which we may write in the form

$$G = -G_{12} = (2e^2/h) \sum_{\alpha'\beta'} T_{\alpha'\beta'} \qquad (8.1)$$

Here, in the first equality, we have used the remark following equation (17) that $G_{11} + G_{12} = 0$. The second equality then follows immediately from equations (7.11b) and (7.16). Equation (8.1) exhibits the fundamental result that, in units of $2e^2/h$, G is equal to the sum of the transmission coefficients of all the propagating channels β' in terminal 2 to all the propagating channels α' in terminal 1.

This deceptively simple equation has wide-ranging utility. It remains valid in an applied magnetic induction field. We therefore use it in Section 8.2 to discuss Aharonov-Bohm magnetoconductance oscillations. In Section 8.3 it helps us to explain the quantisation of G when $\underline{B} = 0$ in quantum point contacts for which $T_{\alpha'\beta'} = 0$ or 1. Finally, in Section 8.4 we follow Buttiker[64] and discuss the integer quantum Hall effect from the point of view of edge states for which the sum of transmission coefficients in equation (8.1) when $\underline{B}$ is large is again integral.

8.2 The Aharonov-Bohm Effect

In 1959 Aharonov and Bohm showed that the conductance of a ring oscillates as a function of the magnetic flux threaded through it.[73] Their argument is simple and we give it below. A decade and a half was to pass before the effect was seen by Washburn and Webb in the form originally predicted.[53]

In Figure 34 we show the 0·82μm diameter gold ring used by Washburn and Webb. The terminals are at the top and bottom of the ring. Electrons entering at the top divide between the left-hand side C_L and the right-hand side C_R. In the wire on either side we may write the one-electron Hamiltonian in the form

$$H = \hbar^2/2m^* [(\underline{p} + e\underline{A}^0)/\hbar]^2 + V(\underline{r}) \qquad (8.3)$$

Here, $\underline{A}^0$ describes the flux threaded through the ring and, as usual, $V(\underline{r})$ describes the confining potential and the elastic scatterers. When $\underline{A}^0$ is slowly-varying we may define a local wave number which is equal to the component of $(\underline{p} + e\underline{A}^0)/\hbar$ along the axis of the wire. Hence, threading a flux ϕ through the ring produces phase shifts

$$\theta_{L(R)} = \int_{C_{L(R)}} (e/\hbar)\, \underline{A}^0 . d\underline{r} \qquad (8.4)$$

in the wave functions of electrons going along $C_{L(R)}$. The relative phase shift between these two paths is

$$\Delta\theta = \theta_L - \theta_R = (e/\hbar) \int_{ring} \underline{A}^0 . d\underline{r} = 2\pi\phi/\phi_0 \qquad (8.5)$$

where $\phi_0 = h/e$ is the flux quantum. We see from equation (8.5) that $\Delta\theta = 2\pi m$, with m integral, when $\phi = m\phi_0$. consequently, all the transmission coefficients $T_{\alpha'\beta'}$ in equation (8.1) are periodic in ϕ with period ϕ_0.

In an attempt to observe this behaviour Sharvin and Sharvin[74] used a hollow tube of Mg with a diameter of 1μm and a length of 1cm. They saw oscillations in G but with flux period $\phi_0/2$ instead of ϕ_0. The reason for this unexpected result provides an interesting application of the theory of weak localisation corrections which is given in Section 6.5. There we set $\underline{B} = 0$ and noted that coherent back-scattering along time-reversed paths reduces the bulk conductivity of a 2DEG below the value which is predicted by Boltzmann transport theory. A similar effect occurs in ring structures. The conductance is reduced below the semi-classical value as a result of constructive interference between multiple scattering paths which return to the input via time-reversed paths going <u>right round</u> the ring in clockwise and anti-clockwise directions.

Weak localisation effects in the bulk are not washed out by system averaging when $\underline{B} = 0$ because the necessary coherence is guaranteed by time-reversal symmetry in every member of an ensemble. Similarly, the corresponding effects in a ring structure also survives system averaging provided that the flux threaded through the ring is small enough. Indeed, the theory predicts precisely what Sharvin and Sharvin observed : G oscillates with a flux period $\phi_0/2$ because <u>each</u> of the two paths involved completely encircles the flux ϕ.[53] The Aharonov-Bohm oscillations with flux period ϕ_0, on the other hand, self-average to zero in the relatively long tube used by Sharvin and Sharvin because different paths C_L and C_R are subject to random phase shifts produced by the different elastic scatterers which are encountered en route.

The wires in the ring shown in Figure 34 are made from a 38nm. thick gold film and are only 40nm. wide. These very small dimensions mean that self-averaging is suppressed and the conductance data obtained with the ring, which is shown at the top of Figure 35, exhibits oscillations with flux period ϕ_0. The Fourier spectrum at the bottom of the Figure shows weak harmonic content with period $\phi_0/2$ which may include contributions from the weak localisation effect seen by Sharvin and Sharvin.

8.3 <u>Quantum Point Contacts</u>

In Section 8.1 we define a quantum point contact to be a two-terminal electronic microstructure in which every transmission coefficient $T_{\alpha'\beta'}$ in equation (8.1) is either 0 or 1. Then G is quantised in units of $2e^2/h$. The real problem is not how to <u>define</u> a quantum point contact, it is how to <u>make</u> one. Similar solutions to the fabrication problem were presented independently in 1988 by a group in the Netherlands[61] and a group in the U.K.[62]

We show the structure used by the Netherlands group in the inset of Figure 36. It consists of 2DEG at a modulation-doped GaAs/AlGaAs heterojunction which is overlayed by a metal gate. When the gate bias V_g is negative electrons are driven away from the region underneath the gate. The two terminals of the device are the wide 2DEGS on either side of the gate. These are so broad that their resistances are unequantised and are independent of V_g. However, to get from one terminal to the other, electrons must pass through the constriction produced by the gate bias. This becomes narrower and narrower as V_g becomes more negative. Consequently fewer and fewer of the channels in the constriction can propagate at the Fermi level.

The constriction is the quantum point contact. We see from the inset that its width $w \tilde{<} 0.25\mu m$. Its length L is less well defined but, (again from the inset) $L \tilde{<} 1.0\mu m$. Both these lengths are much less than the elastic mean free

path in the 2DEG (8.5μm) and the inelastic mean free path at the temperature of the experiment (0·6K). Consequently, the electrons do not make a significant number of collisions with either impurities or phonons while traversing the constriction. Moreover, provided w varies sufficiently slowly, they do not make a significant number of collisions with the edges of the constriction either. Instead, each of the channels which can propagate at the Fermi level in the output terminal either passes through the constriction without reflection or is cut off and reflected back completely. The sum in equation (8.1) therefore reduces to the number of channels which can propagate through the constriction which decreases by one each time another channel is cut off by the progressive reduction of w. This is the origin of the staircase structure of the resistance which is shown in Figure 36. To present the data in its most illuminating form it is necessary to identify and subtract the series resistance of the terminals. The reciprocal of what remains is the conductance of the constriction which we plot against gate voltage in Figure 37. The quantisation in units of $2e^2/h$ is clearly exhibited. Similar results are reported in reference 62.

It can be objected that the assumption on which this interpretation of the data is based is possibly untenable. We have supposed that channels change adiabatically en route through the constriction and this might not be the case because of the sharp changes of width which are involved. However, Stone and Szafer[63] have made detailed calculations of G on the basis of equation (8.1) for the two structures shown at the top of Figure 38 in which spin degeneracy is ignored. In spite of a 4 : 1 change of width between the terminals and the constriction sharp quantisation is predicted.

In Section 7 we developed the Landauer-Buttiker formalism to deal with the thermal conductance κ and the thermopower S of a multi-terminal microstructure. It is interesting to apply these ideas to a quantum point contact. Both κ and S are scalars. At low temperatures κ is related to G by

the Wiedemann-Franz law $K = L_0TG$ (where L_0 is the Lorentz number) which follows immediately from equations (3.2) and (7.12). Moreover, the thermopower S is related to G by the Mott formula (3.9a) with σ replaced by G. Consequently, in a two-terminal microstructure, κ has the same staircase structure as G but with a step height of $2L_0T\,e^2/h$. Moreover the behaviour of S as a function of V_g is described by the theory of the quantum size effects in the thermopower of 2DEGS and 1DEGS which is given in Section 4.3. In a quantum point contact the normal component S_N of S vanishes because G is constant between the steps. The anomalous component S_p has a negative sign in a quantum point contact because G increases whenever ϵ_F moves through a subband minimum in the constriction. Its magnitude has the form which is sketched in Figure 9 (as a function of ϵ_F) and is calculated in detail by Cantrell and Butcher.[40] This behaviour, which remains to be confirmed experimentally. It has been treated recently by Streda.[70]

8.4 The Integer Quantum Hall Effect

When a magnetic induction field $\underline{B}$ is applied in the direction perpendicular to a 2DEG the resistivity ρ in equation (3.2) becomes a 2D tensor. The elements of the tensor are easily evaluated in semiclassical theory by taking account of the Lorentz force which $\underline{B}$ exerts on the electrons. We consider a degenerate electron gas subject to elastic scattering with a momentum relaxation time τ. Then identical results may be obtained either from Boltzmann's equation or, more simply, by solving Newton's equation of motion for the average electron velocity $\langle\underline{v}\rangle$ with a frictional force $-m^*\langle\underline{v}\rangle/\tau$ added to the electromagnetic force $-e[\underline{E} + \langle\underline{v}\rangle \times \underline{B}]$. They are

$$\rho_{zz} = \rho_{xx} = \sigma^{-1} \qquad (8.6a)$$

$$\rho_{zx} = -\rho_{xz} = \omega_c\tau/\sigma \tag{8.6b}$$

where $\omega_c = e B/m^*$ is the cyclotron resonance frequency, $\sigma = n e^2\tau/m^*$ is the conductivity when $\underline{B} = 0$ and Oxz is orientated in the plane of the 2DEG as shown in Figure 39(a).

These results are well known in 3D.[1, 17, 45, 71] They provide a good description of the behaviour of a 2DEG when $\omega_c\tau<<1$. In the opposite extreme, when $\omega_c\tau>>1$, it is necessary to take full account of the quantisation of the circular motion of the electrons in the magnetic induction field. To do so it is convenient to consider a 2DEG waveguide with width w as shown in Figure 39(a). The Cartesian axes Oxyz are oriented according to the convention adopted in Section 7.2 with Oz parallel to the axis of the guide. We are concerned with the solutions of the eigenvalue problem $H\psi = \epsilon\psi$ where the Hamiltonian H has the form given in equation (8.3). To orient $\underline{B}$ in the y direction (perpendicular to the 2DEG) we put $\underline{A}^0 = (0,0,Bx)$. To take account of the confinement of the 2DEG we make V a function of x alone which increases rapidly as the edges of the guide are approached (The confining potential in the y direction, which created the 2DEG in the first place, is irrelevant to the present discussion). To determine ψ we proceed, as in Section 7.2, to write

$$\psi = \exp(ikz)\phi_{\alpha k}(x) \tag{8.7}$$

Substitution into Schrodingers equation gives

$$[p_x^2/2m^* + (x - x_k)^2 m^*\omega_c^2/2 + V]\,\phi_{\alpha k} = \epsilon_{\alpha k}\,\phi_{\alpha k} \tag{8.8}$$

Here, $\epsilon_{\alpha k}$ is the eigenvalue associated with $\phi_{\alpha k}$ and $x_k = k\ell_M^2$ with

$\ell_M = (\hbar/m^*\omega_c)^{1/2}$ denoting the "magnetic" length.

In the interior of the 2DEG we may set V = 0 in equation (8.8). We then have Schrodinger's equation for a harmonic oscillator centred on x_k with frequency ω_c. Hence we may put $\alpha = 0, 1, 2, \cdots$, and write

$$\phi_{\alpha k} = \phi_\alpha (x - x_k) \tag{8.9a}$$

$$\epsilon_{\alpha k} = (\alpha + 1/2)\hbar\omega_c \tag{8.9b}$$

where ϕ_α is the normalised αth Harmonic oscillator wave function and $\epsilon_{\alpha k}$ is the αth Landau level. The spatial extent of $\phi_{\alpha k}$ is determined by ℓ_M which becomes much less than W' when B is large. In that case it is easy to see what happens to $\epsilon_{\alpha k}$ when x_k approaches the edges of the guide. The energy simply increases by an amount determined by the average of V taken with the weighting factor $|\phi_{\alpha k}|^2$. The dispersion curves for the propagating channels therefore have the form shown in Figure 39(b). We see that the group velocity has the same sign as k and is positive (negative) when x_k approaches the top (bottom) edge of the guide as indicated by the arrows in Figure 39(a). These are "edge states". Their importance in the integer quantum Hall effect has been emphasised most recently by Buttiker[64] who cites earlier work on the subject.

In Figure 39(b) we show a line at the Fermi level ϵ_F which lies between the third and fourth Landau levels in the bulk of the 2DEG. It cuts the dispersion curves of the edge states for $\alpha = 0, 1, 2$ at both edges. Consequently, when the Fermi level is perturbed in a resevoir on the left (right) of the electron waveguide, current will be carried only by the top

(bottom) edge states. This observation is central to understanding the integer quantum Hall effect.

To proceed further we have to write down the terminal current/voltage characteristics for a "Hall bar" with the typical geometry shown in Figure 40. To begin with we ignore electron scattering altogether. Then the edge states hug the edges of the Hall bar and propagate round smooth corners as indicated by the arrows in the Figure. This behaviour is the quantum-mechanical analogue of the classical motion of orbit centres along equipotential lines. With this picture in mind, let us consider the current J_1 flowing in terminal 1. It is carried by electrons moving to the right in the top edge states (which originate in the resevoir attached to terminal 1) and by electrons moving to the left in the bottom edge states (which originate in the resevoir attatched to terminal 6). Thus, the situation is analogous to that for a two-terminal network which we treated in Section 8.1. The analogue of equation (8.1) in the present discussion is

$$G_{11} = -G_{16} = (2e^2/h) \sum_{\alpha' \beta'} T_{\alpha' \beta'} \qquad (8.10)$$

where β' now labels a propagating channel in terminal 6 and α' labels a propagating channel in terminal 1. Moreover, since we are ignoring electron scattering, the situation is also analogous to that for a quantum point contact which we treated in Section 8.3. The sum in equation (8.10) is equal to the number, ν, of edge states which can propagate from terminal 6 to terminal 1. Thus we arrive at the current/voltage relationship for terminal 1 : $J_1 = G_\nu(V_1 - V_0)$ where $G_\nu = 2\nu e^2/h$. We may make similar arguments for each terminal. Moreover, ν is the same in every case because it is equal to the number of Landau levels which are occupied in the bulk of the 2DEG. (In Figure 39(b) : $\nu = 3$). Thus we arrive at the complete set of current/voltage relations

for the Hall bar :

$$G_\nu = J_1/(V_1 - V_6) = J_2/(V_2 - V_1) = J_3/(V_3 - V_2)$$

$$= J_4/(V_4 - V_3) = J_5/(V_5 - V_4) = J_6/(V_6 - V_5) \qquad (8.11)$$

We have derived these relations by ignoring electron scattering altogether. However, they remain valid in the presence of weak elastic scattering at low temperatures and high magnetic induction fields when ϵ_F lies between the broadened landau levels. This is because back-scattering is suppressed by the exponentially small spatial overlap of the wavefunctions of edge states at opposite edges when $\underline{B}$ is large.[64] All that elastic scattering can do is transfer electrons between adjacent edge states which has no effect on the sum in equation (8.10) because the electrons continue to move in the same direction.We may therefore make use of equations (8.11) to interpret Hall effect measurements made on a realistic Hall bar. Terminals 2, 3, 5 and 6 are conventionally used as voltage probes and carry no current. Consequently, equation (8.11) shows that $V_1 = V_2 = V_3$ and $V_4 = V_5 = V_6$. It follows that the "longitudinal" resistance

$$R_{2x} = (V_2 - V_3)/J_1 = 0 \qquad (8.12a)$$

and the "Hall" resistance

$$R_{2x} = (V_2 - V_6/J_1 = (V_1 - V_6)/J_1 = G_\nu^{-1} = h/2\nu e^2 \qquad (8.12b)$$

These results hold good while ϵ_F moves <u>between</u> the broadened Landau

levels. The degeneracy D_L of each Landau level per unit area of the 2DEG may be shown to be equal to the inter-Landau-level spacing $\hbar\omega_c$ times the density of states $m^*/\pi\hbar^2$ of the 2DEG when $\underline{B} = 0$, i.e. $D_L = eB/\pi\hbar$. Hence, when ν Landau levels are full, the classical formula (8.6b) reproduces the value for the Hall resistance given in equation (8.12b). What is remarkable about the integer quantum Hall effect is that this value is maintained with high accuracy while ϵ_F moves between Landau levels and, at the same time, $\rho_{zz} = 0$ instead of having the classical value σ^{-1}.

Quantisation of the Hall effect was first seen by von Klitzing et al by varying the gate voltage in a Si MOSFET with B held fixed.[75] We show some typical data in Figure 40.[76] The plateaus in R_{zx} are well developed and remarkably flat as shown in the inset. The additional plateau with $R_{zx} = h/3e^2$ is due to splitting of the spin and valley degeneracy of the ground subband of the 2DEG in Si which we have ignored in our discussion in the interest of simplicity. The vanishing of R_{zz} in the region of each plateau of R_{zx} is also clearly exhibited in the data. These data were soon followed by observations of the integer quantum Hall effect in a GaAs/AlGaAs heterojunction by varying B with n held fixed.[77] The subject has been reviewed by Yennie.[78] It is to be noted that classical behaviour is restored when T is raised enough or B is reduced enough to make the simultaneous partial occupancy of more than one Landau level significant. A theory which adequately describes the transition between the quantal and the classical regimes remains to be developed.

The most unexpected development in the work on heterojunctions was the observation of quantised Hall plateaus with particular fractional values of ν when the lowest Landau level is only partially occupied.[79, 80] We show some typical data in Figure 42.[81] The one electron theory developed here

has nothing to say about the fractional quantum Hall effect. It is a consequence of Coulomb interaction and will be discussed in the lectures given by d'Ambrumenil[82] and Eistenstein.[83]

9. Conclusion

We have looked at three approaches to the theoty of electron transport in low-dimensional semiconductor structures : Boltzmann transport theory, Kubo formalism and the Landauer-Buttiker formalism. The semiclassical Boltzmann equation continues to play a major role in achieving an understanding of electron transport in these systems. Its great attraction is the conceptual simplicity of the formalism and the physical insight which it provides. In addition, it is easy to include in Boltzmann's equation the many different elastic and inelastic scattering mechanisms which often play significant roles in determining the behaviour of the transport coefficients. Finally, Boltzmann transport formalism may be successfully extended to study phonon transport as well as electron transport as we discuss in Section 5.

Boltzmann transport theory is hard to beat as a tool for investigating the main features of electron transport in low-dimensional semiconductor systems. What it misses out are features depending on the phase of the electron wave function (e.g. weak localisation corrections, universal conductance fluctuations and the Aharonov-Bohm effect) or on Landau quantisation of the electron energy spectrum (the quantum Hall effect). The Kubo formalism provides a good description of all these phenomena. However, it is hard to use and provides physical insight only after a long apprenticeship in the interpretation of diagrams.(2)

An outstanding feature of the last two decades has been the shrinking size of the transport structures under experimental investigation. The behaviour of mesoscopic and ballistic structures are now very important research areas. Bulk transport coefficients are not particularly useful in these regimes. One is more concerned with terminal relationships and the Landauer-Buttiker formalism is therefore a natural medium to use. In Section 7 we outline the formalism for dealing with electrical conductivity. It will be developed in detail by Buttiker.(84) We also extend the formalism to include thermoelectric and thermal transport. The results are very simple at low temperatures. The

central quantity is the conductance matrix $G(\epsilon_F)$ of the network when the Fermi level is at ϵ_F. Numerical methods will usually be necessary to calculate $G(\epsilon_F)$ because of the complicated geometry of the structure. However, the calculation is a one-electron problem and considerable progress with it has already been made.(55, 63, 66)

Throughout these lectures we ignore the electron-electron interaction except for some attention to screening and self-consistency. Very often that is a reasonable approximation in transport calculations because the interaction conserves both total energy and total momentum. However, the electron-electron interaction plays an important role in producing corrections to the conductivity which are similar to weak localisation corrections and it dominates the fractional quantum Hall effect.(82, 83) The Kubo formalism again provides a good way to deal with the problem.(2) We have also ignored the strong localisation effects which occur in severly disordered systems and lead to transport by a hopping mechanism. They are reviewed by Fowler et al.(85) Timp. et al.(86, 87) and McInnes and Butcher(88) discuss the behaviour of hopping conductivity in 2D and 1D systems respectively and the general formalism is treated in 3D in the notes for a previous Spring College.(89)

In the last decade most experimental studies of electron transport in small structures at low temperatures have been concerned with electrical conductivity. Thermal and thermoelectric transport measurements are more difficult to make because of the very small temperature differences involved. There has been considerable progress recently in the accurate measurement of small temperature differences when the ambient temperature $T \gtrsim 1K$. Consequently, a rapid expansion of research on thermal and thermoelectric transport has already begun and can be expected to continue.

References

1. F. J. Blatt, Physics of Electronic Conduction in Solids, MaGraw Hill, New York (1986)
2. G. D. Mahan, Many-Particle Physics, Plenum Press, New York (1981)
3. R. Landauer, Conductance determined by transmission : probes and quantised constriction resistance, J. Phys.: Condens. Matter 1, 8099 - 8111 (1989)
4. M. Buttiker, Symmetry of electrical conduction, IBM J. Res. Dev. 32, 303 - 437 (1988)
5. T. Ando, A.B. Fowler and F. Stern, Electronic properties of two-dimensional systems Rev. Mod.Phys. 54, 437 - 672 (1982)
6. B. L. Gallagher, J. P. Oxley, T. Galloway, M. J. Smith and P.N. Butcher, The phonon drag and diffussion thermopower of Si inversion layers, J. Phys. : Condens. Matter 2, 755 - 761 (1990)
7. R. Clark and P. Maksym, Fractional quantum Hall effect in a spin, Phys. World, 2, 39 -44 (1989)
8. C. T. Foxon, Spring College, Trieste (1990)
9. R. Dingle, H. L. Stormer, A.C.Gossard and W. Wiegmann, Electron mobilities in modulation-doped semiconductor heterojunction superlattices, Appl. Phys. Lett. 33, 665 - 667 (1978)
10. G. Bastard, Spring College Trieste (1990)
11. T. J. Thornton, M. Pepper, H. Ahmed, D. Andrews and G.J. Davies, One - dimensional conduction in the 2D electron gas of a GaAs - AlGaAs heterojunction, Phys. Rev. Letts. 56, 1198 - 1201 (1986)
12. L. Kouwenhoven, Spring College, Trieste (1990)
13. F. Stern, Spring College, Trieste (1990)
14. W. J. Skocpol, L. D. Jackel, R. E. Howard, P. M. Mankiewich, D. M. Tennant, A. E. White and R. C. Dynes, Quantum transport in narrow MOSFET channels Surf. Sci. 170, 1 - 3 (1986)
15. M. Pepper, The metal-insulator transition in the impurity band of n-type GaAs induced by a magnetic field and loss of dimension, Phil. Mag. 37B 187 - 198 (1978)
16. A. B. Fowler, A. Harstein and R. A. Webb, Conductance in restricted dimensionality accumulation layers, Phys. Rev. Lett. 48, 196 - 199 (1982)
17. P. N. Butcher, N. H. March and M. Tosi eds., Electrons in Semiconducting Materials and Devices, Plenum Press, New York (1986)
18. D. G. Cantrell and P. N. Butcher, Lifetime, broadening of subband structure in the electrical conductivity of narrow-channel systems. J. Phys. C : Sol. St. Phys. 18, 5111 - 5125. (1985)
19. B. E. Sernelius, K. F. Berggren, M. Tomak and C. M. Fadden, Effects of quantum confinement in a special GaAs field effect transitor : on the dc conductance in the regime of metallic transport, J. Phys. C : Sol. St. Phys. 18, 225 - 240 (1985)

20. D.G. Cantrell and P.N. Butcher, The effect of subband structure on the sign of the thermopower of electrons in a quantum well, J. Phys. C: Sol. St. Phys 18, L587 - 592 (1985)

21. D. G. Cantrell and P. N. Butcher, Lifetime broadening of subband structure in the thermopower of narrow-channel systems, J. Phys. C : Sol. St. Phys 18, 6639 - 6645 (1985)

22. C. Ruf, M. A. Brummell, E. Gmelin and K. Ploog, The influence of subband structure on the thermopower of GaAs - $Al_x Ga_{1-x}$ As heterojunctions, Superlat. and Microstruct. 6, 175 - 178 (1989)

23. M. J. Kearney and P. N. Butcher, A calculation of the effect of subband structure on the thermopower of a quasi-one-dimensional wire, J. Phys. C : Sol. St. Phys. 19, 5429 - 5435 (1986)

24. M. J. Kearney and P. N. Butcher, The effect of lifetime broadening on the conductivity and thermopower of a quasi-1D wire, J. Phys. C : Sol. St. Phys. 20, 47 - 57 (1987)

25. M. J. Smith and P. N. Butcher, Simple models of phonon drag in 3D and quasi-2D, J. Phys. : Condens. Matter. 2, 2375 - 2382 (1990)

26. D. G. Cantrell and P. N. Butcher, A calculation of the phonon-drag contribution to the thermopower of quasi-2D electrons coupled to 3D phonons : I. General theory. J. Phys. C : Sol. St. Phys. 20, 1985 - 1992 (1987)

27. D. G. Cantrell and P. N. Butcher, A calculation of the phonon-drag

contribution to the thermopower of quasi-2D electrons coupled to 3D phonons : II. Applications, J. Phys. C : Sol. St. Phys. 20, 1993 - 2003 (1987)

28. M. J. Smith and P. N. Butcher, A calculation on phonon drag thermopower in a Si MOSFET, J. Phys. : Condens. Matter 1, 1260 - 1273 (1989)

29. S. K. Lyo, Low temperature phonon-drag thermoelectric power in heterojunctions, Phys. Rev. B 38, 6345 - 6347 (1988)

30. M. J. Smith and P. N. Butcher, Inelastic scattering and the temperature dependence of thermoelectric power in quasi-2D systems, J. Phys. : Condens. Matter. 1, 4859 - 4864 (1989)

31. V. Karavolos et al, The effect of interface roughness scattering on the electron diffusion thermopower in a Si MOSFET, J. Phys. : Condens Matter, to be submitted (1990)

32. C. Ruf, H. Obloh, B. Junge, E. Gmelin, K. Ploog and G. Weimann, Phonon-drag effect in GaAs - $Al_x Ga_{1-x}$ As heterostructures at low temperatures, Phys. Rev. B 37, 6377 - 6380 (1988)

33. R. Fletcher, J. C Maan, K. Ploog and G. Weimann, Thermoelectric properties of GaAs - $AlGa_{1-x} Al_x$ As heterojunctions at high magnetic fields. Phys. Rev. B 33, 7122 - 7133 (1986)

34. S. S. Kubakaddi, P. N. Butcher and B. G. Mulimani, Phonon-drag thermopower of a two-dimensional electron gas in a quantising magnetic

field, Phys. Rev. B 40, 1377 - 1380 (1989)

35. S. K. Lyo, Magnetoquantum oscillations of the phonon-drag thermoelectric power in heterojunctions, Phys. Rev. B 40 6458 - 6461 (1989)

36. G. Bergmann, Weak localisation in thin films, Phys. Reports 107, 1 - 58 (1984)

37. S. B. Kaplan and A. Harstein, Mesoscopic coherence phenomena in semiconductor devices, IBM Journ. Res. Develop. 32, 347 - 371 (1988)

38. D. A. Greenwood, The Boltzmann equation in the theory of electrical conduction in metals, Proc. Phys. Soc. (London) 71, 585 - 596 (1958)

39. G. V. Chester and A. Thellung, The law of Wiedemann and Franz, J. Phys. Soc. (London) 77, 1005 - 1013 (1961)

40. J. M. Luttinger, Theory of thermal transport coefficients, Phys. Rev. A 135, 1505 - 1514 (1964)

41. R. Kubo, M. Yokota and S. Nakajima, Statistical-mechanical theory of irreversible processes J. Phys. Soc. Japan 12, 570 - 586, 1203 - 1211 (1957)

42. M. Kearney and P. N. Butcher, Thermal transport in disordered systems, J. Phys. C : Sol. St. Phys. 21, L 265 - 270 (1988)

43. R. T. Syme, M. J. Kelly and M. Pepper, Direct measurement of the thermal conductivity of a two-dimensional electron gas J. Phys Condens. Matter 1, 3375 - 3381 (1988)

44. P. N. Butcher and D. Cotter, The Elements of Nonlinear Optics, Cambridge University Press, London (1990, to be published)

45. P. N. Butcher, in Basic electron transport theory, Electrons in Crystalline Solids, (A. Salam, ed.) pp. 103-165, IAEA. Vienna, (1973)

46. M. Lax, Symmetry Principles in Solid State Physics, Wiley, New York (1974)

47. P. A. Lee and T. V. Ramakrishnan, Disordered electronic systems, Rev. Mod. Phys. 57, 287 - 337 (1985)

48. P. W. Anderson, Absence of diffusion in certain random lattices, Phys. Rev. 109, 1492 - 1505 (1958)

49. D. G Cantrell and P.N. Butcher, The transition between two-dimensional and three-dimensional weak localisation corrections to the Boltzmann conductivity, J. Phys. C : Sol. St. Phys. 18, 6627 - 6638 (1985)

50. M. J. Kearney and P. N. Butcher, Weak localisation in the quasi-one-dimensional regime with many occupied subbands, J. Phys. C : Sol. St. Phys. 21, 2539 - 2553 (1988)

51. D. J. Bishop, D. C. Tsui and R. C. Dynes, Weak localisation in silicon MOSFETS, in Localization, Interaction and Transport Phenomena (B. Kramer, G. Bergmann and Y. Bruynseraeda, eds.) pp. 31 - 37, Springer Verlag , Berlin (1985)

52. A. D. Stone, Universal conductance fluctuations and quantum interference effects in microstructures, in Physics and Technology of Submicron

Structures, (H. Heinreich, G. Bauer and F.Kuchar, eds.) pp. 108 - 127, Springer Verlag, Berlin (1988)

53. S. Washburn and R. A. Webb, Aharonov - Bohm effect in normal metal quantum coherence and transport Adv. Phys. 35, 375 - 422 (1986)

54. W. J. Skocpol, P. M. Mankiewich, R. E. Howard, L. D. Jackel, D. M. Tennant and A. D. Stone, Universal conductance fluctuations in silicon inversion layers, Phys. Rev. Lett. 56, 2865 - 2868 (1986) 58, 2347 - 2350 (1987)

55. A. D. Stone, Magnetoresistance fluctuations in mesoscopic wires and rings, Phys. Rev Lett. 54, 2692 - 2695 (1985)

56. P. A. Lee, D. Stone and H. Fukuyama, Universal conductance fluctuations in metals : effects of temperature, interactions and magnetic field. Phys. Rev. B 35, 1039 - 1070 (1987)

57. F. P. Esposito, B. Goodman and M. Ma, Thermoelectric power fluctuations, Phys. Rev. B 36, 4507 - 4509 (1987)

58. M. J. Kearney, Electron Transport in Disordered Systems, Ph.D. thesis, University of Warwick (1988)

59. T. Galloway, B. 1. Gallagher, P. Beton, J. P. Oxley, M. Carter, S. P. Beaumont, S. Thom and C. D. W. Wilinson, Observation of universal thermopower fluctuations, 8th. International Conference on the Electronic Properties of Two-dimensional Systems, Grenoble, Workbook pp. 558 - 562 (1989)

60. R. Landauer, Spatial variation of currents and fields due to localised

scatterers in metallic conduction, IBM J. Res. Develop. 1, 223 - 231 (1957)

61. B. J. van Wees, H. van Houten, C. W. J. Beenakker, J. G. Williamson, L. P. Kouenhoven, D. van der Marel and C. T. Foxon, Quantised conductance of point contacts in a two-dimensional electron gas. Phys. Rev. Lett. 60, 848 - 850 (1988)

62. D. A. Wharam, D. J. Thorton, R. Newbury, M. Pepper, H. Ahmed, J. E. F. Frost, D. J. Hasko, D. C. Peacock, D. A. Richie and G. A. C. Jones, One-dimensional transport and the quantisation of the ballistic resistance, J. Phys. C : Sol. St. Phys. 21, L209 - 214 (1988)

63. A. D. Stone and A. Szafer, Theory of quantum conduction through a constriction Phys Rev. Lett. 62, 300 - 303 (1989)

64. M. Buttiker, Absence of backscattering in the quantum Hall effect in multiprobe conductors, Phys. Rev. B 38, 9375 - 9389 (1988)

65. C. W. j. Beenakker and H. van Houten, Quenching of the Hall effect, Phys. Rev. Lett. 60 2406 - 2409 (1988)

66. G. Kliczenov, Mechanism of the quenching of the Hall effect, Phys. Rev. Lett. 62, 2993 - 2996 (1989)

67. M. Buttiker, Transmission probabilities and the quantum Hall effect, Phys. Rev. Lett. 62, 229 - 230 (1989)

68. P. N. Butcher, Thermal and electrical transport formalism for electronic microstructures with many terminals, to be published in J. Phys.

Condens. Matter. (1990)

69. U. Sivan and Y. Imry, Multichannel Landauer formula for thermoelectric transport with application to thermopower near the mobility edge Phys. Rev. B. 33, 551 - 558 (1986)

70. P. Streda, Quantised thermopower of a channel in the ballistic regime J. Phys. C : Sol. St. Phys. 1, 1025 - 1027 (1989)

71. A. H. Wilson, The Theory of Metals, London : Cambridge University Press (1954)

72. A. D. Benoit, S.Washburn, P. Umbach, R. B. Laibaultz and R. A. Webb Asymmetry in the magnetoconductance of metal wires and loops, Phys. Rev. Lett 57, 1765 - 1768 (1986)

73. Y. Aharanov and D. Bohm, Significance of electronic potentials in quantum theory, Phys. Rev. 115, 485 - 491 (1959)

74. D. Yu Sharvin and Yu. V. Sharvin, Magnetic-flux quantization in a cylindrical film of a normal metal, JETP. Lett. 34, 272 - 275 (1981)

75. K. von Klitzing, G. Dorda and M. Pepper, New method for high accuracy determination of the fine structure constant based on quantised Hall resistance, Phys. Rev. Lett. 45, 494 - 497 (1980)

76. K. von Klitzing, Two-dimensional systems, a method for the determination of the fine structure constant, Surf. Sci. 113, 1 - 9 (1982)

77. D. C. Tsui and A. C. Gossard, Resistance standard using quantisation of the Hall resistance of GaAs - $Al_xGa_{1-x}As$ heterostructures, Appl. Phys.

Lett. 38, 550 - 552 (1981)

78. D. R. Yennie, Integral quantum Hall effect for non-specialists, Rev. Mod. Phys. 59, 781 - 824 (1989)

79. D. C. Tsui, H.L. Stormer and A. C. Goddard, Two-dimensional magnetotransport in the extreme quantum limit, Phys. Rev. Lett. 48, 1559 - 1562 (1982)

80. H. L. Stormer, A. Chang, D. C. Tsui, J. C. M. Hwang, A. C. Gossard and W. Wiegmann, Fractional quantisation of the Hall effect, Phys. Rev. Lett. 50, 1953 - 1956 (1987)

81. A. M. Chang, P. Bergland, D. C. Tsui, H. L. Stormer and J. C. M. Hwang, Higher-order states in the multiple series, fractional, quantum Hall effect, Phys. Rev. Lett. 53, 997 - 1000 (1984)

82. N. d'Ambrumenil, Spring College, Trieste (1990)

83. J. P. Eisenstein, Spring College, Trieste, (1990)

84. M. Buttiker, Spring College, Trieste (1990)

85. A. B. Fowler, J. J. Wainer and R. A. Webb, Electronic transport in strongly localized structures, IBM J. Res. Dev. 32, 372 - 383 (1988)

86 G.Timp, A. B. Fowler, A. Harstein and P. N. Butcher, Absence of a Coulomb gap in a two-dimensional impurity band, Phys. Rev. B, 33, 1499 - 1502 (1986)

87. G. Timp, A. B. Fowler, A. Harstein and P. N. Butcher, Hopping conduction in a two-dimensional impurity band, Phys. Rev. B, 34, 8771 - 8785

(1986)

88. P. N. Butcher and J. A. McInnes, Hopping transport in one dimensional semi conductor systems, in Physics and Technology of Submicron Structures (H. Heinreich, G. Bauer and F. Kuchar eds.) pp. 218 - 224, Springer-Verlag, Berlin (1988)

89. P. N. Butcher, Electron transport theory for extended and localised states, in Amorphous solids and the liquid state (N. H. March, R. A. Street and M. Tosi) pp. 311 - 359 Plenum Press, New York (1985)

Figure Captions

Fig. 1 Schematic diagram of an n-channel MOSFET.

Fig. 2 The band diagram when an inversion layer (crossed-hatched) is produced.

Fig. 3 Schematic band diagram for heterojunction.

Fig. 4 Schematic band diagram for a quantum well.

Fig. 5 Schematic diagrams of the density of states for (a) a 2DEG and (b) a 1DEG. The minima of the first four subbands are at ϵ_0, ϵ_1, ϵ_2 and ϵ_3.

Fig. 6 Schematic plot of the Boltzmann conductivity $\sigma(\epsilon_F)$ at OK against ϵ_F. The minima of the first three subbands are at ϵ_0, ϵ_1 and ϵ_2.

Fig. 7 The variation of the 2DEG conductivity with Fermi energy for the valuesof $(k_F \ell)_{2D}$ given by the curves. (The depth of the dip A is 6% of the highest value before the dip and the dip at B has a depth equal to 3% of the highest previous value.) The dashed lines indicate the positions of the second and third subband minima.[18]

Fig. 8 Schematic plot of the negative contribution S_N to the thermopower of a 2DEG against Fermi enegy in the neighbourhood of a subband minimum indicated by the dashed line.[20]

Fig. 9 Schematic plot of the positive contribution S_p to the thermopower of

a 2DEG against Fermi energy in the neighbourhood of a subband minimum indicated by the dashed line.[20]

Fig. 10 A plot of S against Fermi energy for a 2DEG. Full curve : $(k_F \ell)_{2D}$ = 50, broken curve $(k_F \ell)_{2D}$ = 6. Both curves are drawn for T = 1K.[21]

Fig. 11 Plots of S against T for a 2DEG when $(k_F \ell)_{2D}$ = 6 for the values of ϵ_F in meV of (A) 4·8, (B) 5·2, (C) 4.0 and (D) 6·0.[21]

Fig. 12 Plots of S against Fermi energy for a 2DEG when $(k_F \ell)_{2D}$ = 2 and T = 1K (A) and 6K (B).[21]

Fig. 13 Experimental plots of -S/T against ϵ_F and n at four temperatures. The minimum is due to quantum size effects in the electron diffusion thermopower. The second subband minimum is at 12·5meV.[22]

Fig. 14 The density of states of a 1DEG as a function of energy for $(k_F \ell)_{1D}$ = 30 (A) and 5 (B). The subband minima are at 0, 5 and 10 meV.[24]

Fig. 15 The electrical conductivity of a 1DEG as a function of chemical potential for $(k_F \ell)_{1D}$ = 30 (A) and 5 (B) at T = 2K. The subband minima are at 0, 5 and 10meV.[24]

Fig. 16 Plots of S for a 1DEG against chemical potential for $(k_F \ell)_{1D}$ = 30 for T = 2K (top curve) and 8K (bottom curve).[24]

Fig. 17 Plots of S for a 1DEG against ϵ_F for $(k_F \ell)_{1D}$ = 5 and T = 2K (top

curve) and 8K (bottom curve).[24]

Fig. 18 Experimental plots of -S against T for n = 3·09 and 3·49 $\times 10^{11} cm^{-2}$. Phonon drag dominates above 1K. S changes sign at 0·35K in the second case because of quantum size effects in the electron diffusion thermopower.[22]

Fig. 19 Data and theory curves for n = 5·47 $\times 10^{11} cm^{-2}$ (b), 8·35 $\times 10^{11} cm^{-2}$ (d) and 14·1 $\times 10^{11} cm^{-2}$ (f).[6] See text for details.

Fig. 20 Plots against q when q_z = 0 of the phonon distribution factor (smooth peak) and the transition rate factor (sharp peak) in the summand of equation (5.33). (a) $T < T_D$, (b) $T = T_D$, (c) $T > T_D$ where T_D is the temperature of the maximum in $-Sg/T^3$ given by equation (5.38).[27]

Fig. 21 Temperature dependence of -Sg in a GaAs/AlGaAs heterojunction.[30] Full curves-theory, Dashed curves-data.[32] The curves are labelled with the power of energy appearing in the electron relaxation time.

Fig. 22 Temperature dependence of -Sg in a GaAs/AlGaAs heterojunction.[30] Chain curve-theory with inelastic scattering. Full curve-theory with elastic scattering., Broken curve-data.[33]. The electron relaxation time has been assumed to be linear in the energy.

Fig. 23 Temperature dependence of the diagonal component of the phonon-drag thermopower tensor in the magnetic quantum limit.[34]

Curve 1 ; piezoelectric scattering. Curve2 : deformation potential scattering. Curve 3 : Both scattering mechanisms. Crosses - experimental data.(33)

Fig. 24 Schematic diagram illustrating two time-reversed multiple scattering processes from $\underline{k}$ to $-\underline{k}$ in a system with time-reversal symmetry. Top arrows : $\underline{k} \rightarrow \underline{k}_1 \rightarrow \underline{k}_2 \rightarrow \underline{k}_3 \rightarrow -\underline{k}$. Bottom arrows ; $\underline{k} \rightarrow -\underline{k}_3 \rightarrow -\underline{k}_2 \rightarrow -\underline{k}_1 \rightarrow -\underline{k}$.

Fig. 25 Schematic illustration of the impulse response function for the current density. Top curve : Boltzmann transport approximation. Bottom curve : weak localisation correction.

Fig. 26 Resistance as a function of temperature for Si MOSFETS with $n = 2{\cdot}03 \times 10^{12} cm^{-2}$ (right-hand curve) and $5{\cdot}64 \times 10^{12} cm^{-2}$ (left-hand curve).(51)

Fig. 27 Magnetoresistance measured as a function of magnetic field for a Si MOSFET with $n = 4{\cdot}52 \times 10^{12} cm^{-2}$ at 0·1K. The smooth curves are theoretical fits to the data with with different parameter values.(51)

Fig. 28 Comparison of conductance fluctuations in units of e^2/h as B varies. Left-hand box : observed in an 0·8μm diameter gold ring,(53) middle box : observed in a quasi-1D Si MOSFET,(54) right-hand box : calculated using an Anderson model.(55) (After reference 52).

Fig. 29 Numerical calculations of the conductance fluctuations in units of e^2/h when the quantity varied is (a) the impurity distribution, (b) the magnetic induction field and (c) the Fermi energy .(56)

Fig. 30 A model conductance function exhibiting universal fluctuations at absolute zero.(58)

Fig. 31 The thermopower as a function of chemical potential at 60mK for the model conductance function given in Figure 30.(58)

Fig. 32 Thermoelectric voltage fluctuations in a GaAs wire due to an electron temperature gradient which increases from 0 for trace A to larger values for traces B and C. The latter two traces are offset by 4 and 7μV respectively.(59)

Fig. 33 Schematic diagram of an independent electron microstructure with N_t terminals labelled 1, 2, 3, $\cdots$ α, $\cdots$ β $\cdots$ $N_t - 1$, N_t.

Fig. 34 Transmission electron photograph of an 0·82μm diametre ring made from a 38nm gold film. The wires are 40nm across.(53)

Fig. 35 (a) Resistance at 40mK of the gold ring shown in Figure 34 as a function of the flux ϕ threaded through the ring. The horizontal double headed arrow indicates the dominant $\phi_0 = h/e$ flux period. The slow modulation is due to universal conductance fluctuations.(53) (b) The Fourier transforms of the data in (a) showing a large peak at $(\Delta H)^{-1} = 130\ T^{-1}$ corresponding to a flux period of ϕ_0 and a smaller peak at the second harmonic $(\Delta H)^{-1} = 260\ T^{-1}$.

Fig. 36 Resistance as a function of gate voltage for the gate structure shown in the inset.(61)

Fig. 37 Conductance of a quantum point contact as a function of gate voltage

This plot is obtained by subtracting the series resistance of the terminals from the data shown in Figure 36.(61)

Fig. 38 Conductance of the 2DEG structures shown at the top of the Figure plotted against Fermi wave number. The width of the terminals is four times the width of the constrictions. The quantity a is the ratio of the length of the transition (between the tapers) to the width of the constriction. The solid lines are exact numerical results for the abrupt transition. The dashed line which is almost hidden by the top curve is for the tapered transition. The dashed lines on the lower three curves show the results of an analytical approximation for the abrupt transition. The curves are offset vertically.(63)

Fig. 39 (a) A laterally confined 2DEG of width w with Cartesian axes Oxyz located and oriented as assumed in the text. The arrows near the top and bottom edges indicate the direction of electron flux in the edge states when $\underline{B}$ points along Oy.
(b) The dispersion curves for the confined 2DEG shown in (a)

Fig. 40 A typical Hall bar. The lines with arrows on them indicate the electron flux in the edge states when the magnetic induction field points out of the paper. Terminal 1 and 4 are current terminals, terminals 2, 3, 5 and 6 are voltage probes.

Fig. 41 The dependence of the Hall resistance R_{zx} and longitudinal resistance R_{zz} on gate voltage V_G (which controls the position of the Fermi level) for a Si MOSFET at 1.5K when B = 18·9T. The inset shows the behaviour for $V_g \sim 12V$ in more detail (After reference 76).

Fig. 42 The dependence of the Hall resistance R_{zx} and the longitudinal resistance R_{zz} on magnetic field (which controls the Landau level spacing) for GaAs/AlGaAs heterojunction at 90mK. (a) R_{zx}, (b) R_{zz}.(81)

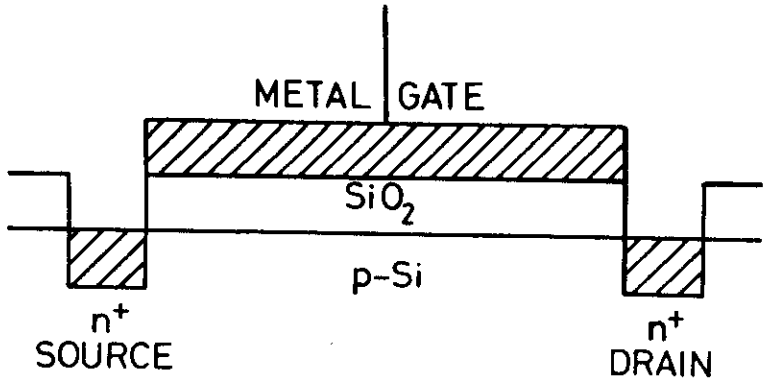
METAL
GATE
SiO_2
p-Si
n^+
SOURCE
n^+
DRAIN

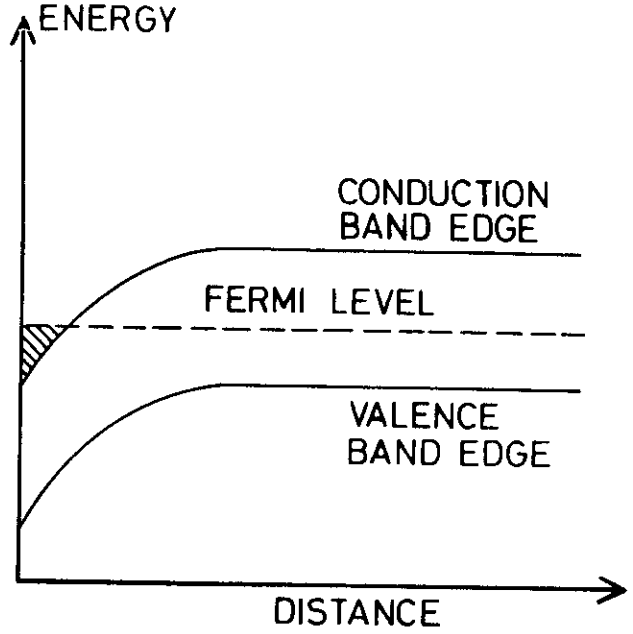
ENERGY
CONDUCTION
BAND EDGE
FERMI LEVEL
VALENCE
BAND EDGE
DISTANCE

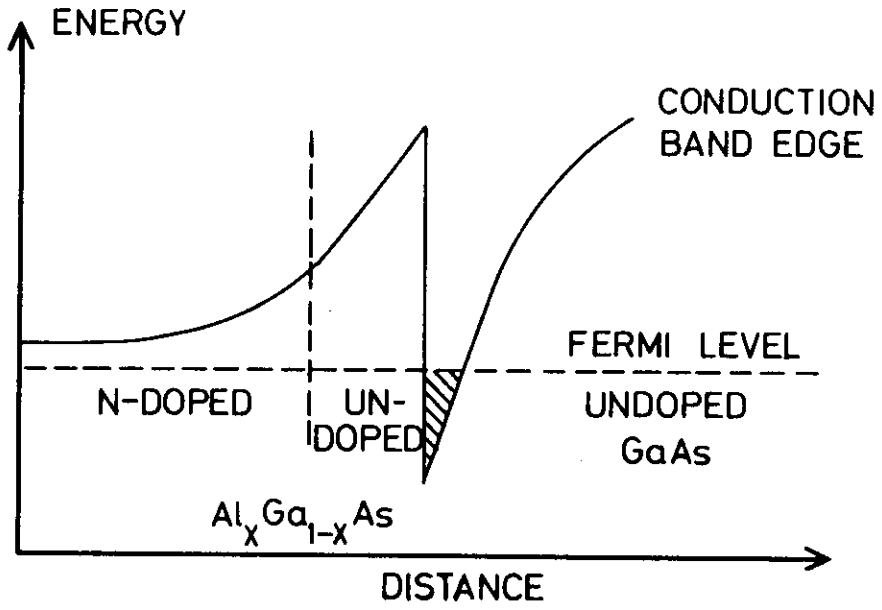
ENERGY
CONDUCTION
BAND EDGE
FERMI LEVEL
N-DOPED
UN-
DOPED
UNDOPED
GaAs
$Al_xGa_{1-x}As$
DISTANCE

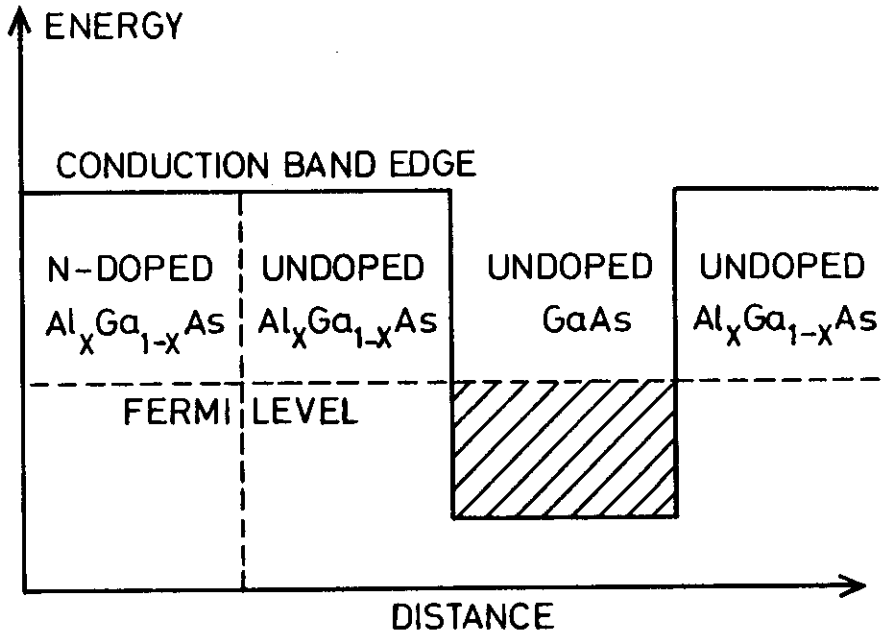
ENERGY
CONDUCTION BAND EDGE
N-DOPED
$Al_xGa_{1-x}As$
UNDOPED
$Al_xGa_{1-x}As$
UNDOPED
GaAs
UNDOPED
$Al_xGa_{1-x}As$
FERMI LEVEL
DISTANCE

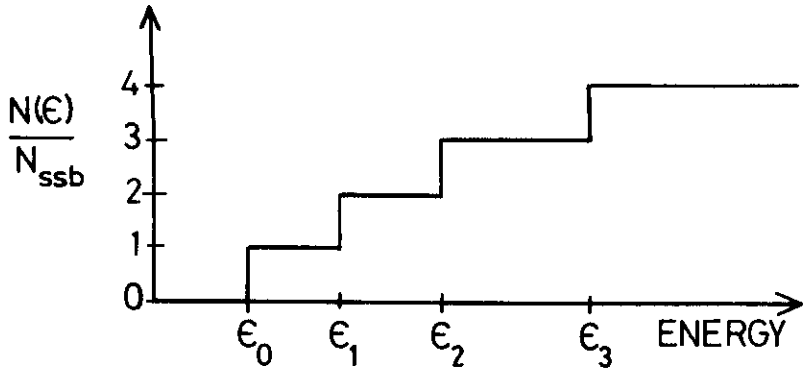
N(E)
N_ssb
4
3
2
1
0
E0
E1
E2
E3
ENERGY

(a)

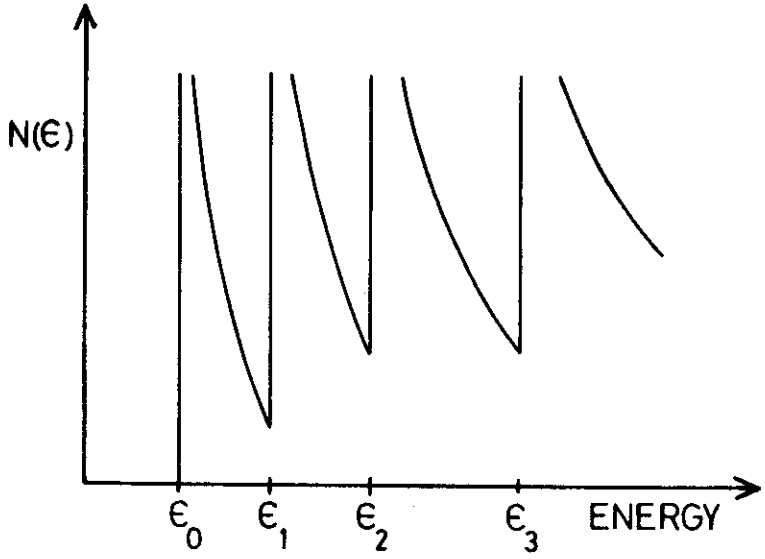
N(E)
E0
E1
E2
E3
ENERGY

(b)

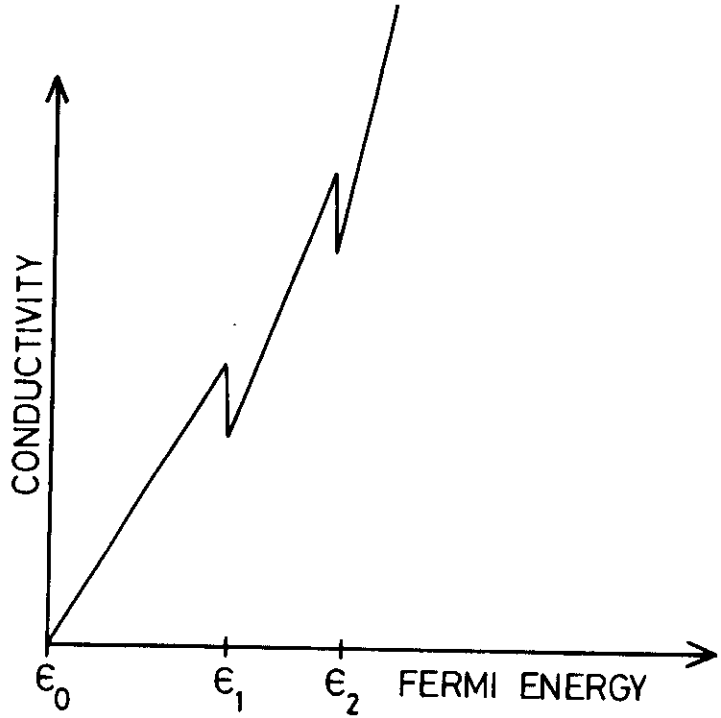
CONDUCTIVITY
E0
E1
E2
FERMI ENERGY

Fig 6

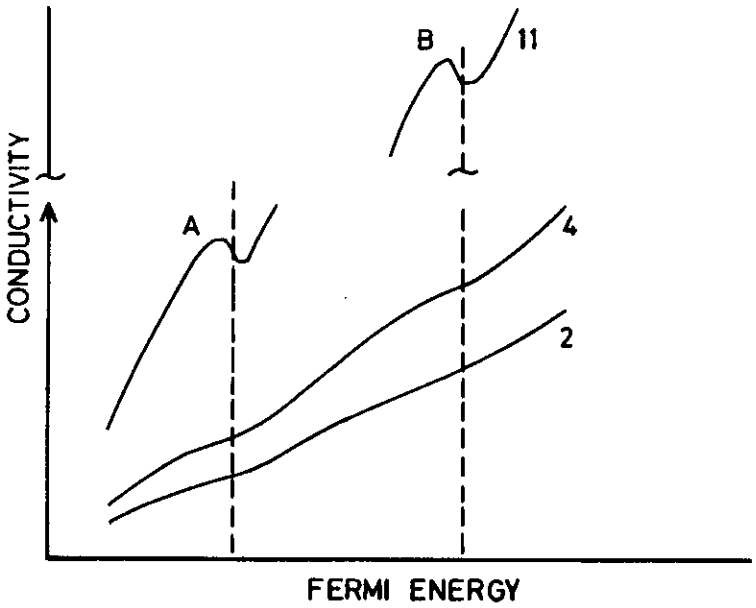

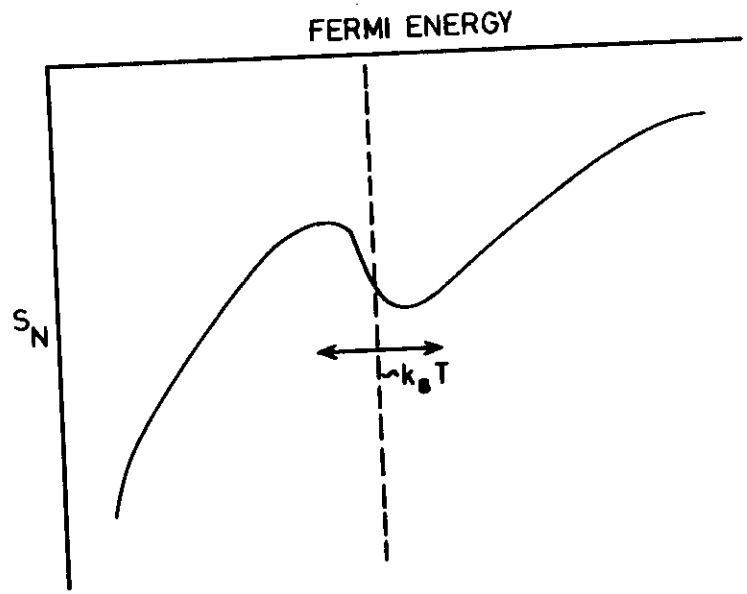

Fig 8

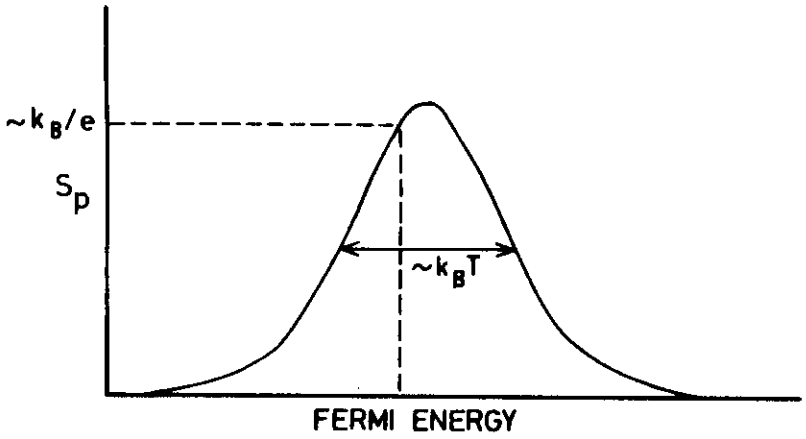

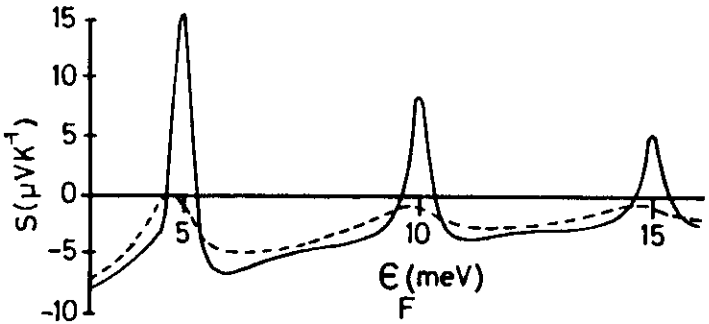

Fig 9

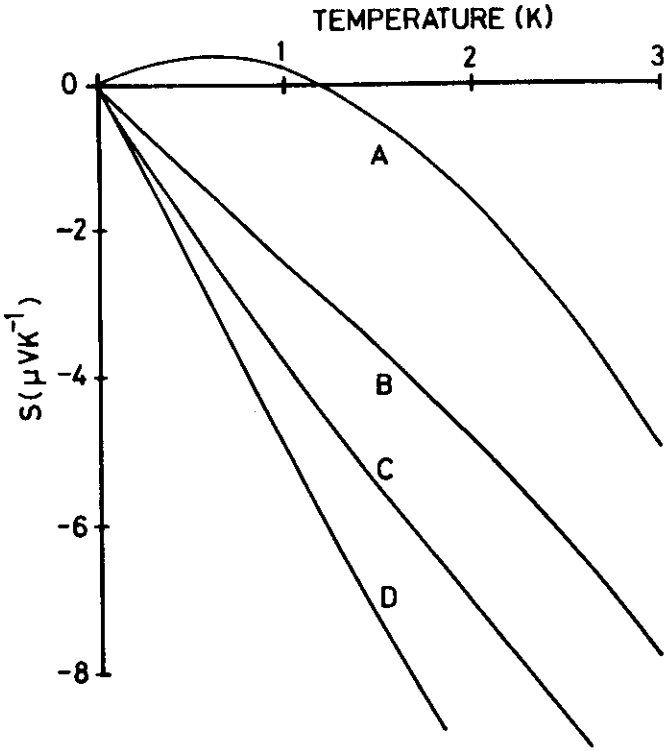
TEMPERATURE (K)
1
2
3
0
-2
-4
-6
-8
S(μVK⁻¹)
A
B
C
D

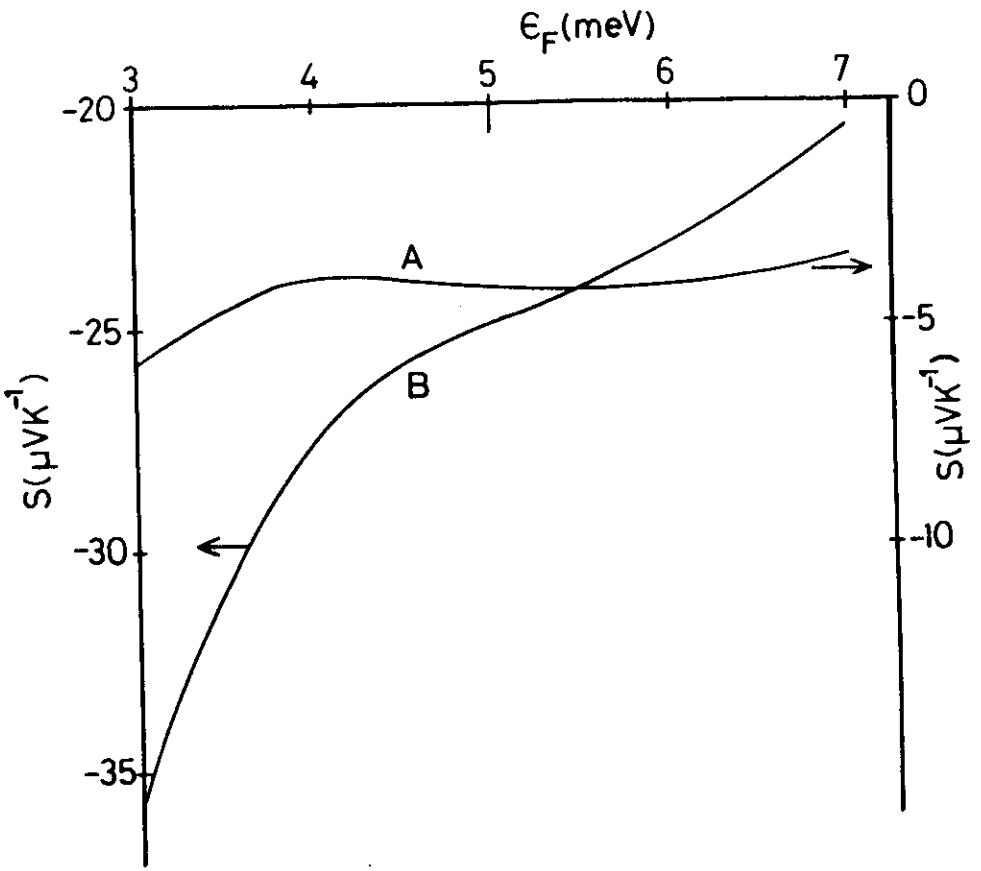
ϵ_F(meV)
3
4
5
6
7
-20
-25
-30
-35
0
-5
-10
S(μVK⁻¹)
S(μVK⁻¹)
A
B

Fig 12

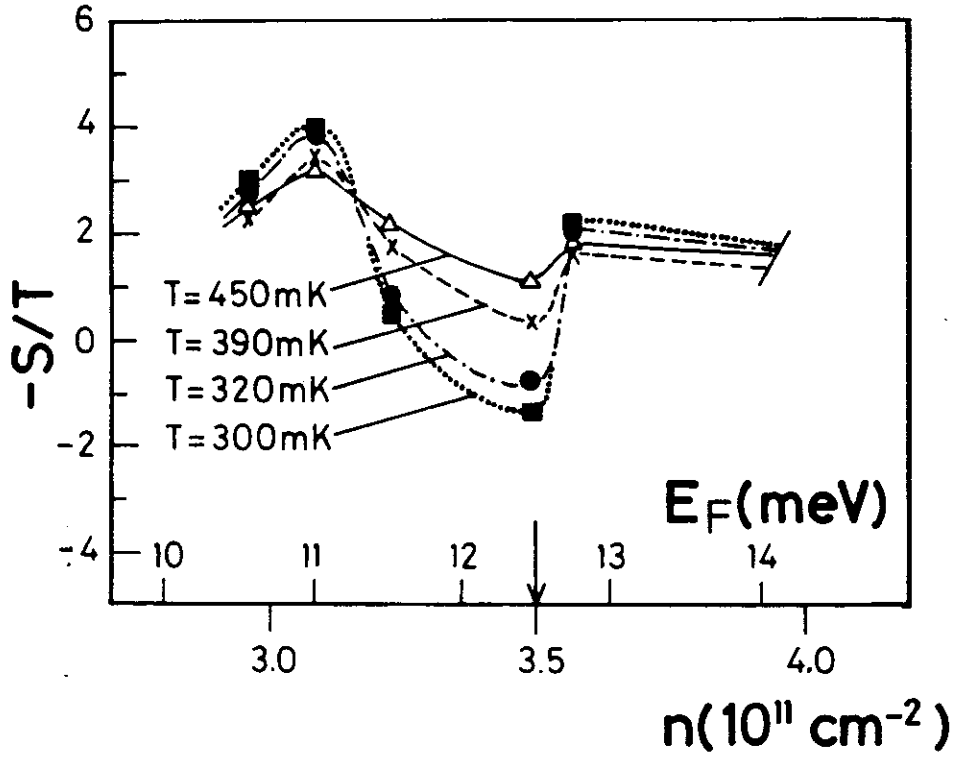
6
4
2
0
-2
-4
-S/T
T=450mK
T=390mK
T=320mK
T=300mK
E_F(meV)
10
11
12
13
14
3.0
3.5
4.0
n(10^11 cm^-2)

Fig. 13

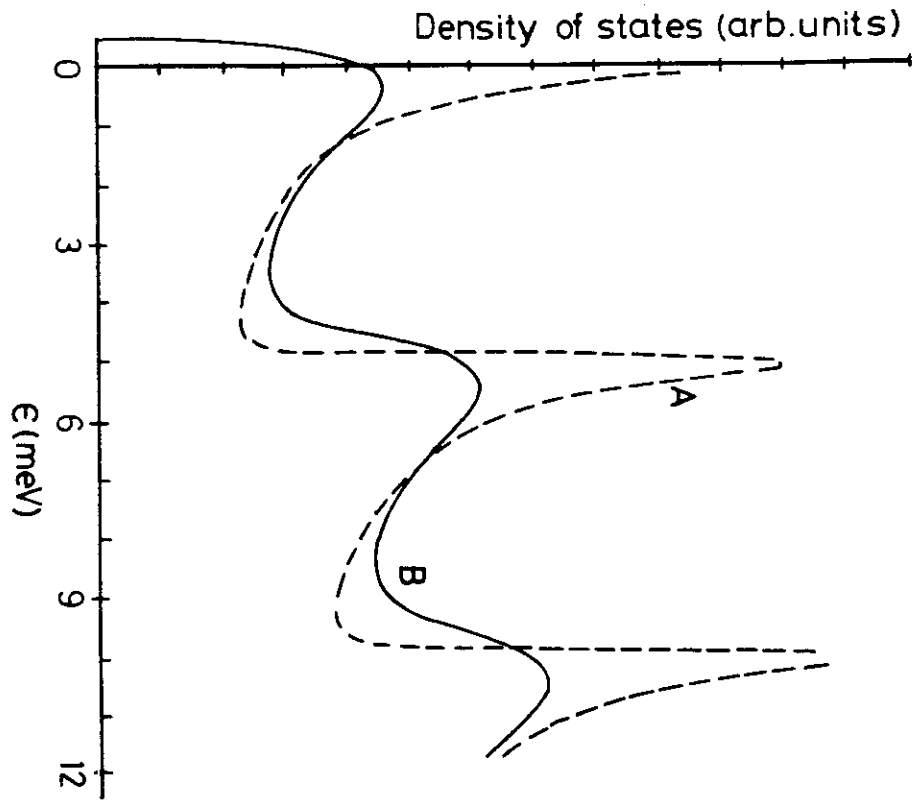
Density of states (arb.units)
0
3
6
9
12
ε(meV)
A
B

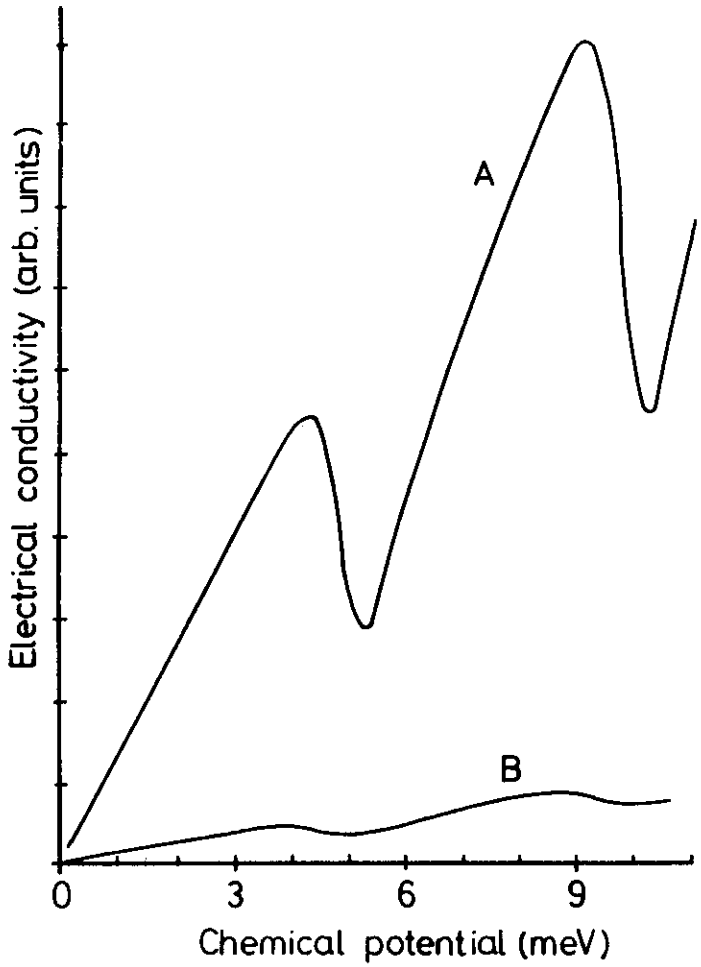
Electrical conductivity (arb. units)
A
B
0
3
6
9
Chemical potential (meV)

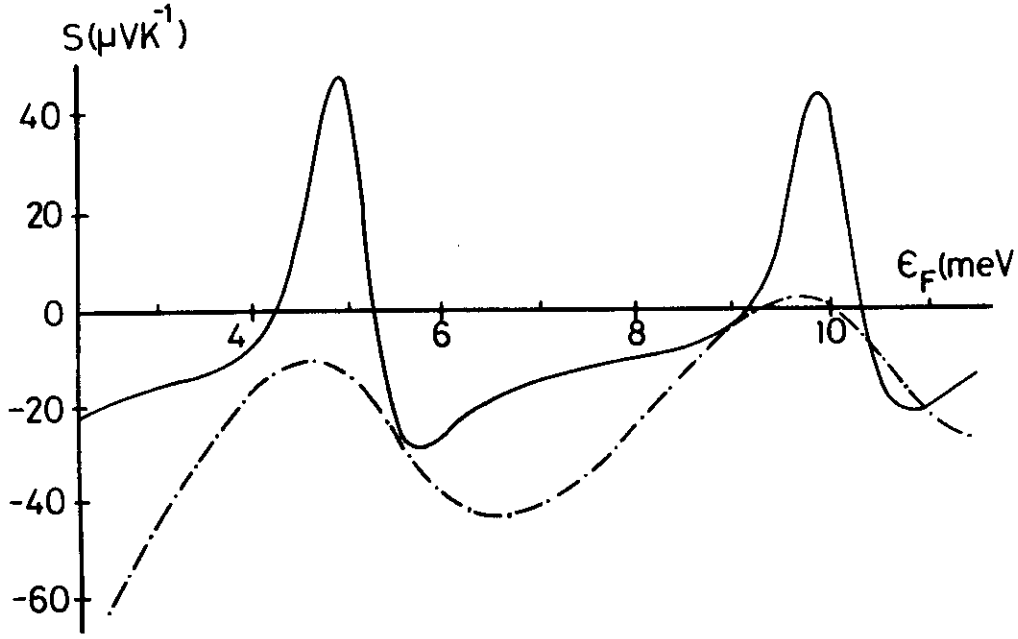
S(μVK⁻¹)
40
20
0
-20
-40
-60
4
6
8
10
ϵ_F(meV

Fig.15

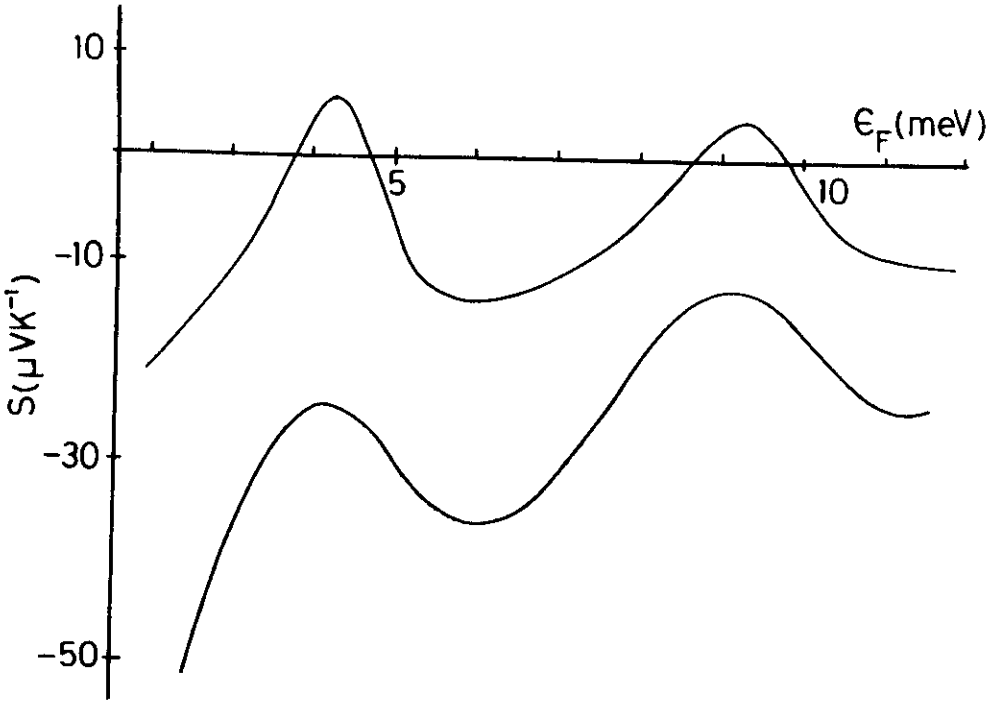
10
-10
-30
-50
S(μVK⁻¹)
5
10
ϵ_F(meV)

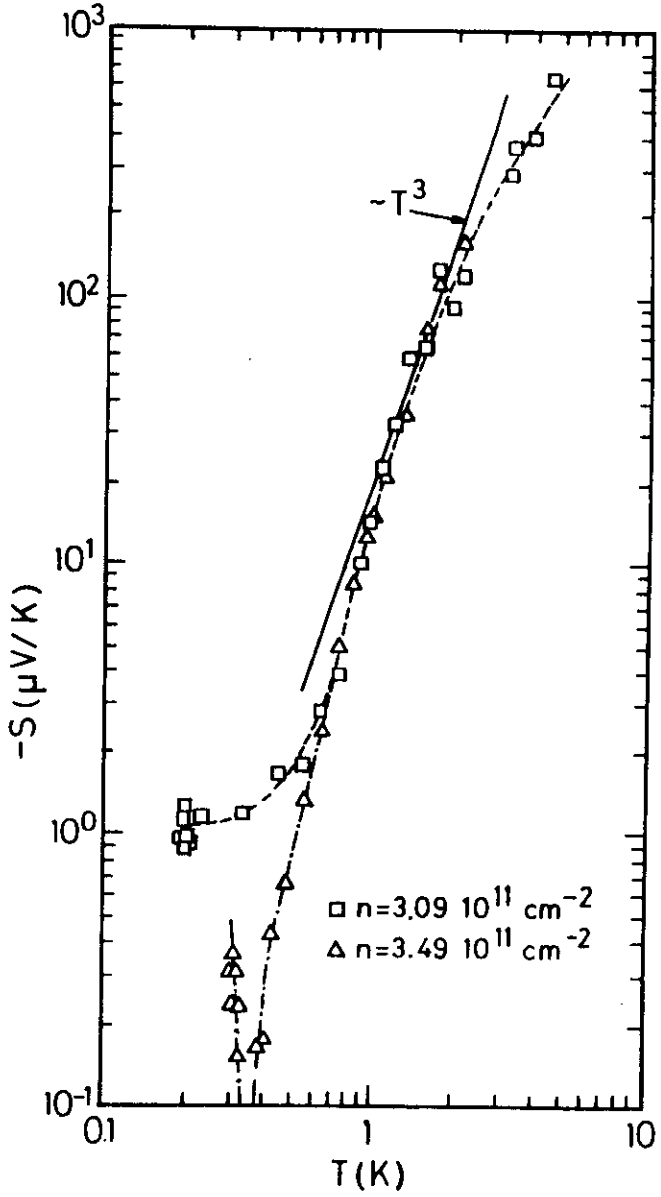
10^3
10^2
10^1
10^0
10^{-1}
-S(μV/K)
~T³
□ n=3.09 10¹¹ cm⁻²
△ n=3.49 10¹¹ cm⁻²
0.1
1
10
T(K)

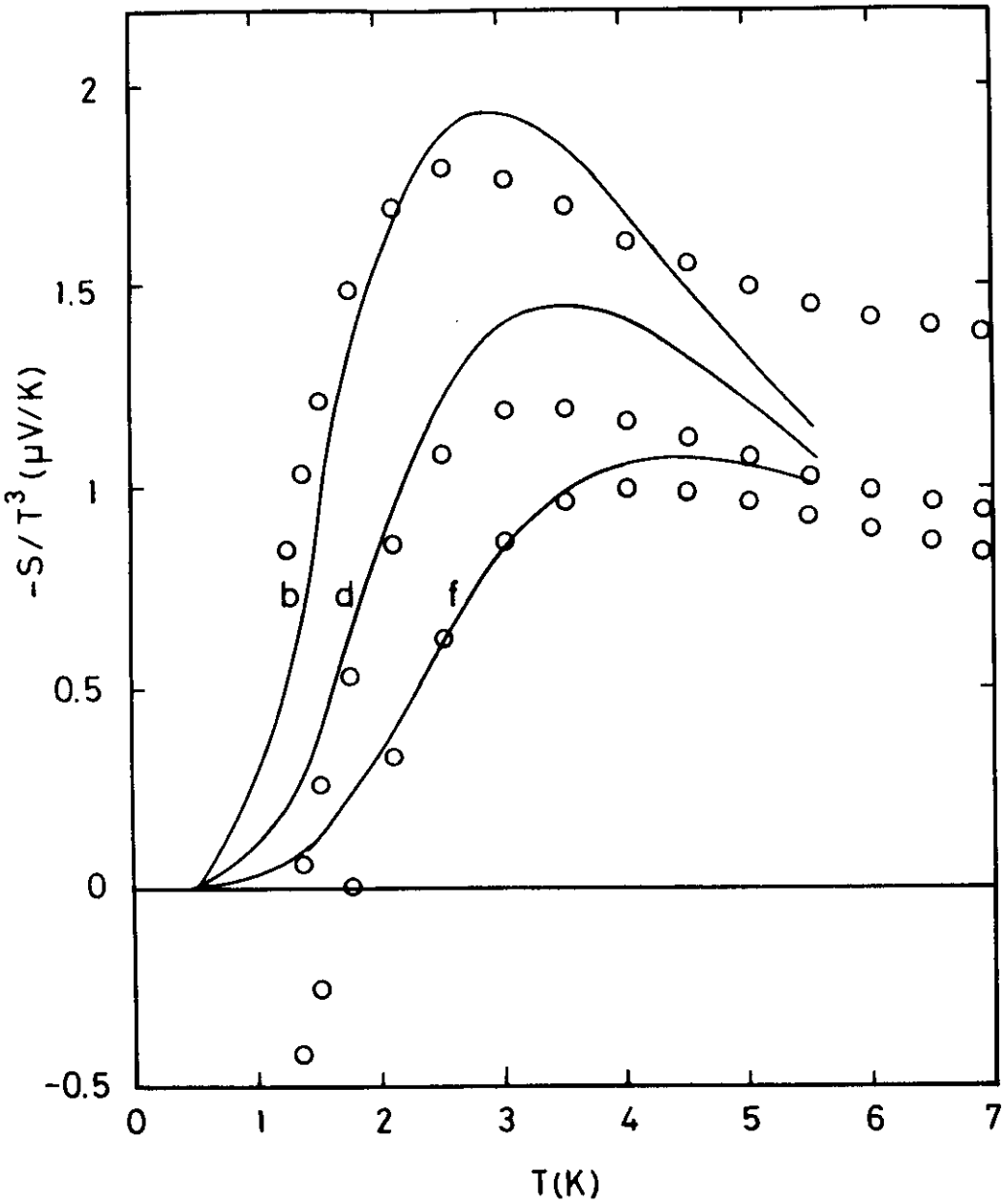
2
1.5
1
0.5
0
-0.5
0
1
2
3
4
5
6
7
T(K)
-S/T³ (μV/K)
b
d
f

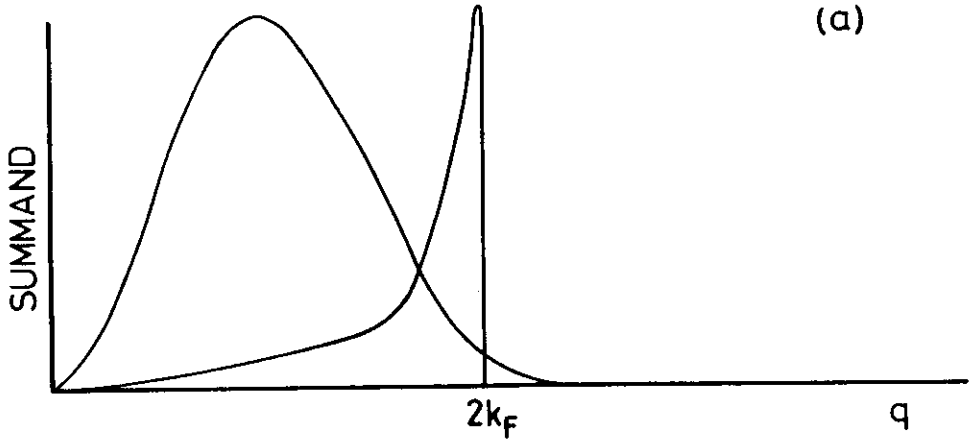
(a)
SUMMAND
2k_F
q

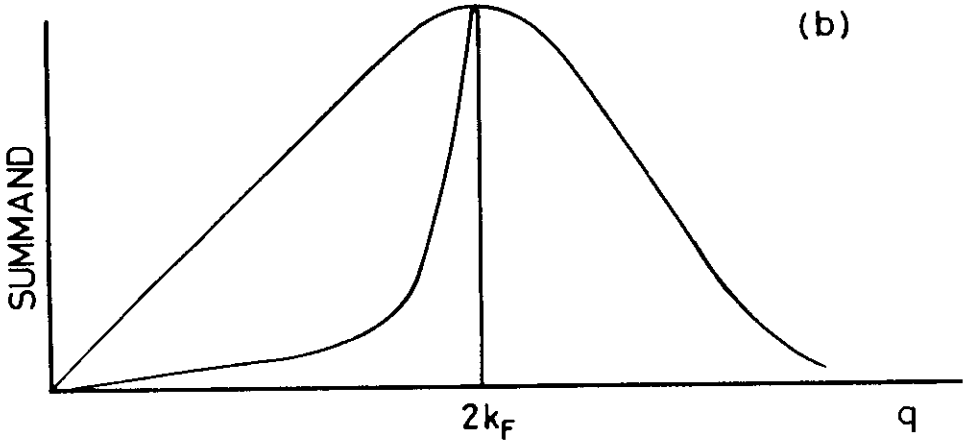
(b)
SUMMAND
2k_F
q

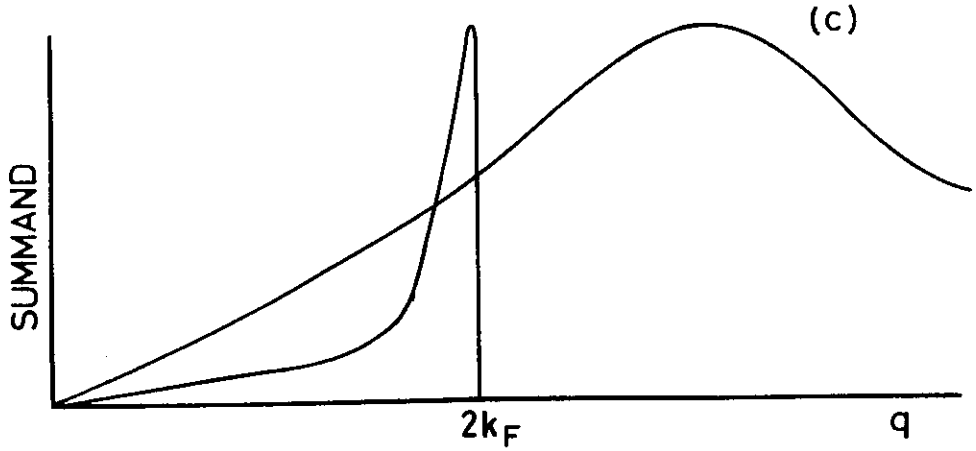
(c)
SUMMAND
2k_F
q

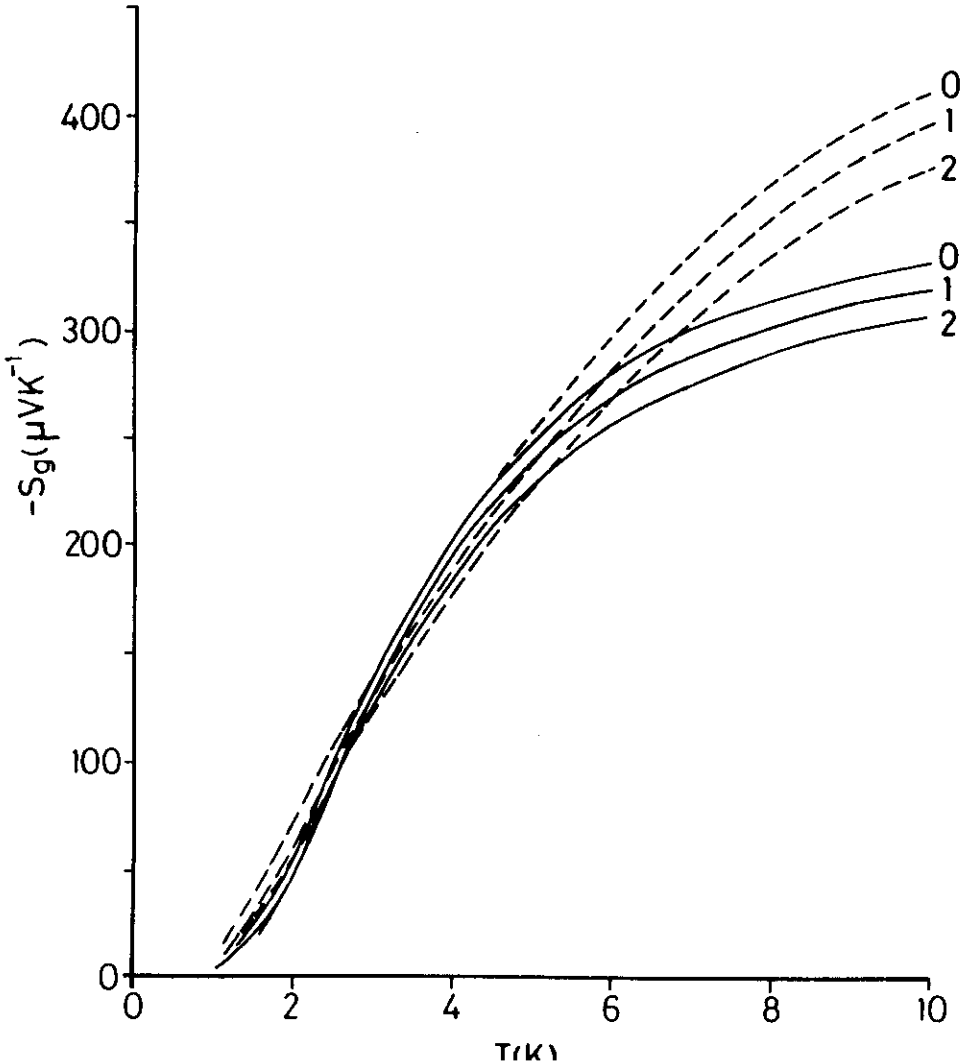
400
300
200
100
0
$-S_g(\mu VK^{-1})$
0
1
2
0
1
2
0
2
4
6
8
10
T(K)

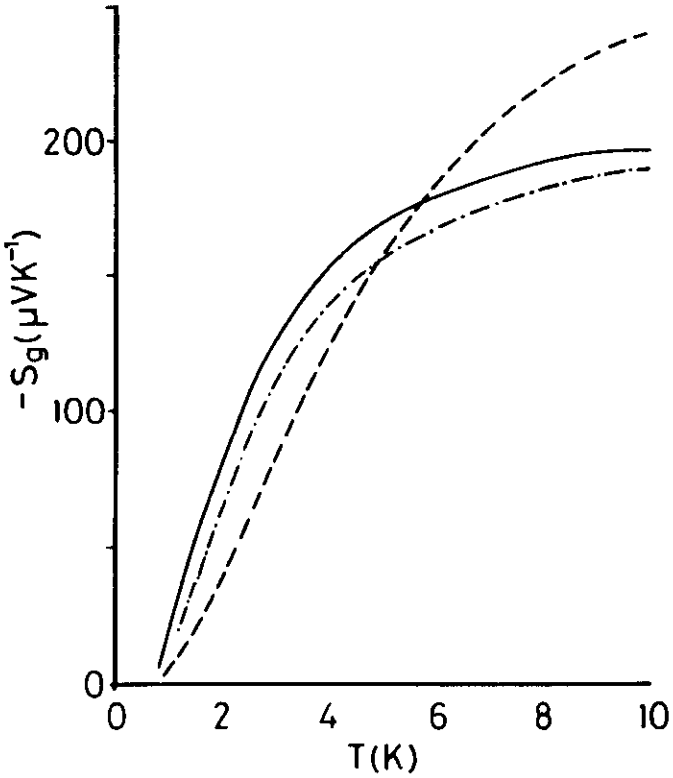
200
100
0
$-S_g(\mu VK^{-1})$
0
2
4
6
8
10
T(K)

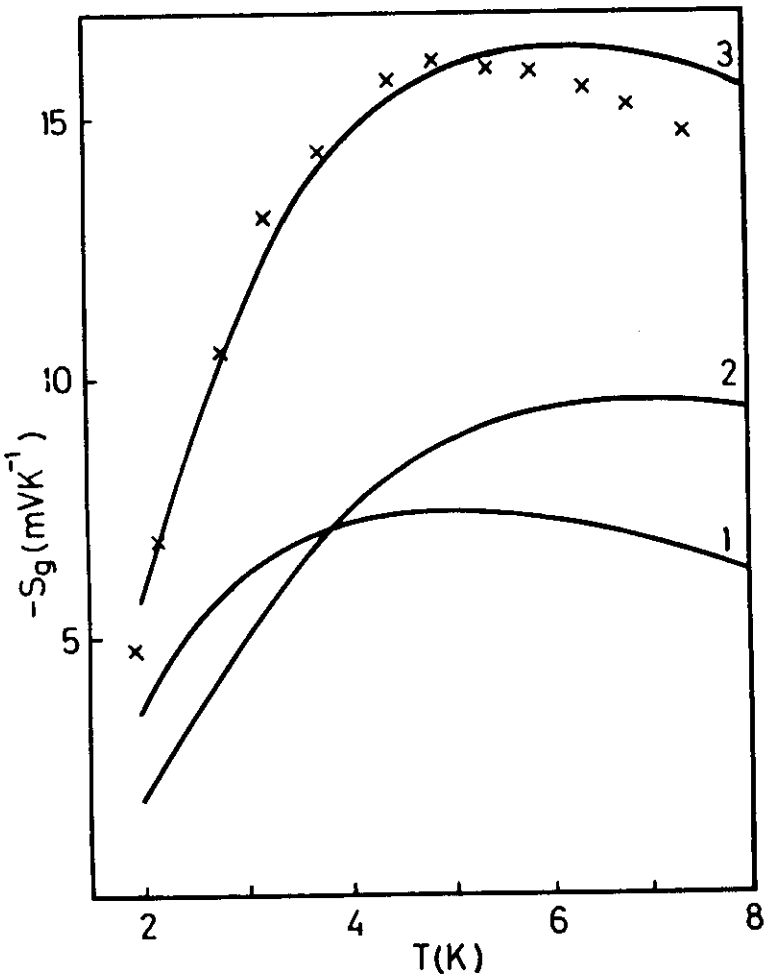

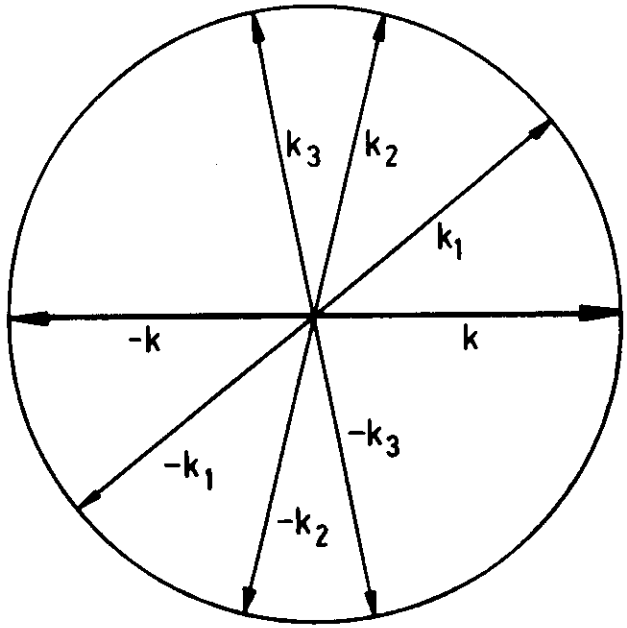

Fig 23

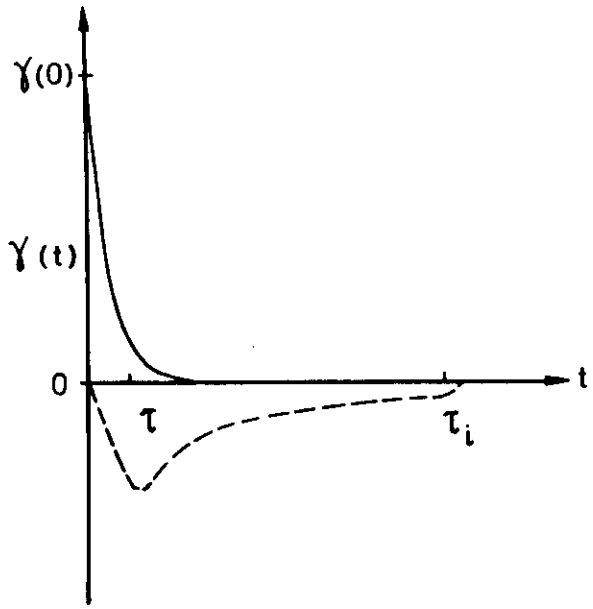
γ(0)
γ (t)
0
t
τ
τi

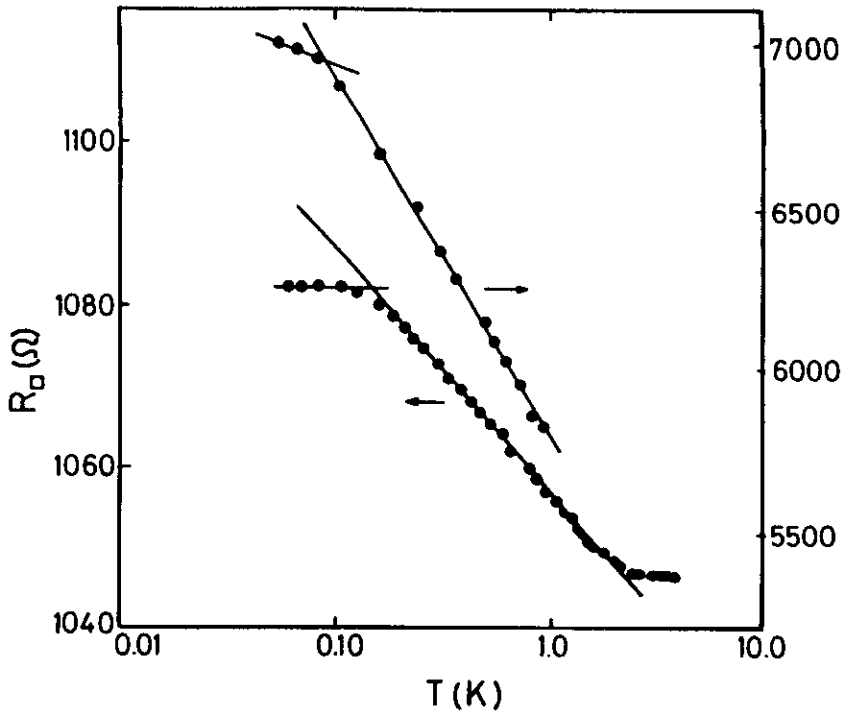
1100
1080
1060
1040
7000
6500
6000
5500
0.01
0.10
1.0
10.0
T (K)
R□ (Ω)

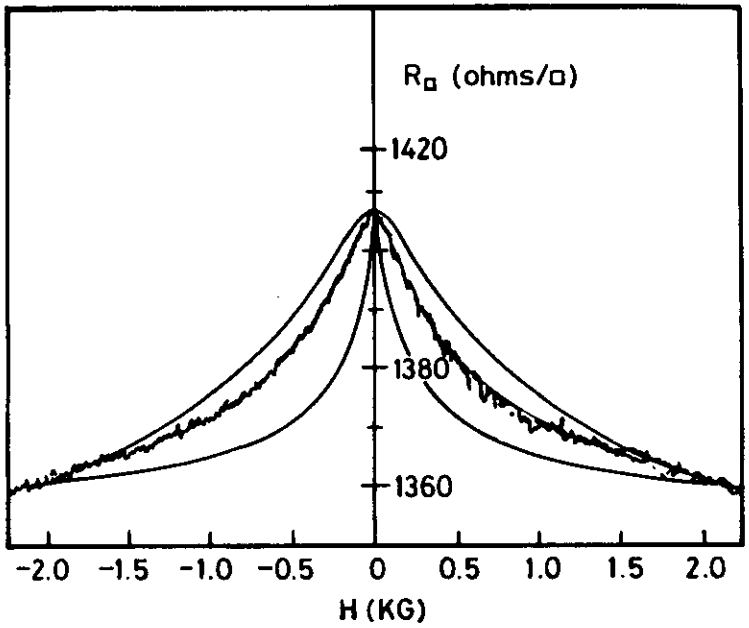
$R_\square$ (ohms/□)
1420
1380
1360
-2.0
-1.5
-1.0
-0.5
0
0.5
1.0
1.5
2.0
H (KG)

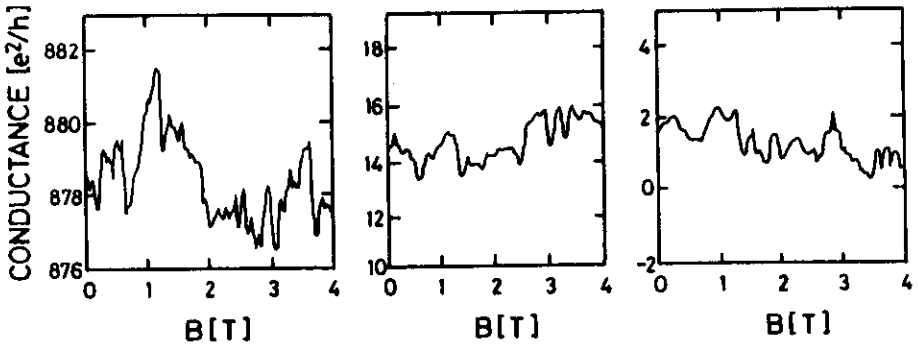
CONDUCTANCE [e²/h]
882
880
878
876
0
1
2
3
4
B[T]
18
16
14
12
10
0
1
2
3
4
B[T]
4
2
0
-2
0
1
2
3
4
B[T]

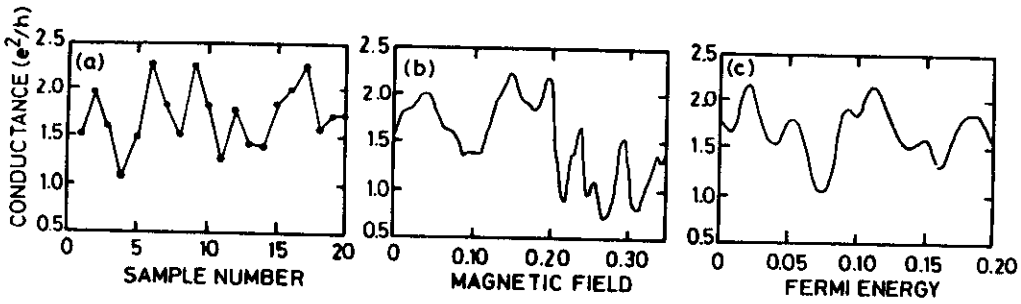
CONDUCTANCE (e^2/h)
(a)
(b)
(c)
SAMPLE NUMBER
MAGNETIC FIELD
FERMI ENERGY

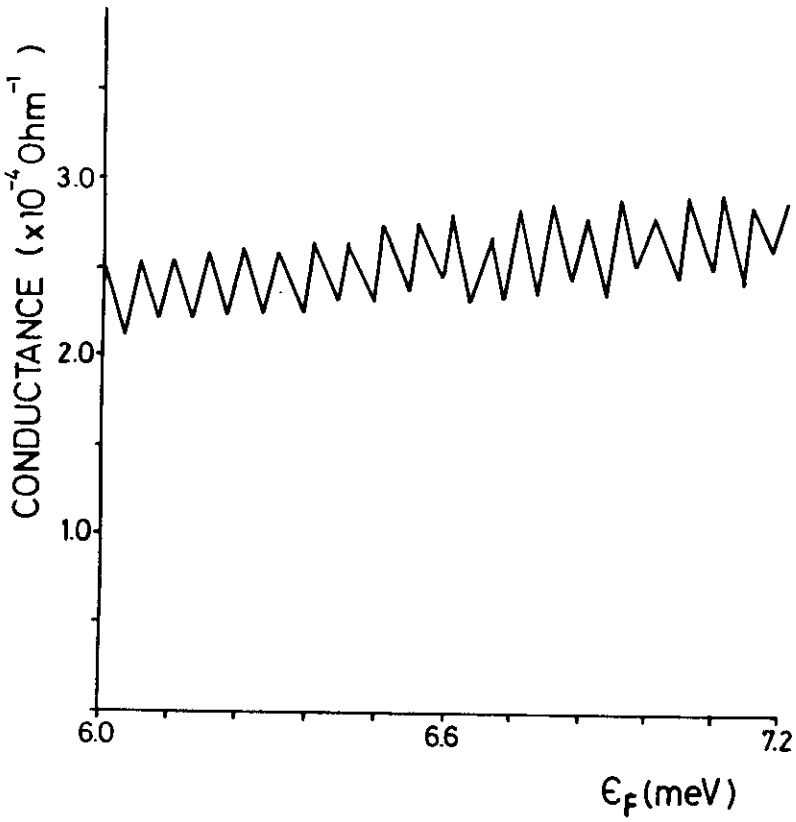
CONDUCTANCE ($\times 10^{-4}$ Ohm^{-1})
ϵ_F (meV)

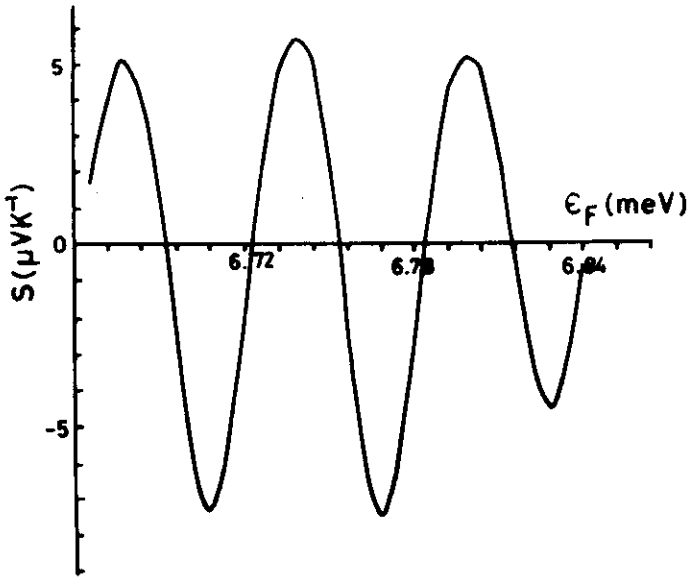
S(μVK⁻¹)
5
0
-5
ϵ_F (meV)
6.72
6.76
6.84

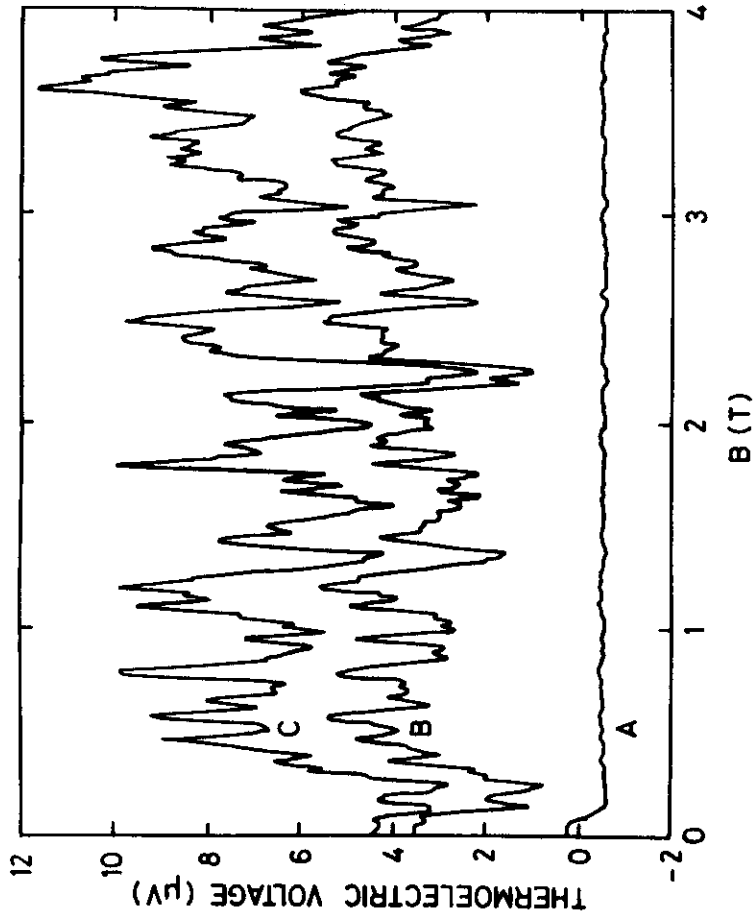
THERMOELECTRIC VOLTAGE (μV)
12
10
8
6
4
2
0
-2
A
B
C
0
1
2
3
4
B (T)

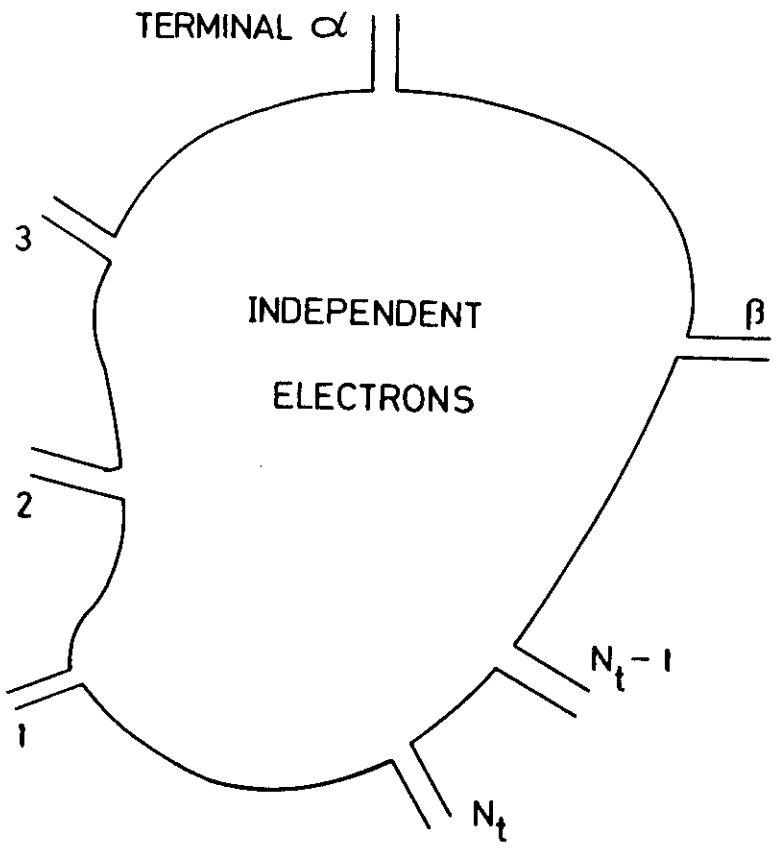

Fig. 33

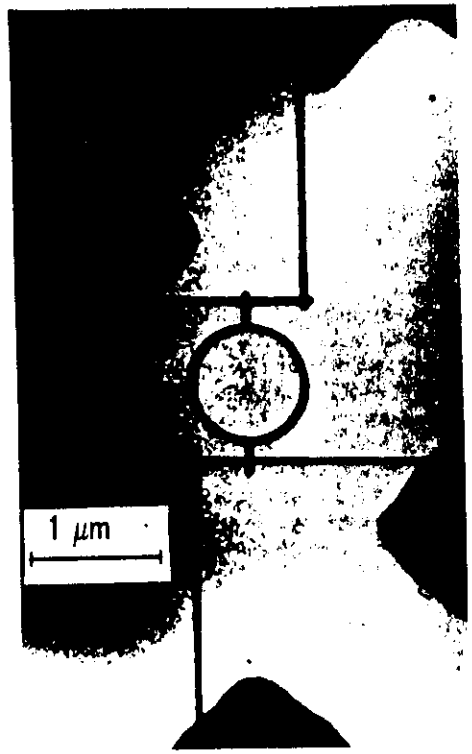

FIG. 34

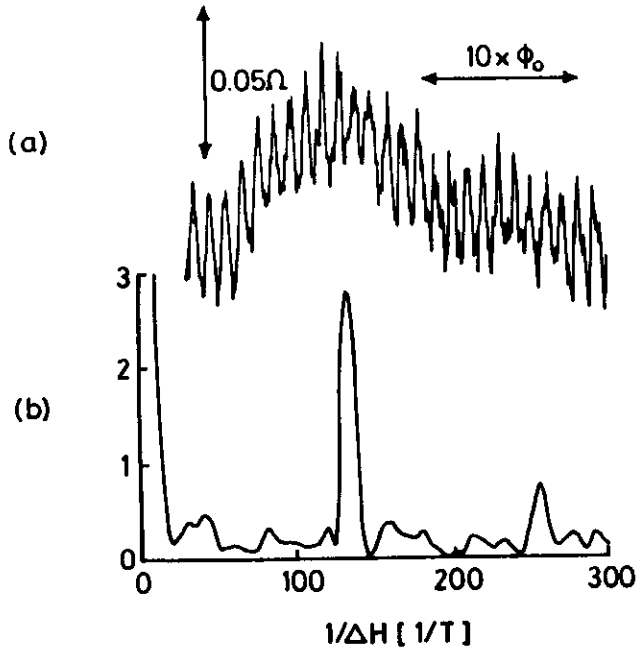
(a)
(b)
0.05Ω
10 × φ₀
3
2
1
0
0
100
200
300
1/ΔH [1/T]

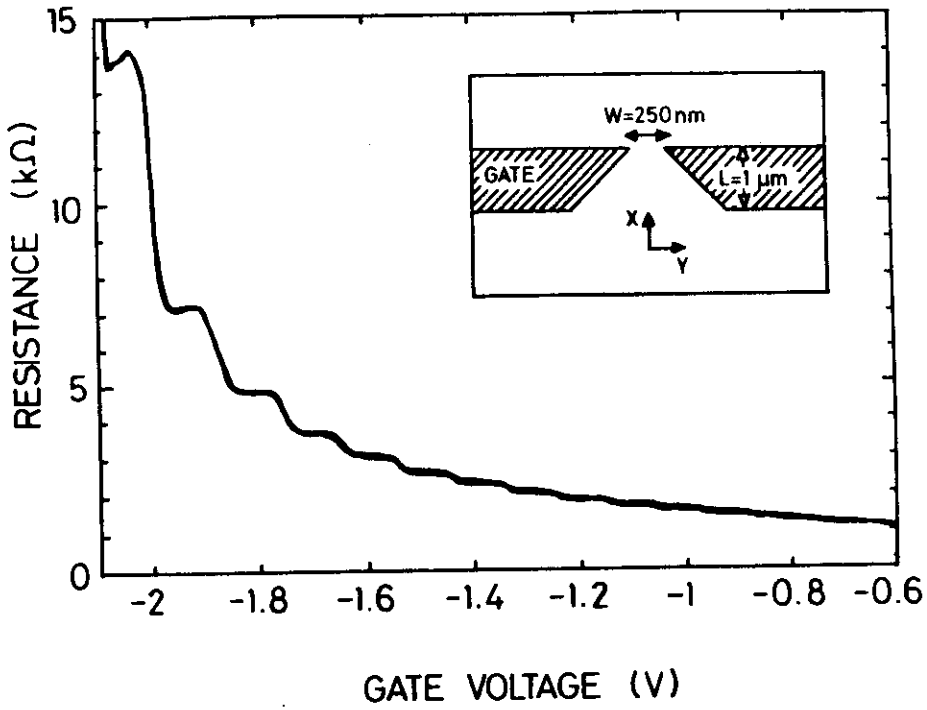
RESISTANCE (kΩ)
15
10
5
0
-2
-1.8
-1.6
-1.4
-1.2
-1
-0.8
-0.6
GATE VOLTAGE (V)
W=250nm
GATE
L=1 μm
X
Y

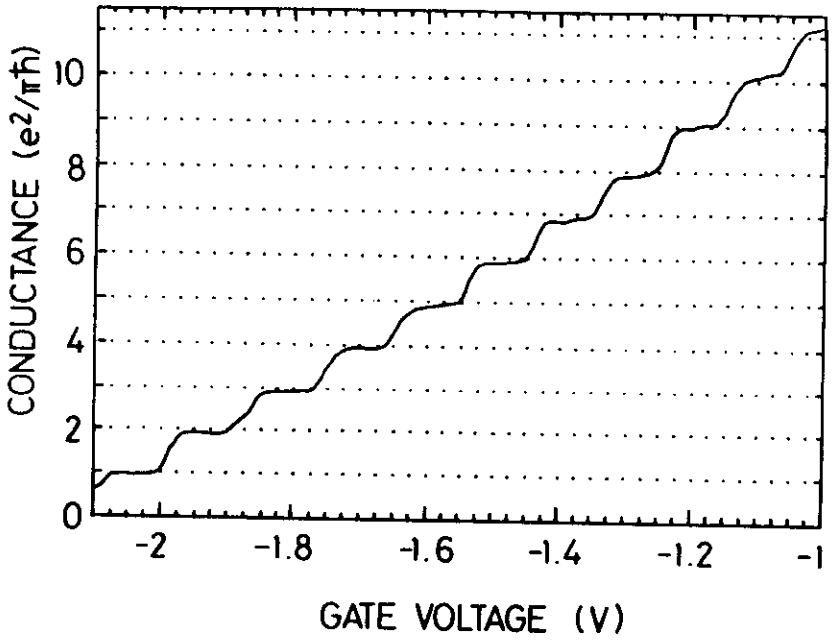
CONDUCTANCE (e²/πħ)
0
2
4
6
8
10
-2
-1.8
-1.6
-1.4
-1.2
-1
GATE VOLTAGE (V)

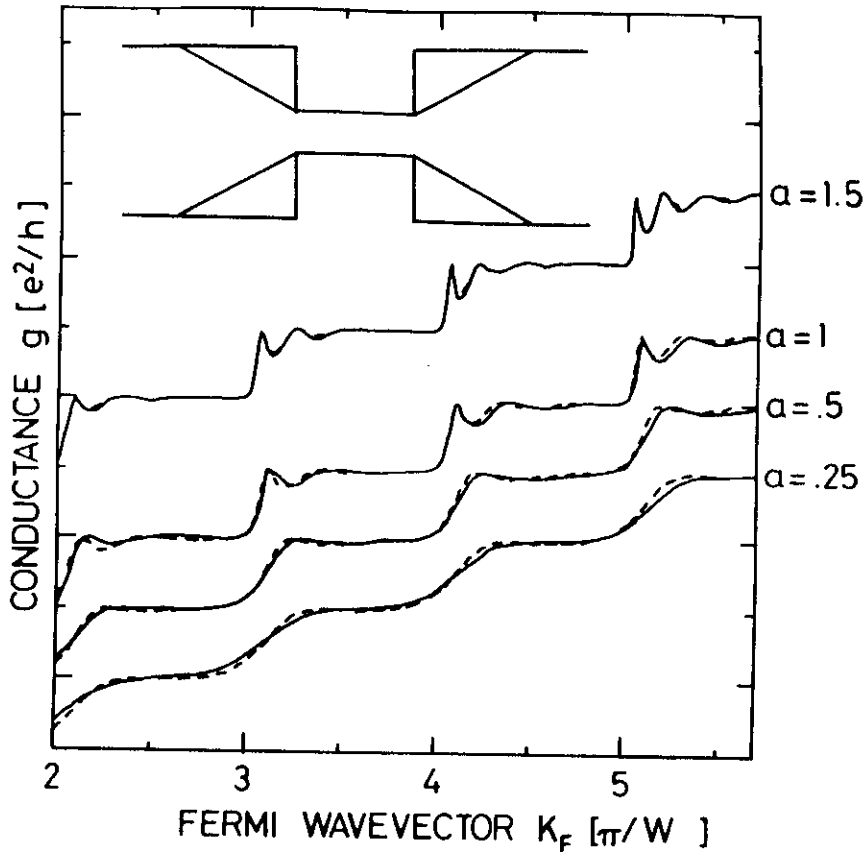
CONDUCTANCE g [e²/h]
α = 1.5
α = 1
α = .5
α = .25
2
3
4
5
FERMI WAVEVECTOR K_F [π/W]

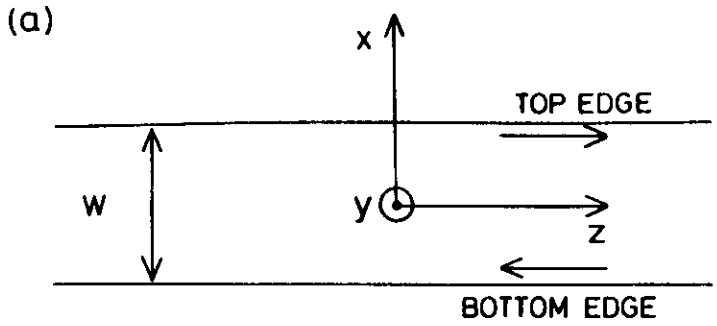
(a)
x
TOP EDGE
W
y
z
BOTTOM EDGE

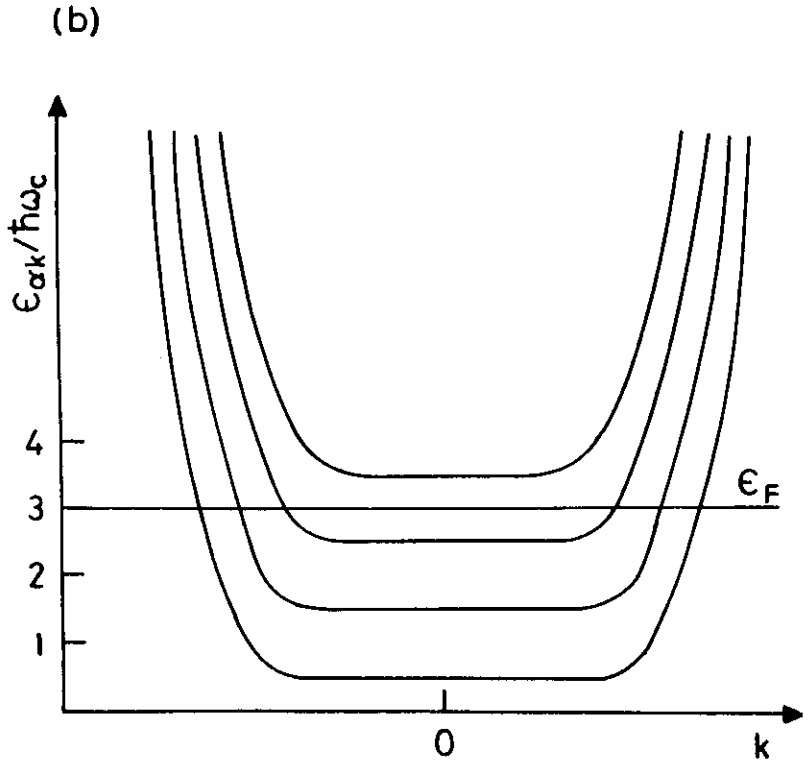
(b)
$\epsilon_{\alpha k}/\hbar\omega_c$
4
3
2
1
ϵ_F
0
k

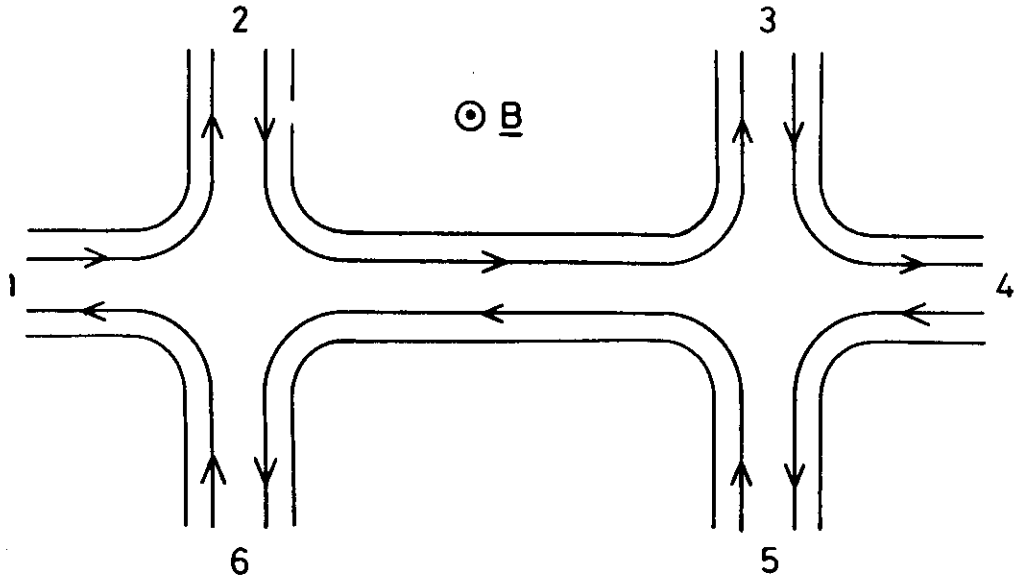
2
3
B
1
4
6
5

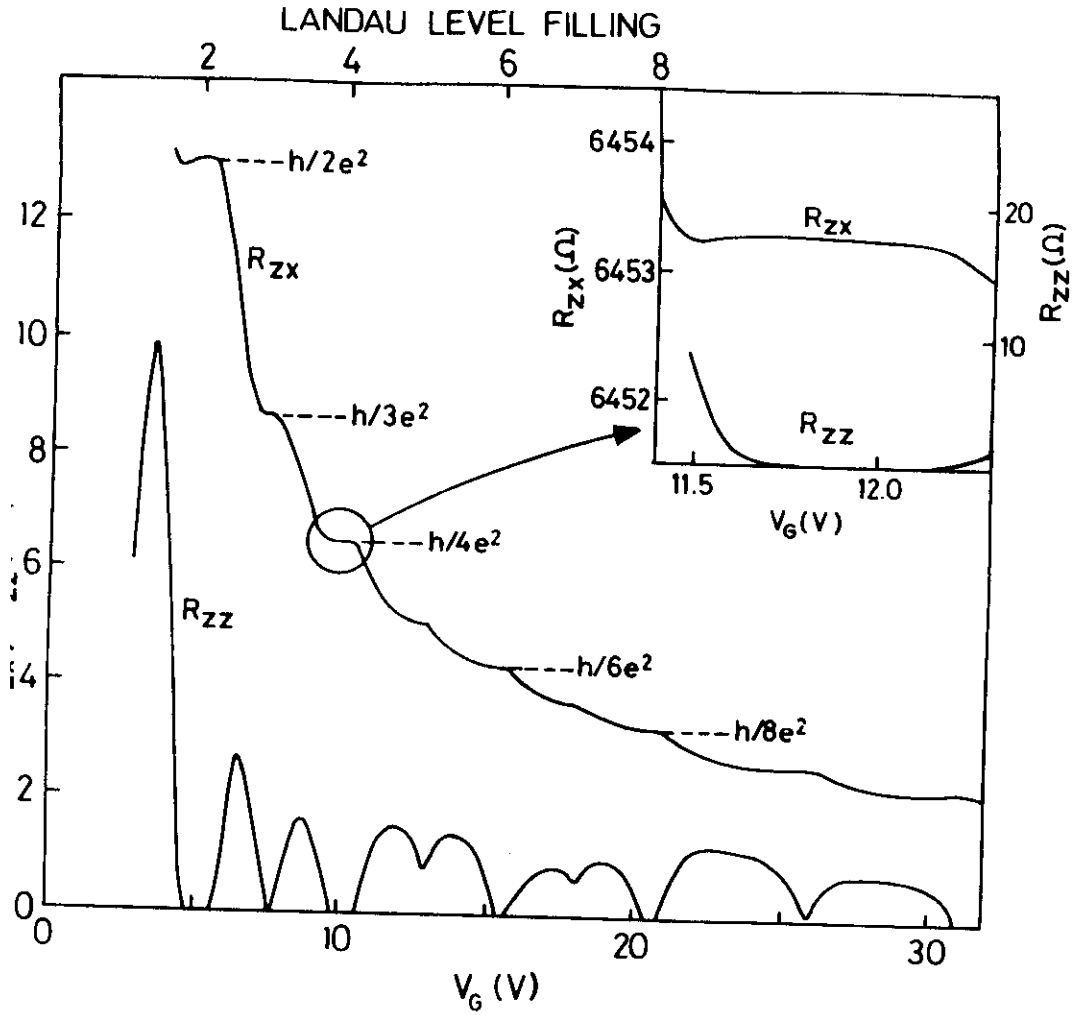
LANDAU LEVEL FILLING
2
4
6
8
h/2e²
h/3e²
h/4e²
h/6e²
h/8e²
Rzx
Rzz
6454
6453
6452
Rzx(Ω)
Rzz(Ω)
20
10
11.5
12.0
VG(V)
12
10
8
6
4
2
0
0
10
20
30
VG (V)

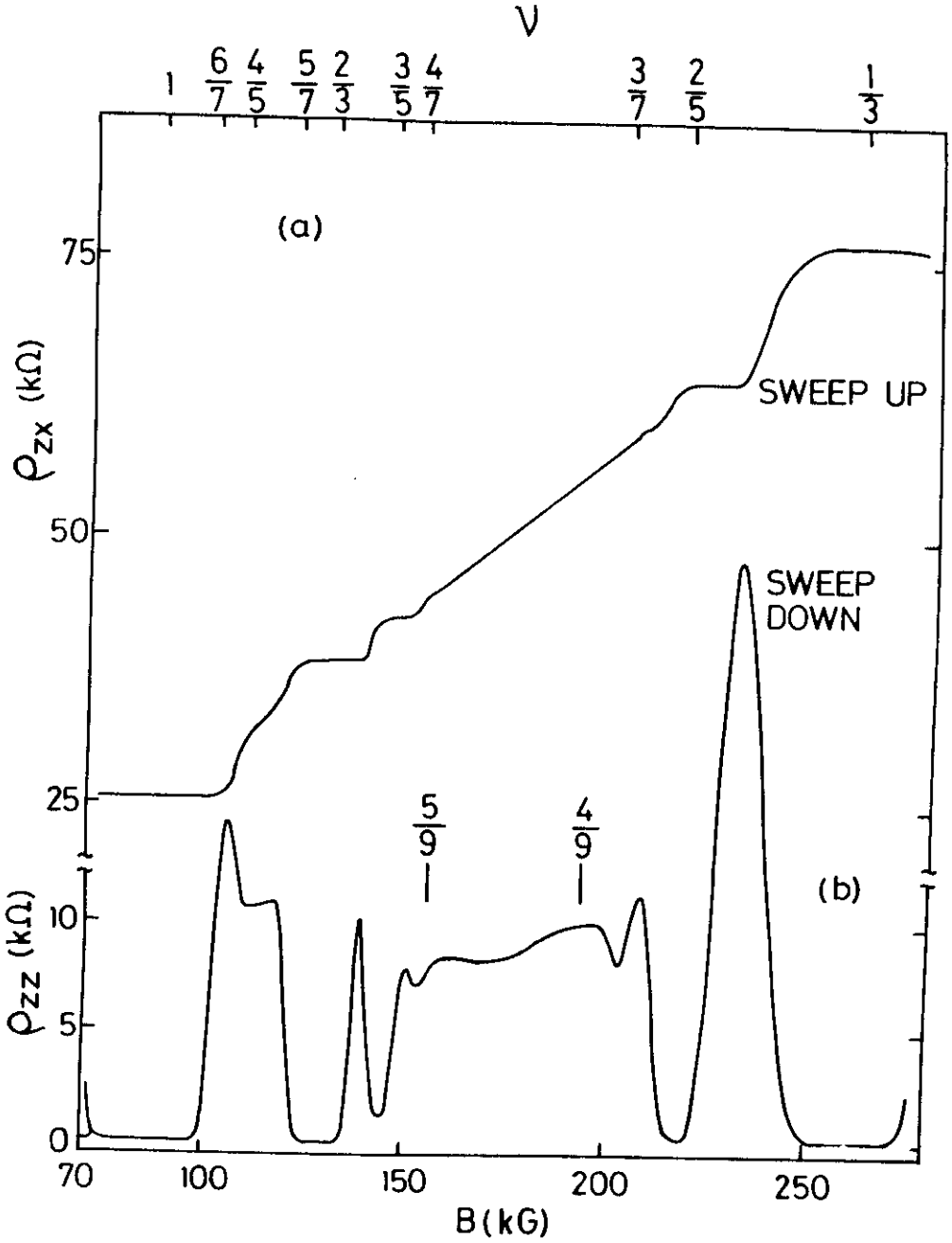
ν
1
6/7
4/5
5/7
2/3
3/5
4/7
3/7
2/5
1/3
(a)
75
50
25
ρzx (kΩ)
SWEEP UP
SWEEP DOWN
5/9
4/9
(b)
10
5
0
ρzz (kΩ)
70
100
150
200
250
B(kG)